



UNIVERSITAT DE
BARCELONA

Glutamine synthetase

- a potential therapeutic target in acute myeloid leukemia

Dissertation

to obtain the two academic degrees
Doctor philosophiae naturalis (Dr. phil. nat.)
and Doctor of Philosophy (PhD)

from the

Goethe University Frankfurt

Faculty of Chemistry, Biochemistry and Pharmacy
Frankfurt am Main, Germany

and the

University of Barcelona

Department of Biochemistry and Molecular Biomedicine,
Faculty of Pharmacy
Barcelona, Spain

by

Johanna Kreitz

born in Troisdorf

Frankfurt am Main

2022

(D 30)

Accepted dissertation by the Faculty of Chemistry, Biochemistry and Pharmacy,
Goethe University Frankfurt

Dean: Prof. Dr. Clemens Glaubitz

Assessors: Prof. Dr. Harald Schwalbe
Prof. Dr. Hubert Serve
Prof. Dr. Marta Cascante

Disputation date: 01.04.2022

TO MY FAMILY

To my brave and determined sister,
to my great and talented brother
and to my parents who have been the most incredible teachers in every way.

You are with me;

Your rod and Your staff, they comfort me.

Psalm 23,4

“A single person can go faster but together we go further.”

Anyone who has accomplished something big will agree that it is rarely if ever a one-man job but rather the sum of work, time and commitment of many. The present work is no exception and is built on the expertise, skills, help and support of the following:

Prof. Dr. Hubert Serve, PD Dr. Frank Schnütgen and Dr. Nina Kurrle,

thank you for taking me on for an incredibly exciting and mind-broadening journey through the world of research and for sharing your knowledge, time and ideas. You have enabled me to gain an understanding of science that will pave the way for anything yet to come.

Prof. Dr. Harald Schwalbe,

thank you for your reliability, focus, teaching and support as a scientist and as a mentor.

Prof. Dr. Marta Cascante and Dr. Silvia Martin,

our cooperation and partnership through the European project HaemMetabolome have been incredibly valuable additives to my time as a PhD candidate. Thank you for the experience and the teaching I received as part of your laboratory group in Barcelona.

iSIAM Alshamleh,

having the support of smart, determined and driven colleagues is an incredibly great value. Finding friends among those that you work with side by side every day is priceless. With you I had the great luck to have both in one person.

Prof. Dr. Thomas Oellerich and Dr. Björn Häupl,

thank you for your cooperation and expertise in proteomics which greatly added to this work. Special thanks to Dr. Björn Häupl for your explanations and for taking time again and again.

Prof. Dr. Daniela Krause and Dr. Rahul Kumar,

thank you for the great support and teamwork during our cooperation. Special thanks to Dr. Rahul Kumar for your scientific support and friendship.

Verena Stolp and Marcel Seibert,

thank you for helping me with 26 mice and for your incredible sense of humor.

Sandra Tzschentke,

thank you so much for all the laughter and hugs we shared and your eagerness and helpfulness as our technical assistant.

Heike Nürnberger, Frank Wempe, Christine Schönfeld, Sarah Weber, Florian Gatzke, Philipp Makowka, Marcel Butzbach, Anastasia Parmon, Ada Clees, Sofia Krujatz, Sifora Kaleab,

thank you for being an unforgettable team and for making every working day a good day.

Dr. Sebastian Mohr, Dr. Ibrahim Polat, Fabian Hahner and James Oo,

thanks a lot for your support and for your friendship.

AG Oellerich and AG Brandts,

working side by side with you was something I always considered a big plus. Thank you!

Content

Abbreviations	7
Abstract	10
Zusammenfassung	13
1 Introduction	18
1.1 Acute myeloid leukemia - development, outcome and treatment	18
1.2 The role of metabolism in AML survival and eradication	22
1.3 Hypoxia and its implications in AML metabolism and survival	26
1.4 Novel metabolic targets identified and investigated in the current work	29
1.4.1 Glutamine synthetase	29
1.4.2 Macropinocytosis and protein metabolism	32
1.5 Aim	34
2 Materials and Methods	35
2.1 Materials	35
2.1.1 Hardware	35
2.1.2 Consumables	36
2.1.3 Software	36
2.1.4 Chemicals, reagents and enzymes	37
2.1.5 Buffers	39
2.1.6 Antibodies and fluorescent stains	40
2.1.7 Commercially available kits	40
2.1.8 Oligonucleotides and vector maps	41
2.1.9 Cell lines, primary AMLs, patient data and bacterial strain	45
2.2 Methods	47
2.2.1 Cell culture	47
2.2.2 Western blotting	48
2.2.3 Gene editing techniques	49
2.2.4 Growth, viability and colony assays	52
2.2.5 ATP-based viability assay for IC ₅₀ determination	52
2.2.6 Flow cytometry-based experiments	54
2.2.7 Glutamine consumption assay	55
2.2.8 Immunofluorescence microscopy	56
2.2.9 Mass spectrometry-based experiments	57
2.2.10 Nuclear magnetic resonance (NMR) analysis	59
2.2.11 <i>In vivo</i> mouse study	60
3 Results	62
3.1 GS expression is upregulated in AML on transcriptomic and proteomic level	62
3.2 Genetic deletion of GS reduces AML cell growth	66

3.3	The role of GS in glutamine synthesis	70
3.4	The role of GS in ammonium detoxification	73
3.5	Endocytic protein uptake and catabolism contribute to amino acid metabolism	81
3.6	GS-mediated ammonium detoxification is important for protein-derived amino acid metabolism	88
3.7	The adaptive role of the urea cycle/arginine biogenesis pathway upon GS deletion 93	
4	Discussion.....	97
4.1	The function of GS is relevant for the metabolization of endocytosed proteins	97
4.2	The adaptive role of the urea cycle/arginine biogenesis pathway upon GS deletion 101	
4.3	AML cells conduct macropinocytosis and metabolize protein-derived amino acids 103	
5	Conclusion	106
6	References.....	107
7	Appendix	121
7.1	¹⁵ N- and non-labeled <i>Arthrospirulina maxima</i> cell extract preparation.....	121
8	Declaration for collaborative work.....	122
9	Eidesstattliche Erklärung	123
10	Curriculum vitae.....	124

Abbreviations

αKG	α-Ketoglutarate
ALL	Acute lymphoblastic leukemia
AML	Acute myeloid leukemia
APL	Acute promyelocytic leukemia
ARG	Arginase
ASL	Argininosuccinate lyase
ASS1	Argininosuccinate synthetase 1
ATP	Adenosine triphosphate
BCAAs	Branched-chain amino acids
BCL-2	B-cell lymphoma 2
BSA	Bovine Serum Albumin
CBF	Core binding factor
CLL	Chronic lymphocytic leukemias
CPS1	Carbamoyl phosphate synthetase 1
CR	Complete remission
CRISPR	Clustered regularly interspaced short palindromic repeats
D2O	Deuterium oxide
DMSO	Dimethylsulfoxide
DNMT3A	DNA methyltransferase 3A
DSMZ	Deutsche Sammlung von Mikroorganismen und Zellkulturen GmbH
DTT	Dithiothreitol
DQ-BSA	Dye quenched-bovine serum albumin
EDTA	Ethylenediaminetetraacetic acid
EIPA	Ethyl-isopropyl amiloride
FCS	Fetal calf serum
FLT3	FMS-related tyrosine kinase 3
FLT3-TKI	FLT3 tyrosine kinase inhibitors
FSC-A	Forward scatter area
FSC-H	Forward scatter height
GC-MS	Gas chromatograph coupled to mass spectrometry
GDH	Glutamate dehydrogenase
GS	Glutamine synthetase
HCl	Hydrochloric acid
hFLT3L	Human FLT3-ligand
HIF	Hypoxia inducible factor
hIL3	Human interleukin 3

HSC	Hematopoietic stem cells
hSCF	Human stem cell factor
HSPCs	Healthy hematopoietic stem and progenitor cells
hTPO	Human thrombopoietin
IDH	Isocitrate dehydrogenase
ITD	Internal tandem duplication
LSC	Leukemic stem cells
MgCl ₂	Magnesium chloride
MSO	L-methionine sulfoxamine
mTOR	Mammalian target of rapamycin
Na ₃ VO ₄	Sodium orthovanadate
NaCl	Sodium chloride
NaF	Sodium fluoride
NaOH	Sodium hydroxide
NADPH	Reduced nicotinamide adenine dinucleotide phosphate
NH ₄ Cl	Ammonium chloride
NMR	Nuclear magnetic resonance
NPM1	Nucleophosmin
NSCLC	Non-small cell lung cancer
NSG	NOD SCID gamma
NTC	Non-target control
OS	Overall survival
OTC	Ornithine transcarbamoylase
OXPPOS	Oxidative phosphorylation
P5CS	Pyrroline-5-carboxylate synthase
PBS	Dulbecco's Phosphate Buffered Saline
PEI	Polyethylenimine
PFA	Paraformaldehyde
PI3K	PI3 kinase
PO ₄	Sodium phosphate
PPP	Pentose phosphate pathway
RIPA	Radioimmunoprecipitation assay
RUNX1	Runt-related transcription factor 1
SDS	Sodium dodecyl sulfate
SDS-PAGE	SDS polyacrylamide gel electrophoresis
sgRNA	Single guide RNA
SILAC	Stable isotope labeling by amino acids in cell culture

TBS-T	Tris-buffered saline with Tween
TCA	Tricarboxylic acid
TCGA	The Cancer Genome Atlas
TMSP	Trimethylsilylpropanoic acid
WT	Wildtype

Abstract

Acute myeloid leukemia (AML) is one of the most frequently occurring and fatal types of leukemia. Initiated by genetic alterations in hematopoietic stem and progenitor cells, rapidly proliferating cancer cells (leukemic blasts) infiltrate the bone marrow and damage healthy hematopoiesis. Subgroups of AML are defined by underlying molecular and cytogenetic abnormalities, which are decisive for treatment and prognosis. For AML patients that can be intensively treated, the first line treatment remains a combination of cytarabine and anthracycline, which was developed in the 1970s. While this treatment regimen clears the disease and reinstates normal hematopoiesis (complete remission, CR) in 60% to 80% of patients below the age of 60, CR rates in patients above the age of 60 are only 40% to 50%. Relapse and refractory disease are the major cause of death of AML patients, despite large efforts to improve risk-adjusted post-remission therapy with further chemotherapy cycles and, if possible, allogeneic bone marrow transplantation. Elderly patients are particularly difficult to treat because of age-related comorbidities and because their disease tends to relapse more often than the disease of younger patients. Thus, the cure rates of AML vary with age, with 5-year survival rates of about 50% in young patients, and less than 20% in patients above the age of 65 years. With the median age of AML patients being 68 years, the need for novel therapeutic options is immense. The recent approval of eight new agents (venetoclax, midostaurin, gilteritinib, glasdegib, ivosidenib, enasidenib, gemtuzumab ozogamicin and CPX-351 (liposomal cytarabine and daunorubicin)) has added considerably to the therapeutic armamentarium of AML and has increased cure rates in specific subgroups of AML. However, the high heterogeneity among patients, clonal evolution and commonly occurring drug resistance, which cause the high relapse rates, remain a substantial problem in the treatment of AML. Therefore, a better understanding of currently used therapeutics and further development of novel therapeutics is urgently needed.

In recent years, attention has increasingly focused on therapeutic strategies to interfere with the metabolic requirements of cancer cells. The last three decades have provided extensive insights into the diversity and flexibility of AML metabolism. AML cells use different sources of nutrients compared to normal hematopoietic progenitor cells and reprogram their metabolic pathways to fulfill their exquisite anabolic and energetic needs. As a result, they develop high metabolic plasticity that enables them to thrive in the bone marrow microenvironment, where oxygen and nutrient availability are subject to constant change.

Cancer cells, specifically AML cells, have a strong dependency for the amino acid glutamine. Glutamine serves in energy production, redox control, cell signaling as well as an important nitrogen source. The only enzyme capable of *de novo* glutamine synthesis is glutamine

synthetase (GS). GS catalyzes glutamine production from glutamate and ammonium. In AML, the metabolic role and dependency of GS is poorly understood. Here, we investigated the effects of GS deletion on AML growth, and its functional relevance in AML metabolism. Genetic deletion of GS resulted in a significant decrease of cell growth *in vitro*, and impaired leukemia progression *in vivo* in a xenotransplantation mouse model. Interestingly, the dependency of AML cell growth on GS was shown to be independent of its functional role in glutamine synthesis. Glutamine starvation did not increase the dependency of the AML cells on GS, nor did increased glutamine availability rescue the GS-knockout-associated growth disadvantage. Instead, functional studies revealed the role of GS in the detoxification of ammonium. GS-deficient cells showed elevated ammonium secretion as well as a higher sensitivity towards the toxic metabolite. Exogenous provision of ¹⁵N-labeled ammonium was detoxified by GS-driven incorporation into glutamine. Studies on cells that had gained resistance to GS-knockout-mediated growth inhibition indicated enzymes involved in the urea cycle and the arginine biogenesis pathway to compensate for a loss of GS. Together, these findings unveiled GS as an important ammonium scavenger in AML.

Clinical studies on AML patients revealed increased ammonium concentrations in the blast-infiltrated bone marrow compared to peripheral blood. In line with this finding, proteome and transcriptome analysis of AML blasts showed a significant upregulation of GS in AML compared to healthy progenitors, further indicating its importance in ammonium detoxification. Analyzing pathways that contribute to ammonium production revealed protein uptake followed by amino acid catabolism as a yet not identified mechanism supporting AML growth. Protein endocytosis and subsequent proteolytic degradation were shown to rescue AML cells from otherwise growth-inhibiting glucose or amino acid depletion. Furthermore, protein metabolization led to the reactivation of the mammalian target of rapamycin (mTOR) signaling pathway, which was deactivated upon leucine and glutamine depletion, revealing protein consumption as an important alternative source of amino acids in AML.

To drive energy production, protein-derived amino acids undergo deamination resulting in carbon backbones that replenish the tricarboxylic acid (TCA) cycle. The present study established a link between amino acid-derived ammonium accumulation and GS-dependent ammonium removal. The link was revealed through the addition of ¹⁵N-labeled cell extracts which resulted in a GS-driven incorporation of released ammonium into glutamine.

We further investigated if prolonged periods of hypoxia (> 7 days) influence the dependency of AML cells on GS. Despite the great impact of oxygen availability on cell metabolism, the relevance of GS in AML was not affected by hypoxia.

In summary, the current work exposed a previously undiscovered role of GS in ammonium detoxification which could be linked to amino acid catabolism. This essential function of GS poses it as a potential therapeutic target in AML. We further revealed AML cells to conduct macropinocytosis and to metabolize extracellular protein which has so far not been elucidated in AML. We could show that the uptake of protein through endocytosis-driven pathways fulfills the anabolic and energetic needs of AML cells, especially under nutrient starvation.

Zusammenfassung

Die akute myeloische Leukämie (AML) ist eine der am häufigsten auftretenden und tödlich verlaufenden Leukämiearten. Ausgelöst durch genetische Veränderungen in hämatopoetischen Stamm- und Vorläuferzellen, infiltrieren schnell proliferierende Krebszellen (leukämische Blasten) das Knochenmark und schädigen die gesunde Hämatopoese. Untergruppen der AML werden durch zugrundeliegenden molekularen und zytogenetischen Anomalien definiert, die für die Behandlung und Prognose entscheidend sind. Die genetischen Veränderungen von etwa 50 % aller *de novo* AML-Patienten beinhalten große chromosomale Umlagerungen. Dazu gehören häufige chromosomale Translokationen wie t(8:21) und t(15:17), die nach strukturellen Veränderungen oder Unterdrückung von myeloischen Transkriptionsfaktoren die normale myeloische Reifung behindern. Zusätzlich treten in > 97 % der AML-Fälle genetische Mutationen von verschiedenen Genen auf. Die am häufigsten mutierten Gene sind die Nukleophosmin (25 % - 30 %), die FMS-verwandte Tyrosinkinase 3 (20 %) und die DNA-Methyltransferase 3A (18 % - 22 %). Mutationen in diesen Genen fördern die Leukämieentwicklung, indem sie das Blasten-Wachstum stimulieren oder die normale Hämatopoese blockieren.

Die Primärbehandlung in der Therapie der AML ist nach wie vor eine Kombination aus Cytarabin und Anthrazyklin, die in den 70er Jahren entwickelt wurden. Während dieses Behandlungsschema bei 60 % bis 80 % der Patienten unter 60 Jahren eine komplette Remission (CR) erreicht und eine normale Blutbildung wiederherstellt, sind die CR-Raten bei Patienten über 60 Jahren mit 40 % bis 50 % deutlich niedriger. Rezidiv und refraktäre Erkrankung sind die Haupttodesursache von AML-Patienten, trotz großer Anstrengungen zur Verbesserung der risikoadjustierten Nachremissionstherapie mit weiteren Chemotherapiezyklen und, wenn möglich, allogener Knochenmarktransplantation. Ältere Patienten sind besonders schwierig zu behandeln, weil sie altersbedingte Komorbiditäten aufweisen und weil ihre Erkrankung häufiger zu Rückfällen neigt als die von jüngeren Patienten. So variieren die Heilungsraten der AML mit dem Alter, mit 5-Jahres-Überlebensraten von etwa 50 % bei jungen Patienten und weniger als 20 % bei Patienten über 65 Jahren. Da das Durchschnittsalter von AML-Patienten bei 68 Jahren liegt, ist der Bedarf an neuen therapeutischen Optionen immens. Die jüngste Zulassung von acht neuen Wirkstoffen (Venetoclax, Midostaurin, Gilteritinib, Glasdegib, Ivosidenib, Enasidenib, Gemtuzumab Ozogamicin und CPX-351 (liposomales Cytarabin und Daunorubicin)) hat das therapeutische Behandlungsspektrum der AML erheblich erweitert und die Heilungsraten in bestimmten Untergruppen der AML erhöht. Die hohe Heterogenität unter den Patienten, die klonale Evolution und die häufig auftretende Medikamentenresistenz, die die hohen Rückfallraten verursachen, bleiben jedoch ein wesentliches Problem bei der Behandlung der AML. Daher

ist ein besseres Verständnis der derzeit verwendeten Therapeutika und die Weiterentwicklung neuartiger Therapeutika dringend erforderlich.

In den letzten Jahren hat sich die Aufmerksamkeit zunehmend auf therapeutische Strategien gerichtet, die in die metabolischen Anforderungen von Krebszellen eingreifen. Die letzten drei Jahrzehnte haben umfangreiche Einblicke in die Vielfalt und Flexibilität des AML-Stoffwechsels geliefert. AML-Zellen nutzen andere Nährstoffquellen als normale hämatopoetische Vorläuferzellen und programmieren ihre Stoffwechselwege um, um ihre anabolen und energetischen Bedürfnisse zu erfüllen.

Die bestehenden Forschungsergebnisse zeigen, dass jeder wichtige Stoffwechselweg bei AML umprogrammiert ist. Die beschleunigte Glykolyse, die oft als Warburg-Effekt bezeichnet wird, ist seit langem als eindeutige Signatur von Krebszellen bekannt, da sie die Ausbeute an zellulären Bausteinen erhöht. Dies gilt auch für AML-Zellen, die stark auf ein hohes glykolytisches Profil angewiesen sind, was zusätzlich eine Medikamentenresistenz verleiht.

Die metabolische Umprogrammierung beeinflusst auch den mitochondrialen Stoffwechsel, der den Tricarbonsäurezyklus und die oxidative Phosphorylierung umfasst. Diese Stoffwechselwege steuern biosynthetische Prozesse und die Energieproduktion und sind zentral für das Überleben und die Proliferation der AML. Unsere eigenen unveröffentlichten Daten weisen darauf hin, dass insbesondere FLT3-ITD-positive AML in hohem Maße von der Aktivität des Tricarbonsäurezyklus abhängig sind. Durch das Umschalten zwischen verschiedenen Nährstoffquellen entwickeln AML-Zellen eine hohe metabolische Plastizität, die es ihnen ermöglicht, in der Mikroumgebung des Knochenmarks zu wachsen, in der die Verfügbarkeit von Sauerstoff und Nährstoffen einem ständigen Wandel unterworfen ist.

Krebszellen, insbesondere AML-Zellen, haben eine starke Abhängigkeit von der Aminosäure Glutamin. Glutamin dient der Energieproduktion, der Redox-Kontrolle, den Zellsignalprozessen sowie als wichtige Stickstoffquelle. Das einzige Enzym, das in der Lage ist, Glutamin *de novo* zu synthetisieren, ist die Glutaminsynthetase (GS). GS katalysiert die Produktion von Glutamin aus Glutamat und Ammonium.

In soliden Krebsarten wurde die Bedeutung von GS ausgiebig untersucht. Eine erhöhte GS-Expression wird bei vielen soliden Krebsarten beobachtet, jedoch variiert die Korrelation mit dem Fortschreiten des Krebses oder der Aggressivität. Die spezielle Abhängigkeit von Krebszellen von GS ist schwer zu definieren und variiert zwischen den verschiedenen Krebsarten und auch in Abhängigkeit von der Verfügbarkeit von extrazellulärem Glutamin. Bei mehreren soliden Krebsarten wurde gezeigt, dass die GS-Abhängigkeit auf Bedingungen mit Glutaminmangel beschränkt ist. Wenn extrazelluläre Glutaminreserven erschöpft sind, spielt

GS eine kritische Rolle bei der Wiederauffüllung der intrazellulären Glutaminreserven und somit bei der Aufrechterhaltung stickstoffabhängiger anaboler Prozesse wie der Nukleotidbiosynthese.

Trotz der Bedeutung von GS im Glutamin-Stoffwechsel bei vielen soliden Krebsarten wurde die metabolische Rolle und Abhängigkeit der GS bei AML nur unzureichend verstanden. In der vorliegenden Arbeit untersuchten wir die Auswirkungen einer GS-Depletion auf das AML-Wachstum und ihre funktionelle Bedeutung im AML-Stoffwechsel. Die genetische Deletion von GS führte zu einer signifikanten Abnahme des Zellwachstums *in vitro* und beeinträchtigte die Entwicklung der Leukämie *in vivo*. Dies wurde in AML-Zelllinien mit verschiedenen genetischen Veränderungen gezeigt, in welchen die Depletion von GS zu ausgeprägten Wachstumsdefiziten führte. Die Bedeutung von GS für das AML-Wachstum wurde außerdem in einem Xenotransplantations-Mausmodell bestätigt, bei dem THP1-Zellen mit einem GS-Knockdown injiziert wurden. *In vitro* zeigten die GS-Knockdown-Zellen im Vergleich zu den Kontrollzellen eine signifikant verminderte Fähigkeit zu wachsen und Kolonien zu bilden. *In vivo* verlängerte der Knockdown von GS signifikant das Überleben der Mäuse und verringerte die Fähigkeit zur Tumorbildung sowie die Infiltration von Knochenmark, Lymphknoten und Organen.

Interessanterweise erwies sich die Abhängigkeit des AML-Zellwachstums von GS als unabhängig von seiner funktionellen Rolle bei der Glutaminsynthese. Unabhängig vom extrazellulären Glutaminspiegel zeigten GS-Knockout-Zellen die gleiche reduzierte Wachstumsrate. Selbst die Versorgung der Zellen mit 600 mg/l Glutamin, doppelt so viel wie unter Standard-Kulturbedingungen, befreite die Zellen nicht von dem GS-Knockout-induzierten Verlust der Proliferation. Diese Ergebnisse deuteten auch darauf hin, dass AML-Zellen stark auf exogenes Glutamin angewiesen sind, nicht aber auf *de novo* synthetisiertes Glutamin. Dies wurde durch eine Metabolon-Analyse bestätigt, die gleiche intrazelluläre Glutaminwerte unter ausreichenden Glutaminbedingungen in GS-Knockout-Zellen im Vergleich zu Kontrollzellen ergab.

Anstatt den Zellen als primäre Quelle für Glutamin zu dienen, zeigten funktionelle Studien die Rolle von GS bei der Entgiftung von Ammonium. Ammonium wird in allen Zellen des Körpers während des Metabolismus von stickstoffhaltigen Verbindungen und hauptsächlich im Prozess der Aminosäuredeaminierung produziert. Es dient als wichtige Stickstoffquelle und als Schlüsselmetabolit bei der pH-Kontrolle. Ammonium übt jedoch zytotoxische Wirkungen aus, die zu einer Störung des intrazellulären pH-Werts, elektrochemischer Gradienten oder

enzymatischer Reaktionen sowie zu Veränderungen der Protonengradienten und damit zur Hemmung endo- und exozytotischer Prozesse führen können, wenn es nicht abgefangen wird. Unsere Arbeit zeigte, dass GS-defiziente Zellen eine erhöhte Ammoniumsekretion aufweisen sowie eine höhere Empfindlichkeit gegenüber dem toxischen Metabolit ausüben. Mechanistische Studien mit Massenspektrometrie und magnetischer Kernresonanz bestätigten den spezifischen Einbau von ¹⁵N-markiertem Ammonium in Glutamat in einer von GS katalysierten Reaktion.

Untersuchungen an Zellen, die eine Resistenz gegen GS-Knockout-vermittelte Wachstumshemmung erlangt hatten, zeigten, dass Enzyme, die am Harnstoffzyklus und am Arginin-Biogeneseweg beteiligt sind, den Verlust von GS kompensieren. Zusammengenommen enthüllten diese Befunde die Rolle von GS bei der Ammonium-Entgiftung in AML.

Klinische Studien an AML-Patienten ergaben erhöhte Ammonium-Konzentrationen im durch Blasten infiltrierten Knochenmark im Vergleich zum peripheren Blut. In Übereinstimmung mit diesem Befund zeigten Proteom- und Transkriptomanalysen von AML-Blasten eine signifikante Hochregulierung von GS in AML im Vergleich zu gesunden hämatopoetischen Stamm- und Vorläuferzellen, was ein weiterer Hinweis auf die Bedeutung von GS bei der Ammonium-Entgiftung ist.

Die Analyse von Stoffwechselwegen, die zur Ammoniumproduktion beitragen, zeigte die Proteinaufnahme, gefolgt von Aminosäurekatabolismus, als einen noch nicht identifizierten Mechanismus, der das AML-Wachstum unterstützt. Es konnte gezeigt werden, dass die Protein-Endozytose und der anschließende proteolytische Abbau der Proteine AML-Zellen vor einem ansonsten wachstumshemmenden Glukose- oder Aminosäuremangel rettet. Darüber hinaus führte die Proteinmetabolisierung zur Reaktivierung des mTOR-Signalwegs (Abkürzung für „mammalian target of rapamycin“, auf Deutsch „Ziel des Rapamycins im Säugetier“), der bei Leucin- und Glutaminmangel deaktiviert wurde, was die Proteinaufnahme als wichtige alternative Aminosäurequelle bei AML aufzeigt.

Um die Energieproduktion voranzutreiben, werden aus Proteinen gewonnene Aminosäuren desaminiert, was zu Kohlenstoffketten führt, die den Tricarbonsäurezyklus wieder auffüllen. In der vorliegenden Studie wurde eine Verbindung zwischen der Aminosäure-abgeleiteten Ammonium-Akkumulation und der GS-abhängigen Ammonium-Entfernung hergestellt. Die Verbindung wurde durch die Zugabe von ¹⁵N-markierten Zellextrakten aufgedeckt, was zu einer GS-gesteuerten Inkorporation von freigesetztem Ammonium in Glutamin führte.

Wir konnten die Interdependenz zwischen Proteinaufnahme und -katabolismus und der funktionellen Rolle von GS weiter verdeutlichen. Ein starker Beweis für die Abhängigkeit des Proteinstoffwechsels von GS-Funktionen ergab sich aus der beobachteten Abnahme der Aufnahme und Proteolyse von Bovinem Serumalbumin (BSA) bei GS-Inhibition. Wir stellten die Hypothese auf, dass die Akkumulation von Ammonium bei GS-Abnahme die Fähigkeit der Zellen, Proteine zu verwerten und zu wachsen, beeinträchtigt. Die abnehmende Aufnahme und Proteolyse von BSA bei Zugabe von Ammoniumchlorid bestätigte tatsächlich, dass die Ammoniumakkumulation hemmende Auswirkungen auf die Proteinaufnahme und -verwertung hat. Darüber hinaus konnten wir zeigen, dass der Zwang zum Proteinabbau (durch Zugabe von Proteinen) bei GS-Knockout-Zellen ihren Wachstumsnachteil noch verstärkte. Die hemmenden Effekte von Ammonium auf den Proteinstoffwechsel sind wahrscheinlich die Ursache dafür, dass die Endozytose-vermittelte Proteinaufnahme ein pH-sensitiver Prozess ist, der durch eine Absenkung des pH-Wertes gehemmt wird, ein Effekt, der durch die Ammoniumanreicherung induziert wird.

Wir haben weiter untersucht, ob längere Perioden von Hypoxie (> 7 Tage) die Abhängigkeit der AML-Zellen von GS beeinflussen. Trotz des großen Einflusses der Sauerstoffverfügbarkeit auf den Zellstoffwechsel wurde die Relevanz von GS in AML durch Hypoxie nicht beeinflusst. Zusammenfassend zeigte die aktuelle Arbeit eine bisher unentdeckte Rolle von GS bei der Ammonium-Entgiftung auf, die mit dem Aminosäure-Katabolismus verbunden sein könnte. Diese essentielle Funktion von GS macht GS zu einem potentiellen therapeutischen Angriffspunkt in der AML. Weiterhin konnten wir zeigen, dass AML-Zellen Makropinozytose betreiben und extrazelluläres Protein verstoffwechseln, was bisher in der AML noch nicht aufgeführt wurde. Wir konnten zeigen, dass die Aufnahme von Protein durch Endozytose-getriebene Wege den anabolen und energetischen Bedarf der Zellen erfüllt, insbesondere unter Nährstoffmangel.

Zukünftige Studien sind erforderlich, um die Verbindung zwischen dem proteinbasierten Aminosäurekatabolismus und der Ammoniumentfernung durch GS weiter zu bestätigen. Auch sind weitere präklinische Studien erforderlich, um die Toxizität der GS-Hemmung an gesunden Zellen zu beurteilen, bevor die Entwicklung von GS-Inhibitoren in Betracht gezogen werden kann.

1 Introduction

1.1 Acute myeloid leukemia - development, outcome and treatment

The hematopoietic system is responsible for the continuous production of the versatile array of blood cells. It consists of self-renewing hematopoietic stem cells that inhabit the bone marrow and give rise to multipotent progenitor cells which further differentiate into mature and functional cells of the lymphoid and myeloid lineage (Dharampuriya *et al.*, 2017) (Figure 1). Depending on the lineage and the cell type, blood cells fulfill different functions vital to the body, including the delivery of oxygen (erythrocytes), the formation of both adaptive (T cells, B cells) and innate (granulocytes, megakaryocytes and macrophages) immunity and the regulation of hemostasis (platelets).

Genetic abnormalities acquired by hematopoietic precursors can dramatically interfere with normal hematopoiesis and can cause the onset of acute myeloid leukemia, an aggressive and life-threatening hematological malignancy (reviewed in Khwaja *et al.*, 2016 and De Kouchkovsky and Abdul-Hay, 2016). AML is characterized by the clonal expansion of immature and non-functional myeloid cells (termed as blasts) in the bone marrow, which can further infiltrate the peripheral blood and other tissues and organs. The abnormal growth and differentiation of the blasts interferes with the growth and production of healthy blood cells and decreases vital cell populations such as red blood cells, platelets and white blood cells. AML is defined by a blast count in the bone marrow or blood of 20% or higher (Vardiman *et al.*, 2002). (In healthy individuals the blast count in the bone marrow is below 5% with no blasts in the peripheral blood.) Depletion of the terminally differentiated myeloid cells leads to bone marrow failure with rapid onset of consequential symptoms and fatality if left untreated. The incidence of AML increases with age and is most dominant at a median age of 68 years (National Cancer Institute Surveillance, 2020). Despite continuous improvements in the treatment of AML, overall long-term survival remains poor. Increased age and decreased fitness are associated with lower rates of CR and overall survival (OS) (reviewed in De Kouchkovsky *et al.*, 2016). Population-based studies reported 5-year OS rates of below 20% in patients 60 years of age or older and approximately 50% in patients below the age of 60 (Juliusson *et al.*, 2009; Pulte *et al.*, 2016; Sossa *et al.*, 2018).

One of the major challenges in the treatment of AML is the highly heterogeneous nature of the genetic and epigenetic alterations in AML cells (Chen *et al.*, 2013; Papaemmanuil *et al.*, 2016; Martignoles *et al.*, 2018). Improvements in genomic technologies in recent years (e.g. next-generation sequencing) have given unprecedented insights into genomic alterations arising during AML pathogenesis, including their frequency and pattern of cooperativity (Figure 1).

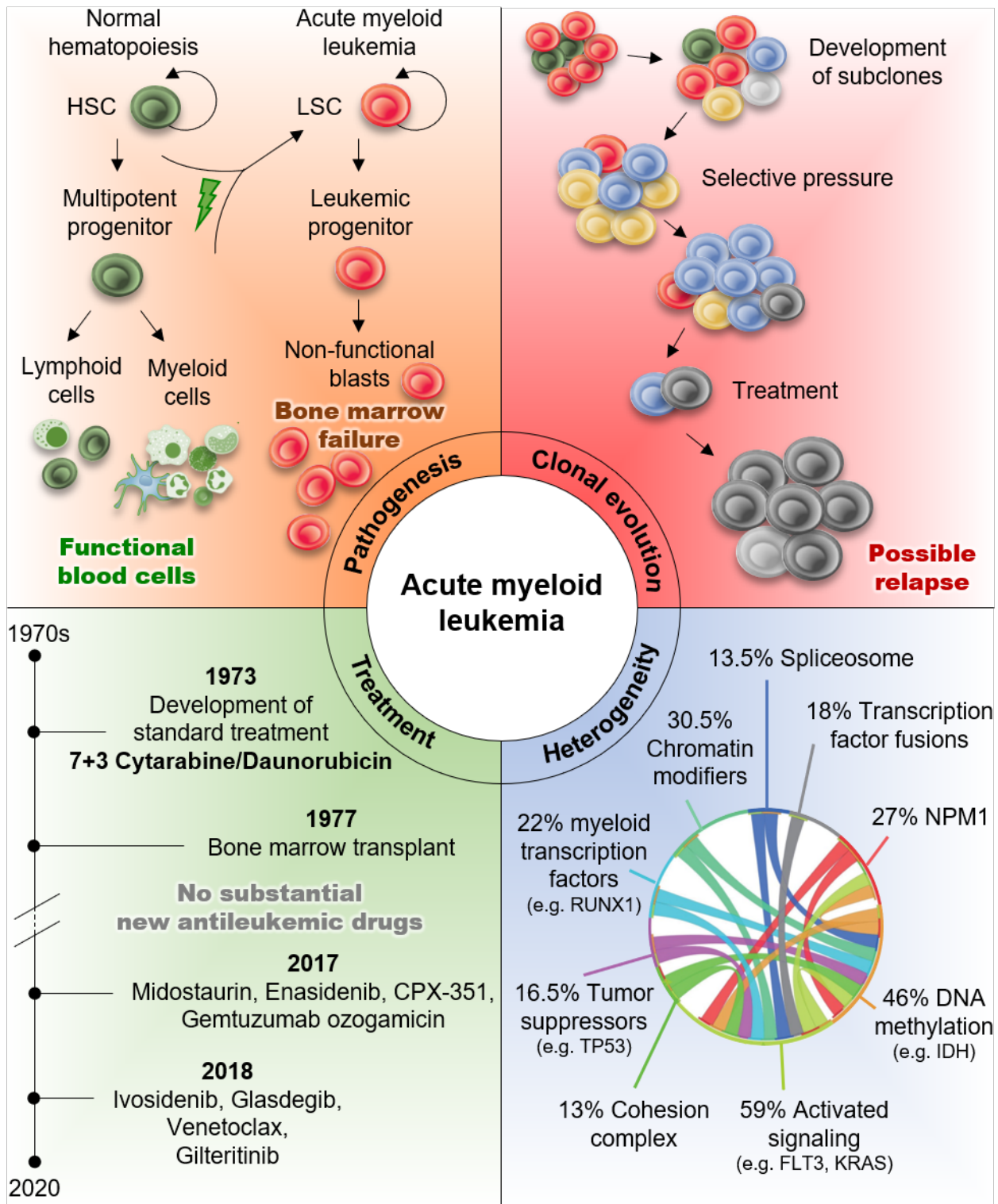


Figure 1. Acute myeloid leukemia

Pathogenesis: Oncogenic events in hematopoietic stem and progenitor cells can lead to the onset of AML, followed by an expansion of non-functional AML blasts that cause bone marrow failure. **Clonal evolution:** The clonal composition and mutational profile changes during AML progression due to selective pressure induced also by chemotherapy. Treatment-resistant clones can arise and cause relapse. **Heterogeneity:** AML is a highly heterogeneous disease, where genetic events as shown by the connecting ribbons, can form complex patterns of cooperation (adapted from Chen *et al.*, 2013). **Treatment:** After the development of the standard treatment regimen in the 1970s, new drugs are on their way.

H/LSC = hematopoietic/leukemic stem cells; NPM1 = nucleophosmin 1; IDH = isocitrate dehydrogenase; FLT3 = FMS-like tyrosine kinase 3; RUNX1 = runt-related transcription factor 1

Furthermore, it has shed light on the dynamics of the clonal evolution that occurs during AML development, treatment and relapse (Martignoles *et al.*, 2018; Vosberg, 2019).

Genetic alterations of about 50% of all *de novo* AML patients involve large chromosomal translocations. The most important types of chromosomal translocations in AML include (1) recurrent translocations, defining a disease type, (2) balanced translocations, not resulting in losses or gains of biological material, (3) translocation-derived fusion genes, resulting in the expression of new proteins with altered function and (4) translocations which involve transcription factors, fusing their DNA binding motif with other functional motifs that change their function (Grimwade *et al.*, 2016). Specific AML cases are the core binding factor (CBF) leukemias (which display inv(16) or t(8;21)), and the acute promyelocytic leukemia (APL), characterized by translocation of RARalpha (t(15;17)).

Additionally, genetic mutations of a long list of different genes (co-)occur in > 97% of AML cases. The most recurrently mutated genes are nucleophosmin (NPM1; 25% - 30%), FMS-related tyrosine kinase 3 (FLT3; 20%) and DNA methyltransferase 3A (DNMT3A; 18% - 22%). Mutations in these genes promote leukemia development by stimulating blast proliferation or blocking normal hematopoiesis (Grimwade *et al.*, 2016; Papaemmanuil *et al.*, 2016). Different types of mutations can co-occur in complex patterns and imply cross-talk between the AML-driving pathways (reviewed in Chen *et al.*, 2013; Figure 1). During the course of AML, clones with different sets of mutations and chromosomal abnormalities arise and are subject to selective pressure (Martignoles *et al.*, 2018; Vosberg, 2019; Figure 1). Shaped by extracellular growth conditions, in particular during AML therapy, where clonal susceptibility can differ tremendously, the heterogeneous clones form ever-changing complex clonal hierarchies that contribute to AML relapse (Shlush *et al.*, 2017). Identification of the underlying genetic abnormalities as well as the age and fitness of the patient are crucial prognostic factors that influence physicians' decisions on the patients' treatment (Estey *et al.*, 2017). Chemotherapy, including the standard 7+3 cytarabine and anthracycline induction (7 days of cytarabine and simultaneously 3 days of an anthracycline, most often daunorubicin), and allogeneic hematopoietic stem cell transplantation constitute the core of AML treatment (Chen *et al.*, 2019). In 60% to 80% of *de novo* AML patients below the age of 60 years and 40% to 50% above the age of 60 years, induction therapy achieves CR (von dem Borne *et al.*, 2016). What renders however the susceptibility to this intensive line of treatment is increased age, poor performance status and specific genetic aberrations. Furthermore, minimal residual disease often persists in CR and requires consolidation therapy (e.g. intermediate-dose cytarabine) to prevent relapse which is a common cause of death in AML (reviewed in Ravandi *et al.*, 2018). Following 40 years of no game-changing new drugs for the standard care of AML patients, the

FDA recently approved eight novel drugs (venetoclax, midostaurin, gilteritinib, glasdegib, ivosidenib, enasidenib, gemtuzumab ozogamicin and CPX-351 (Figure 1)) which provide novel opportunities for AML cohorts in different clinical situations (Short *et al.*, 2020). Continuous search for novel therapeutic targets in AML is required to provide further treatment options that eradicate the disease as rapidly as possible. Understanding the cellular metabolism of AML that is reprogrammed to fulfill the cancer's energetic and synthetic needs may eventually lead the way to drugs that exploit the differences of these mechanisms between AML and normal cells of the hematopoietic system (reviewed in Chapuis *et al.*, 2019; Kreitz *et al.*, 2019). In fact, one of the first successful chemotherapeutic agents in the treatment of acute leukemias, aminopterin and methotrexate, were effective as they blocked tetrahydrofolate metabolism (Farber and Diamond, 1948). Gaining further insights into the metabolic requirements of AML cells and elucidating novel vulnerabilities will be the focus of the current work.

1.2 The role of metabolism in AML survival and eradication

Cellular metabolism comprises the set of anabolic and catabolic processes that generate energy and biomass central to cellular growth (Palm and Thompson, 2017). The metabolic processes are fed by extracellular nutrients such as amino acids, glucose and macromolecules that are imported into the cell. A hallmark of cancer is a fundamentally rewired network of nutrient uptake and metabolization to fulfill its high energetic and anabolic demands (reviewed in Pavlova and Thompson, 2016).

AML is no exception to the general concept that metabolic alterations play a key role in cancer proliferation and drug resistance (reviewed in Kreitz *et al.*, 2019). The strategies used by AML cells to gain metabolic flexibility, increase yields of energy and biomass and maintain tumor proliferation under starvation are numerous and only partially understood (Figure 2). The existing body of research shows that every major metabolic pathway is rewired in AML. Accelerated glycolysis, often referred to as the Warburg effect, has long been known to be a distinct signature of cancer cells as it increases yields of cellular building blocks (Ganapathy-Kanniappan, 2018). This also holds true for AML cells that rely heavily on a high glycolytic profile, which additionally confers drug resistance (Chen *et al.*, 2014).

Metabolic reprogramming also affects mitochondrial metabolism that encompasses the TCA cycle and oxidative phosphorylation (OXPHOS). These pathways drive biosynthetic processes and energy production and are central to AML survival and proliferation (reviewed in Kreitz *et al.*, 2019). Our own unpublished data indicate that especially FLT3-ITD positive AML are highly dependent on TCA cycle activity (Alshamleh *et al.*, unpublished data). Switching between different sources that maintain the TCA cycle significantly contributes to the metabolic plasticity of AML cells. An important anaplerotic precursor is glutamine, which can enter the TCA cycle upon glutaminolysis (Emadi, 2015). Rewiring glutamine metabolism further contributes to redox control (Gregory *et al.*, 2019) and activity of the mTOR complex 1 (mTORC1) (Willems *et al.*, 2013), a central hub for cell growth and nutrient signaling.

Metabolic reprogramming in AML occurs far beyond the examples given above and differs between AML sub-types as well as sub-clones. Certain metabolic alterations can be linked to AML driver mutations. FLT3-ITD-driven AMLs for example rely on glycolysis, which they promote through upregulation of the key glycolytic enzyme hexokinase 2 (Ju *et al.*, 2017). When treated with glycolysis-constraining FLT3 tyrosine kinase inhibitors (FLT3-TKI), FLT3-ITD mutated AMLs switch to glutaminolysis as the central carbon source (Gallipoli *et al.*, 2018). This confers resistance towards FLT3-TKIs, exemplifying how AML metabolic plasticity can abolish treatment sensitivity.

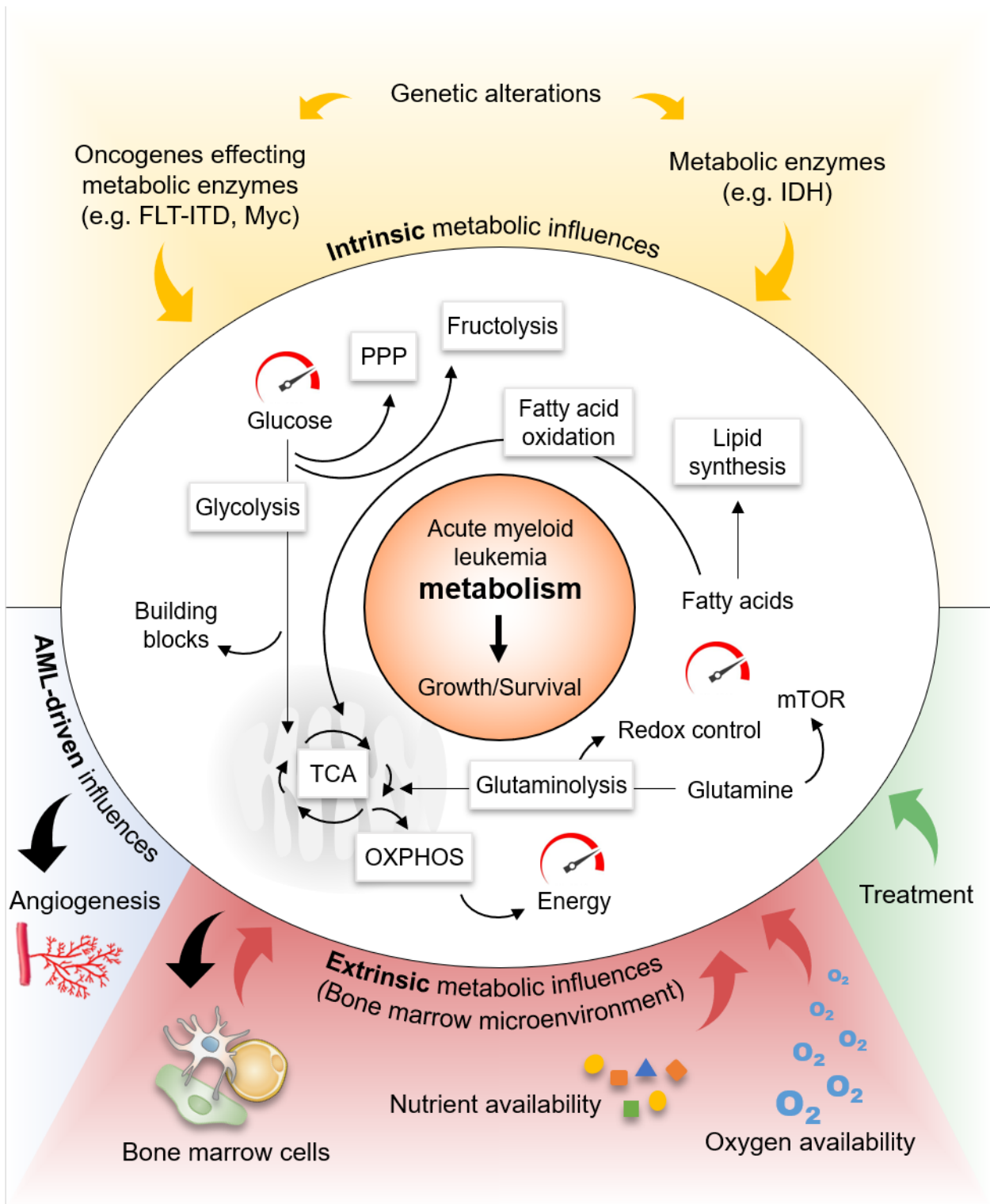


Figure 2. Intrinsic and extrinsic factors shape the diverse metabolism of AML

Both directly and indirectly, genetic alterations fundamentally change the metabolic pathways that drive AML growth and survival. AML metabolism is characterized by a high plasticity that allows the cancer cells to switch between different metabolic pathways and adapt to changes in the bone marrow microenvironment (e.g. nutrient and oxygen availability). Metabolic rewiring can also confer treatment resistance. To fulfill metabolic requirements, AML cells also actively change the microenvironment through the induction of angiogenesis or the manipulation of non-malignant cells.

PPP = pentose phosphate pathway; ITD = internal tandem duplication; IDH = isocitrate dehydrogenase; TCA = tricarboxylic acid cycle; mTOR = mammalian target of rapamycin

The flexible nature of AML metabolism is also key to surviving and thriving in the bone marrow microenvironment that also dictates tumor behavior (Forte *et al.*, 2019). AML cells respond metabolically to changes in oxygen and nutrient availability, oxidative stress and signals from surrounding cells. They do so in part by actively shaping the environment to their advantage, inducing vascularization (Han *et al.*, 2016) or insulin resistance in non-malignant cells in order to increase their share of glucose (Ye *et al.*, 2018) (Figure 2).

Exploiting the metabolic strategies of AML cells in the development of AML therapeutics is the aspired goal that has been pursued in the last decades. Multiple new drugs targeting AML metabolism have been developed and are currently tested in preclinical and clinical trials (reviewed in Castro *et al.*, 2019 and Chapuis *et al.*, 2019). Targets being therapeutically evaluated include glycolysis, amino acid and fatty acid metabolism, signaling pathways (e.g. mTORC1) and metabolic enzymes such as isocitrate dehydrogenases (IDHs). IDHs are involved in multiple metabolic and epigenetic cellular processes (Yang *et al.*, 2012). Mutations in IDHs which are present in approximately 20% of patients were first identified to cause a loss of the normal function in catalyzing isocitrate into α KG. Further studies revealed that IDH mutations not only abolish normal catalytic activity, but also induce a gain of function leading to the production of oncogenic R-2-hydroxy-glutarate, ultimately inducing differentiation arrest in hematopoietic stem cells (Medeiros *et al.*, 2017). Mutated IDH represents an appealing target as it is a metabolic addiction specific to AML cells. Further, its inhibition induces differentiation of the leukemic cells and offers a promising treatment option for relapsed and refractory AML. Numerous therapeutic agents against IDH mutations are evaluated (pre-)clinically at present (Liu and Gong, 2019). Most promising are enasidenib (AG-221) (Reed *et al.*, 2019) and ivosidenib (AG-120) (Roboz *et al.*, 2020) which have been approved for the treatment of relapsed and refractory AML and in the case of ivosidenib also for the treatment of newly-diagnosed IDH1 mutated AML patients above the age of 75 years.

After decades of no new antileukemic drugs, the novel agent venetoclax in combination with a hypomethylating agent is now considered to be a new standard of care for AML patients above 75 years of age or intolerant to intensive induction therapy (Jonas and Pollyea, 2019; Pollyea *et al.*, 2019). The success of venetoclax is in part linked to its indirect inhibitory effects on metabolic dependencies in AML. Venetoclax selectively inhibits B-cell lymphoma 2 (BCL-2), an anti-apoptotic protein commonly overexpressed in hematological malignancies including chronic lymphocytic leukemias (CLL) (Schena *et al.*, 1992; Hanada *et al.*, 1993), acute lymphoblastic leukemia (ALL) (Gala *et al.*, 1994) and AML (Zhou *et al.*, 2019). The agent further reduces mitochondrial respiration and TCA cycle activity, an effect independent of BCL-

2 inhibition and currently under investigation (Lagadinou *et al.*, 2013; Pollyea *et al.*, 2018; Roca-Portoles *et al.*, 2020).

To further exploit metabolic dependencies in targeted therapy, scientists and clinicians need to continuously unravel the complexity of AML metabolism. It requires taking into consideration the extracellular microenvironment that significantly influences the metabolic processes (Jiang and Nakada, 2016; van Gastel *et al.*, 2019; Tabe *et al.*, 2020). A major niche factor that governs metabolic rewiring in the cell is oxygen abundance. Oxygen is needed to provide the energy released during mitochondrial respiration and is vital for cellular metabolism. The bone marrow niche where AML cells reside is in a chronic state of low oxygen supply, often addressed as physiological hypoxia (< 6% O₂) (Joel A Spencer *et al.*, 2014). Hypoxia has been shown to impact AML proliferation, differentiation and resistance to chemotherapy (Irigoyen *et al.*, 2017). Its influence on AML metabolism however, has not been well explored.

1.3 Hypoxia and its implications in AML metabolism and survival

In medicine, “hypoxia” defines a condition of inadequate oxygen supply. In regard to malignancies, the term has been adapted to describe regions within the tumor or its microenvironment with low oxygen concentrations (Bertout *et al.*, 2008; Ast and Mootha, 2019). It generally refers to concentrations far below that of arterial blood (10% – 13% O₂; 75 - 100 mmHg), typically ranging from 2% to 0.1% O₂ (15 - 0.75 mmHg). In contrast to hypoxia, the term “normoxia” commonly refers to atmospheric oxygen conditions (21% O₂; 160 mmHg). Hypoxia has emerged as an important player in solid malignancies, where it contributes to treatment resistance, metastatic propagation, metabolic alterations, immune response modulations and consequently, increased mortality (Parks *et al.*, 2017).

Hypoxia inducible factor (HIF) proteins are the master regulators in mediating cellular adaptations to physiologically and pathologically encountered hypoxia (reviewed in Majmundar *et al.*, 2010). In response to low oxygen concentrations, HIFs drive the transcriptional initiation of genes involved in cellular metabolism (particularly glucose metabolism), angiogenesis, apoptosis, differentiation and proliferation. HIFs are also main drivers of stem cell maintenance and sustain quiescence of hematopoietic stem cells (Simsek *et al.*, 2010; Takubo *et al.*, 2010). HIF α isoforms HIF α 1 and HIF α 2 have both common and distinct targets. While HIF α 1 is thought to be the main isoform participating in early responses to acute hypoxia, HIF α 2 has been recognized as key regulator of chronic hypoxia (Koh and Powis, 2012). Due to abnormal or insufficient tumor vascularization, solid tumors frequently exhibit high levels of HIF α expression, which is considered a marker of poor prognosis (Bertout, Patel and Simon, 2008). In solid malignancies hypoxia-driven HIF signaling was shown to support cancer development by promoting extracellular matrix remodeling, cell migration and invasion.

In hematopoietic malignancies, the role of hypoxia has long been neglected as they develop in an environment naturally low of oxygen. The bone marrow is among the least oxygenated environments of the body, harboring an oxygen gradient from 6% to nearly anoxic concentrations of 0.1% (Spencer *et al.*, 2014; Figure 3). Defining the role of hypoxia and HIF in AML has proven challenging. HIF-induced responses have shown to impact AML proliferation, differentiation and chemoresistance (reviewed in Deynoux *et al.*, 2016). The role of HIFs in AML development and maintenance remains however controversial, as HIFs were found to act as both oncogenes and tumor suppressor genes. This is also reflected in studies evaluating the therapeutic implications of HIFs. Many studies affirmed beneficial effects through HIF targeting (Wang *et al.*, 2011; Kawada *et al.*, 2013; Coltella *et al.*, 2015; Abdul-Aziz *et al.*, 2018); some, however, showed contradictory results and call into question the notion

that inhibition of the HIF pathway benefits leukemia treatment (Velasco-Hernandez *et al.*, 2014; Velasco-Hernandez *et al.*, 2019).

In part, these discrepancies may be due to considerable differences in hypoxia intensity and duration in studies remodeling the hypoxic bone marrow microenvironment *in vitro*. As HIF activities are regulated in a time-dependent manner, their responses differ between acute and chronic hypoxia (Koh and Powis, 2012). In order to define the duration of acute hypoxia and the beginning of chronic hypoxia, Fuhrmann *et al.* (2013) observed HIF-induced responses to hypoxia (1% O₂) over 96 hours. Using the AML cell line THP1 as the cell model, the group showed that after 72 hours the protein expression of both HIF isoforms and mRNA of classical HIF target genes returned towards basal levels. Hence, incubation of 72 hours was chosen to study chronic hypoxia. Chronic hypoxia was found to reduce mitochondrial mass independent of HIF. Further research pointed towards increased glutaminolysis for α KG production and a shift towards fatty acid synthesis and utilization in chronic hypoxia (Fuhrmann *et al.*, 2019). In contrast, cellular respiration in acute hypoxia was predominantly pyruvate-centered.

In summary, hypoxia is an important factor of the bone marrow microenvironment and may be a major determinant of AML metabolism. Thus, mirroring the oxygen conditions of the bone marrow *in vitro* has the potential to provide a better understanding of niche-specific AML metabolism and to identify novel metabolic vulnerabilities. The distinct metabolic modifications observed in acute hypoxia and chronic hypoxia, however, emphasize the importance of allowing sufficient time for cellular adaptation to chronic hypoxia prior to examining AML metabolism. We hypothesize that responses to chronic hypoxia on the proteomic and metabolic level require more than 72 hours, which Fuhrmann *et al.* (2013) defined as the beginning of chronic hypoxia on mRNA level. Therefore, the present study aimed at characterizing the influence of hypoxia over extended periods of time (> 7 days; Figure 3).

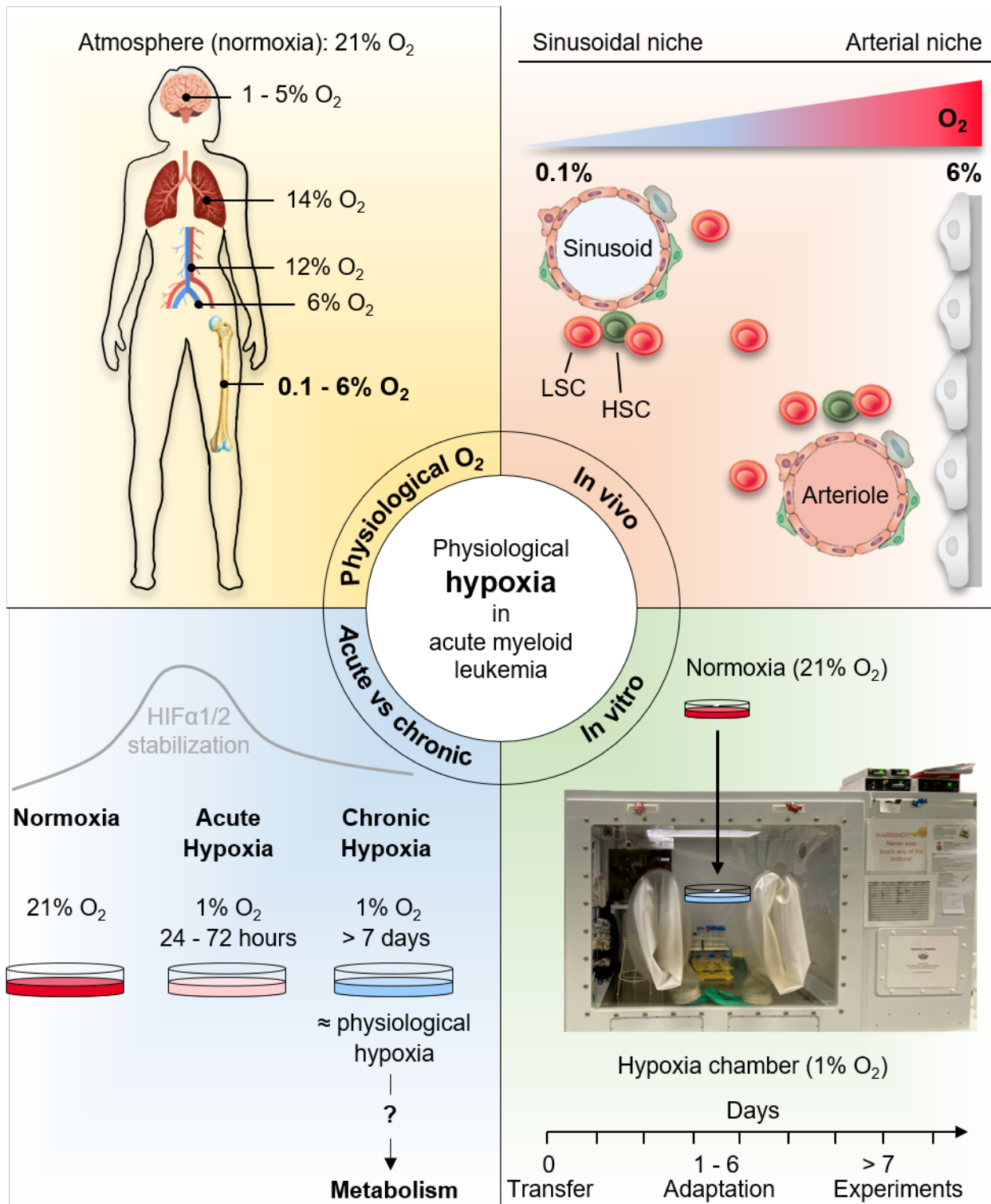


Figure 3. Studying the metabolic impact of physiological hypoxia on AML

Physiological O_2 : Cellular availability of oxygen significantly changes between different parts of the body and is among the lowest in bone marrow where AML cells reside. **In vivo:** The bone marrow niche harbors an oxygen gradient from ~ 6% O_2 in the arterial zone to nearly anoxic 0.1% O_2 in sinusoidal areas. **In vitro:** In order to mirror the hypoxic niche of the bone marrow *in vitro* the current study employed a hypoxia chamber that was downregulated to 1% O_2 , resembling the lower end of the bone marrow oxygen gradient. Prior to experiments, cells were adapted to the low oxygen environment. **Acute vs chronic:** HIF α 1/2 stabilization experiments previously defined the duration of acute and the beginning of chronic hypoxia. In the current study we analyzed AML metabolism in chronic hypoxia (1% O_2 , adapted > 7 days). HSC = hematopoietic stem cells; LSC = leukemic stem cells; HIF = hypoxia inducible factor

1.4 Novel metabolic targets identified and investigated in the current work

1.4.1 Glutamine synthetase

While the previous sections presented the general aspects of AML metabolism and the role of hypoxia as a metabolic regulator, this section will address metabolic mechanisms investigated in the current work with a special focus on amino acid metabolism.

Amino acids are important metabolites that fuel multiple biosynthetic pathways and are required to fulfil the energetic and anabolic needs of both healthy and malignant cells including AML (Tabe *et al.*, 2019). An important enzyme in amino acid metabolism is GS.

GS, encoded by the gene *GLUL*, catalyzes the conversion of glutamate and ammonium to glutamine (Eisenberg *et al.*, 2000). It is the only enzyme capable of *de novo* glutamine synthesis and a key enzyme in glutamine metabolism. In this reaction, ATP and glutamate bind to the active sites of GS. Glutamate is phosphorylated and induces a conformational change. This allows the binding of ammonium and its transfer to glutamate to yield glutamine. Another biochemical function of GS is the clearance of ammonium ions which makes it essential also in the detoxification of ammonium (Nelson *et al.*, 2009).

The functional role of GS is often tissue specific (Castegna and Menga, 2018). In muscle, the main tissue of glutamine storage and release, GS plays an important role in glutamine production (He *et al.*, 2010). Glutamine is among the most important amino acids and serves as an essential carbon and nitrogen source in many biosynthetic processes (Yoo *et al.*, 2020). In AML, Glutamine has long been recognized as a key metabolite where it serves as an anaplerotic substrate for the TCA cycle (Jacque *et al.*, 2015) and is utilized in the activation of mTOR signaling (Willems *et al.*, 2013) and in redox control (Gregory *et al.*, 2018) (Figure 4).

Next to endogenous synthesis through GS, glutamine can be acquired from exogenous sources. Through the membrane transporters SLC1A5 and SLC7A5/SLC3A2, glutamine can be obtained from the plasma where it is the most abundant amino acid (Pochini *et al.*, 2014). It can further be derived from protein catabolism (Cruzat *et al.*, 2018). In AML, only the contribution of plasma glutamine to AML metabolism has been investigated. Multiple studies showed an increased uptake of circulating glutamine by AML cells (indicated by reduced glutamine concentrations in the plasma of AML patients (Rudman *et al.*, 1971; Wang *et al.*, 2013)) and an exquisite dependence on the glutamine transporter SLC1A5 (Willems *et al.*, 2013; Ni *et al.*, 2019).

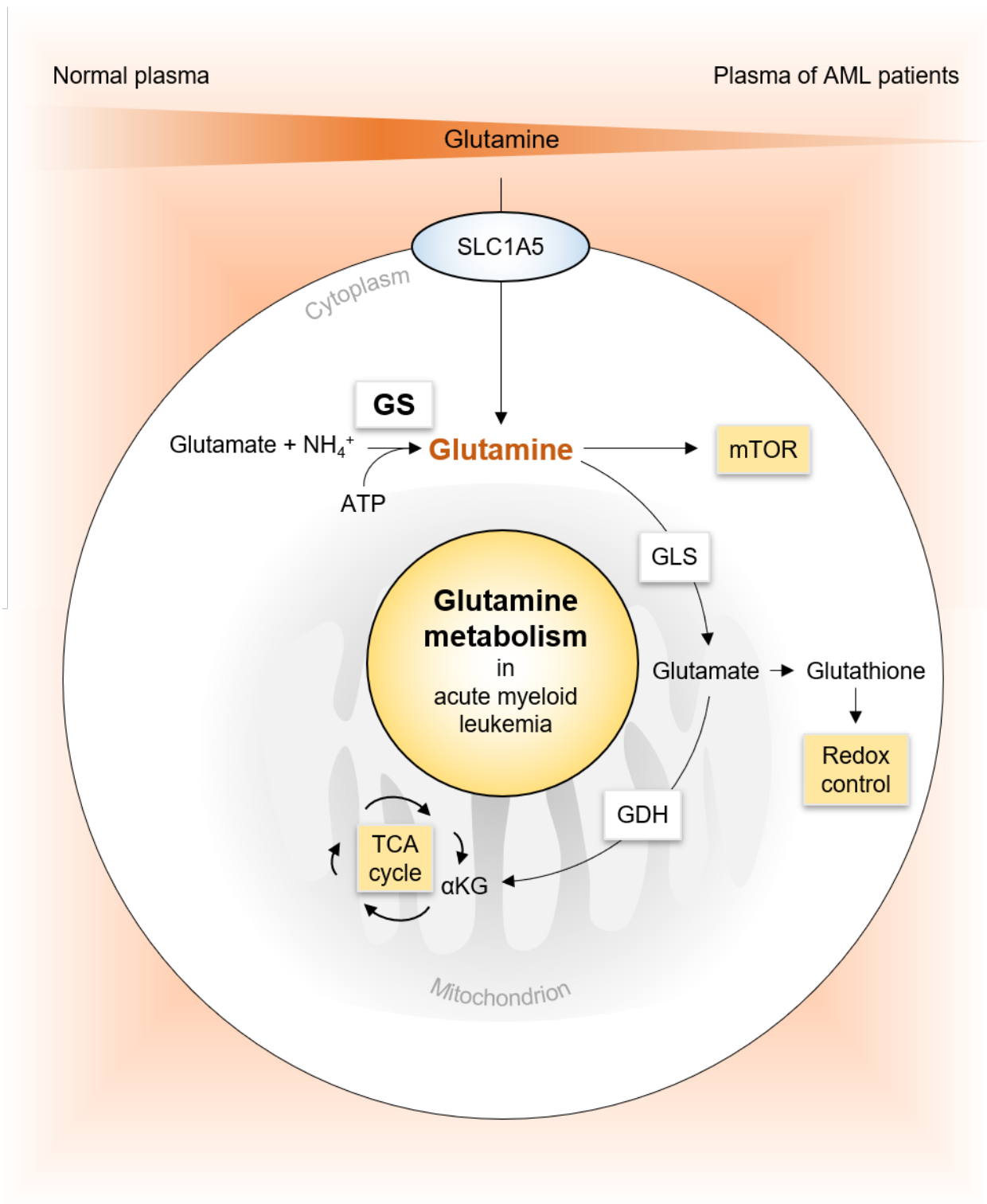


Figure 4. Glutamine metabolism in AML

AML cells depend on the transporter SLC1A5 for glutamine uptake and import high amounts of extracellular glutamine shown by decreased glutamine concentrations in the plasma of AML patients. Endogenously, glutamine can be produced *de novo* through GS-driven conjugation of glutamate and ammonium. AML cells utilize glutamine for different metabolic processes including mTOR activation, redox control (through the conversion to glutathione) and TCA anaplerosis (through the conversion to αKG).

NH₄⁺ = ammonium; GS = glutamine synthetase; GLS = glutaminase; GDH = glutamate dehydrogenase; TCA = tricarboxylic acid; mTOR = mammalian target of rapamycin; αKG = α-ketoglutarate

The other function of GS in detoxifying ammonium is mostly prominent in the brain and the liver, where GS is present ubiquitously. The liver acts as the main ammonium-detoxifying organ and metabolizes ammonium in the periportal region to urea in the urea cycle (Hakvoort *et al.*, 2017). GS in the pericentral region is essential to remove residual ammonium from the hepatic circulation and has a much higher affinity for ammonium than the gate keeper enzyme of the urea cycle (carbamoyl phosphate synthetase 1 (CPS1)). Deletion of GS in mouse liver has shown to cause severe hyperammonemia highlighting the importance of GS in liver-mediated ammonium detoxification (Qvartskhava *et al.*, 2015).

In brain physiology, GS is also crucial for the removal of ammonium which freely crosses the blood-brain barrier (reviewed in Castegna and Menga, 2018). It is mainly expressed by astrocytes which are located in close proximity to the blood-brain barrier. GS further attenuates neurotoxicity by scavenging the neurotransmitter glutamate which is released by neurons and recycled by astrocytes through GS. The pivotal role of GS as ammonium detoxifier in the brain was shown by increased ammonium concentrations upon GS inhibition through L-methionine sulfoxamine (MSO) in rats (Cooper *et al.*, 1979).

GS was further shown to be essential for early mouse embryogenesis where it was hypothesized to be crucial for ammonium detoxification during amino acid catabolism that serves embryonic energy production (He *et al.*, 2007).

The importance of GS in human embryogenesis is underlined by the observation that congenital GS deficiency is extremely rare. Only four cases of congenital GS deficiency have been reported to date and caused decreased glutamine levels and hyperammonemia with severe consequences (epileptic encephalopathy, organ failure) (reviewed in Spodenkiewicz *et al.*, 2016; Ünal *et al.*, 2018).

In summary, GS is an essential metabolic enzyme that serves both glutamine production and ammonium detoxification.

1.4.2 Macropinocytosis and protein metabolism

To fulfill the metabolic requirements for amino acids, amino acids can also be derived from extracellular proteins, which account for the biggest component of extracellular fluid (approximately 70% of the soluble substances) (Stehle *et al.*, 1997). This has been shown to play a role especially in cancer cells where protein-derived amino acids supply central carbon metabolic pathways (reviewed in Recouvreux and Commisso, 2017).

Unlike free amino acids, proteins are large molecules that can only be taken up through endocytic mechanisms. In cancer cells, the driving mechanism for protein uptake has been shown to be macropinocytosis. Macropinocytosis is an evolutionarily conserved mechanism that mediates non-specific endocytosis of extracellular fluids (King and Kay, 2019). It is activated by members of the RAS superfamily of small guanosine triphosphatases (GTPases; RAS, RAC, CDC42, ARF6, and RAB5) and membrane phospholipids (particularly phosphatidylinositols) and occurs through actin-driven cell surface ruffles that result in the formation and internalization of macropinosomes (Egami *et al.*, 2014). Especially RAS-driven cancers were found to employ macropinocytosis for the internalization of proteins (reviewed in Recouvreux and Commisso, 2017). Commisso *et al.* (2013) was the first to report internalized proteins in RAS-driven pancreatic cancer cells to serve as supply route for amino acids. Newer studies have since followed confirming macropinocytosis-mediated nutrient uptake in other solid malignancies including prostate cancer (Kim *et al.*, 2018) and RAC-driven lung cancer (Hodakoski *et al.*, 2019a).

Whether macropinocytosis-driven protein uptake also contributes to the expansion of non-malignant mammalian cells is largely unknown. A recent report on T cells was the first to demonstrate that amino acids derived from extracellular proteins also support the growth of cells beyond cancer cells (Charpentier *et al.*, 2020). Here, macropinocytosis was shown to give access to protein-derived amino acids and to promote T cell growth by sustaining mTORC1 activity.

Other purposes of macropinocytosis in the hematopoietic system have long been known to comprise important immune cell function. Here, hematopoietic cells such as macrophages and immature dendritic cells employ this mechanism in order to scan their microenvironment for antigenic proteins (Canton, 2018).

As of hematological malignancies, including leukemias, lymphomas and multiple myeloma, there is some evidence that this endocytic process is active (Nishimura *et al.*, 2008; Watanabe *et al.*, 2011; Hou *et al.*, 2013; Zheng *et al.*, 2019). In fact, indirect evidence of the activity of macropinocytosis in hematological malignancies can be drawn from the observation of low

levels of albumin (the most dominant plasma protein (Stehle *et al.*, 1997)) observed in patients with AML (Komrokji *et al.*, 2009; Wang *et al.*, 2020), myelodysplastic syndromes (Komrokji *et al.*, 2012; Sevindik *et al.*, 2015) and chronic lymphocytic leukemia (Wung *et al.*, 2018) suggesting high cellular uptake of albumin. Nevertheless, this area remains poorly understood and further research is needed, especially on the specific metabolic functions of macropinocytosis and protein metabolism in AML.

Since this high turnover of protein and amino acid metabolism results in large amounts of ammonium ions, it would be further interesting to understand the mechanisms by which AML cells cope with the high ammonium levels and the role played by GS in this process.

1.5 Aim

The current thesis aimed at gaining a greater understanding of the metabolic dependencies in AML. Amino acid metabolism contributes greatly to fulfilling the energetic and anabolic needs of AML cells. Among the most essential amino acid is glutamine. Glutamine can be acquired endogenously through GS-mediated *de novo* synthesis or exogenously through the uptake of glutamine or proteins, which contribute to amino acid pools upon protein catabolism. While glutamine import has gained much attention, the contribution of GS or protein catabolism to intracellular glutamine pools has so far not been investigated. Therefore, we examined the dependency of AML cells on GS and analyzed its role in glutamine production. Since GS is a key enzyme in the removal of ammonium, we further evaluated its functional role in ammonium detoxification. To establish that GS metabolism is also relevant under physiological oxygen conditions (1% O₂), which have been shown to impact the metabolic needs of AML cells, we additionally examined GS-mediated processes under prolonged periods of hypoxia (1% O₂, > 7 days).

Next, we investigated the endocytic uptake and catabolism of extracellular proteins and evaluated its contribution to intracellular amino acid pools and amino acid metabolism. As endocytosis of proteins and their subsequent metabolism creates large amounts of ammonium ions, we investigated the functional role of GS in detoxifying this ammonium.

2 Materials and Methods

2.1 Materials

2.1.1 Hardware

Device	Manufacturer
Agilent 5975C MS	Agilent Technologies, USA
Agilent 7890A GC	Agilent Technologies, USA
Analytical balance	Sartorius, Germany
AV950 MHz Bruker spectrometer equipped with a 5 mm TCI cryoprobe	Bruker, USA
Bacteria shaker Roth KS 15A	Roth, Germany
BD FACSCelesta™	BD Biosciences, USA
BD LSRFortessa™	BD Biosciences, USA
CASY (automatic cell counter)	OMNI Life Science, Germany
COBAS Mira Plus Chemistry Analyzer	Horiba ABX, Japan
Concentrator Plus vacuum dryer	Eppendorf, Germany
Confocal microscope LSM710	Zeiss, Germany
Confocal microscope LSM800	Zeiss, Germany
Cytospin™ 4 Centrifuge	Thermo Fisher Scientific, USA
Hamilton syringe	Gilson, Germany
HP 5ms capillary column	Agilent Technologies, USA
Hypoxia chamber	BioSpherix Medical, USA
Incubator Heracell 150i	Thermo Fisher Scientific, USA
Incubator Heraeus B6030	Thermo Fisher Scientific, USA
Infinite 200 PRO multimode plate reader	TECAN, Switzerland
Laminar flow; Sterile bank Class II Nuaire	Zapf Instruments, Germany
Mastercycler ^R Pro	Eppendorf, Germany
Microcentrifuges 5424	Hettich, Germany
Microscope Zeiss ID03	Zeiss, Germany
NanoDrop 2000c	Thermo Fisher Scientific, USA
Neubauer counting chamber	Paul Marienfeld GmbH & Co. KG, Germany
Odyssey® Fc Imaging System	LI-COR, USA
PAGE Power supply - Power Pac 1000	Bio-Rad, USA
PAGE system - XCELL SureLock™	Invitrogen, USA
pH-meter - Hanna pH 210	Hanna instruments, USA
Photometer	Eppendorf, Germany
Pipettes	Gilson, USA
Rotanta 460	Hettich, Germany
Rotina 35	Hettich, Germany
SciVet abc animal blood cell counter	SciVet, Germany
SONOPULS mini20 Ultrasonic homogenizer	Bandelin, Germany
Table centrifuge - Himac CT15RE	Hitachi, Japan
Thermomixer comfort	Eppendorf, Germany
Vibra-Cell sonicator	Sonics & Materials Inc., USA
Vortexer VF-2 Janke&Kunkel	IKA, Germany

Water bath GFL1083	GFL, Germany
Wet Transfer blot module - XCELL II™ Blot Module	Invitrogen, USA

2.1.2 Consumables

Consumable	Manufacturer
1.5 - 2 ml tubes	Sarstedt, Germany
15 - 50 ml tubes	Sarstedt, Germany
Cell culture plates	Greiner bio-one, Austria
Corning Costar Stripette serological pipettes (5 - 50 ml)	Merck, Germany
Microfilter (0.22 µm, 0.45 µm)	Merck Millipore, Germany
Nylon cells strainer (40 µm)	Falcon, USA
PCR tubes	Greiner bio-one, Austria
Polystyrene cuvettes (10x4x45 mm)	Sarstedt, Germany
Polystyrene sample tubes (5 ml, 75x12 mm)	Sarstedt, Germany
Shigemi 3 mm NMR tubes	Cortecnet, France
Superfrost Plus microscope slides	Thermo Fisher Scientific, USA
Syringes	Braun, Germany
Tips	StarLab, Germany
Trans Blot Transfer Medium Pure Nitrocellulose Membrane	Biorad, USA

2.1.3 Software

Software/web service	Supplier or web address
ApE-A plasmid editor	by M. Wayne Davis (University of Utah)
BD FACSDiva™ Software	BD Biosciences, USA
Benchling (CRISPR predictor)	https://benchling.com/
Bioinformatics & evolutionary genomics	http://bioinformatics.psb.ugent.be/webtools/Venn/
BloodSpot database	http://servers.binf.ku.dk/bloodspot/
CCTop - CRISPR/Cas9	http://crispr.cos.uni-heidelberg.de/
Clustal Omega	http://www.ebi.ac.uk/Tools/msa/clustalo/
Ensembl	http://www.ensembl.org/index.html
GraphPad Prism 8	GraphPad software, USA
i-control software version 1.11.1.0	TECAN, Switzerland
Image Studio software	LI-CORE, USA
Mendeley	Elsevier, Netherlands
Microsoft Office	Microsoft, USA
Perseus version 1.5.6.0	https://maxquant.net/perseus/
R version 3.6.0	R Foundation for Statistical Computing, Austria
Reactome	https://reactome.org/
SnapGene® software	GSL Biotech, USA
SynergyFinder web application (version 2.0)	https://synergyfinder.fimm.fi/synergy/
TopSpin 3.5	Bruker, USA

2.1.4 Chemicals, reagents and enzymes

Compound	Manufacturer
10X ligase buffer	NEB, USA
2-Propanol	Sigma-Aldrich, USA
4X loading dye	Roth, Germany
5X Roti-Quant reagent	Roth, Germany
Acrylamide 40%	Amresco, USA
Adenosine diphosphate (ADP)	Sigma-Aldrich, USA
Agarose	Roth, Germany
Ammonium chloride	Sigma-Aldrich, USA
Ammonium- ¹⁵ N chloride	Sigma-Aldrich, USA
Ampicillin sodium salt	Roth, Germany
APS 10%	Roth, Germany
BamHI restriction enzyme	NEB, USA
Bovine Serum Albumin lyophilized powder, BioReagent, suitable for cell culture	Sigma-Aldrich, USA
BsmBI restriction enzyme	NEB, USA
cOmplete™ EDTA-free Protease Inhibitor Cocktail	Roche, Switzerland
cOmplete™, EDTA-free Protease Inhibitor Cocktail	Roche, Switzerland
DC™ Protein Assay Reagent A (Lowry reagent)	Bio-Rad, USA
DC™ Protein Assay Reagent B (Lowry reagent)	Bio-Rad, USA
Deuterium oxide (D ₂ O)	Deutero, Germany
Dextran, Alexa Fluor™ 555; 10,000 MW	Thermo Fisher Scientific, USA
Dextran Oregon Green™ 488; 70,000 MW	Thermo Fisher Scientific, USA
Digitonin	Merck, Germany
Dimethylsulfoxide (DMSO)	Sigma-Aldrich, USA
Dithiothreitol (DTT)	AppliChem, Germany
DMEM	Thermo Fisher Scientific, USA
DQ™ Red BSA	Invitrogen, USA
Dulbecco's Phosphate Buffered Saline (PBS)	Sigma-Aldrich, USA
Ethanol	Sigma-Aldrich, USA
Ethylenediaminetetraacetic acid (EDTA)	Roth, Germany
Ethyl-isopropyl amiloride (EIPA)	Tocris Bioscience, GB
Fetal calf serum (FCS)	Sigma-Aldrich, USA
Fluoroshield	Sigma-Aldrich, USA
Glutamate dehydrogenase (GDH)	Roche, Switzerland
Glutaminase	Sigma-Aldrich, USA
Glycine	PanReac, Spain
Hanks balanced salt solution	Sigma-Aldrich, USA
HEPES	Roth, Germany
HPLC-grade chloroform	Roth, Germany
HPLC-grade methanol	VWR Chemicals Intern., USA
human FLT3-ligand (hFLT3L)	Peprotech, USA
human interleukin 3 (hIL3)	Peprotech, USA
human stem cell factor (hSCF)	Peprotech, USA
human thrombopoietin (hTPO)	Peprotech, USA

HyClone fetal calf serum (FCS)	GE Healthcare, USA
Hydrazine	PanReac, Spain
Hydrochloric acid (HCl)	Roth, Germany
IMDM medium (#36150)	Stemcell, Canada
Invitrogen™ UltraPure Water	Invitrogen, USA
IPI549	MedChem Express, Germany
L-ARGININE:HCL (U-13C6, 99%; U-15N4, 99%)	Eurisotop, GB
LB broth mix for LB medium	Roth, Germany
LB-Agar	Roth, Germany
L-glutamine solution	Sigma-Aldrich, USA
L-Leucine, suitable for cell culture, 98.5-101.0%	Sigma-Aldrich, USA
L-Lysine:2HCL (13C6, 99%; 15N2, 99%)	Eurisotop, GB
L-Methionine sulfoxamine	Sigma-Aldrich, USA
Magnesium chloride (MgCl ₂)	Merck, Germany
MBQ-167	MedChem Express, Germany
Methanol	Merck, Germany
MethoCult H4100	Stemcell, Canada
MOPS SDS running buffer	Invitrogen, USA
NaOH	Roth, Germany
Natrium azide (NaN ₃)	Sigma-Aldrich, USA
Nicotinamide adenine dinucleotide (NAD ⁺)	Sigma-Aldrich, USA
Nitrocellulose membrane	Bio-Rad, USA
Novex NuPAGE 20X Transfer buffer	Thermo Fisher Scientific, USA
Nrul restriction enzyme	NEB, USA
Paraformaldehyde (PFA)	Merck, Germany
Penicillin/Streptomycin (100x)	Thermo Fisher Scientific, USA
Pierce Universal Nuclease	Thermo Fisher Scientific, USA
Polybrene	Fluka BioChemika, Switzerland
Polyethylenimine (PEI)	Sigma-Aldrich, USA
Ponceau S	AppliChem, Germany
Potease inhibitor cocktail	Merck, Germany
Precision Protein Standard	Biorad, USA
Puromycin	InvivoGen, USA
Radioimmunoprecipitation assay (RIPA) buffer	ChromoTek, Germany
Roti®-Histofix 4%	Roth, Germany
RPMI 1640 Medium (21875034)	Thermo Fisher Scientific, USA
RPMI 1640 Medium w/o L-Glutamine, Leucine (Powder)	USBiological, USA
RPMI 1640 Medium, without glucose (111879020)	Thermo Fisher Scientific, USA
RPMI 1640 medium without glutamine	Thermo Fisher Scientific, USA
SILAC RPMI (w/o L- Arg, L-Lys)	Thermo Fisher Scientific, USA
Sodium acetate	PanReac, Spain
Sodium chloride (NaCl)	Roth, Germany
Sodium dodecyl sulfate (SDS)	AppliChem, Germany
Sodium fluoride (NaF)	Sigma-Aldrich, USA
Sodium hydroxide (NaOH)	Roth, Germany
Sodium orthovanadate (NA ₃ VO ₄)	Sigma-Aldrich, USA

SuperSignal® West Femto Luminol/ Enhancer Solution	Thermo Fisher Scientific, USA
SuperSignal® West Femto Stable Peroxide Solution	Thermo Fisher Scientific, USA
SuperSignal® West Pico Luminol/ Enhancer Solution	Thermo Fisher Scientific, USA
SuperSignal® West Pico Stable Peroxide Solution	Thermo Fisher Scientific, USA
T4 DNA ligase	NEB, USA
TEMED	Roth, Germany
Trimethylsilylpropanoic acid (TMSP)	Merck, Germany
Tris-HCl	Roth, Germany
Triton X-100	Sigma-Aldrich, USA
Trypan blue	Thermo Fisher Scientific, USA
Trypsin (10x)	PAA Laboratories, Austria
Tween-20	Roth, Germany
UltraPure™ DNase/RNase-Free Distilled Water	Thermo Fisher Scientific, USA
X-Vivo 10	Lonza, Switzerland

2.1.5 Buffers

Buffer	Composition
4% (w/v) paraformaldehyde (PFA) solution	80 mM PIPES pH 6.8 2 mM MgCl ₂ 4% (w/v) PFA 5 mM EGTA pH 8.0 in ddH ₂ O
Bis-Tris Buffer	1.25 M Bis-Tris pH 6.5 in ddH ₂ O
Blocking buffer	5% (w/v) non-fat milk powder in TBS-T
Erythrocyte lysis buffer	155 mM NH ₄ Cl 10 mM KHCO ₃ 0.1 mM EDTA pH 8.0 in ddH ₂ O
NMR buffer	100 mM sodium phosphate (PO ₄) 10% (v/v) D ₂ O 0.5 mM TMSP (reference compound) pH 7
Radioimmunoprecipitation assay (RIPA) lysis buffer	150 mM sodium chloride 1.0% (v/v) Triton X-100 0.5% (w/v) sodium deoxycholate 0.1% (w/v) sodium dodecyl sulfate (SDS) 50 mM Tris-HCl pH 7.5
SDS lysis buffer	50 mM Tris-HCl pH 8, 100 mM NaCl 1 mM EDTA pH 8 0.5% (w/v) SDS
Transfer buffer	Novex NuPAGE 20X Transfer buffer prepared in H ₂ O 10% (v/v) methanol
Tris-buffered saline with Tween (TBS-T)	100 mM Tris-HCl pH 7.4 150 mM NaCl 0.05% (v/v) Tween-20

2.1.6 Antibodies and fluorescent stains

Primary antibodies for immunological detection

Antibody	Species	Clonality	Dilution	Brand
4EBP1 (Ser65)	Rabbit	Monoclonal	1:1000	Cell Signaling Technology, USA
CPS1	Rabbit	Polyclonal	1:1000	Cell Signaling Technology, USA
GS (ab178422)	Rabbit	Monoclonal	1:1000	Abcam, GB
Nucleolin (C23 (H-20): sc-13057)	Rabbit	Polyclonal	1:500	Santa Cruz Biotechnology, USA
p-4EBP1 (Ser65)	Rabbit	Monoclonal	1:1000	Cell Signaling Technology, USA
p70S6K (T389)	Rabbit	Monoclonal	1:1000	Cell Signaling Technology, USA
p-p70S6K (T389)	Rabbit	Monoclonal	1:1000	Cell Signaling Technology, USA
Vinculin	Mouse	Monoclonal	1:1000	Sigma-Aldrich, USA

Secondary antibodies for immunological detection

Antibody	Species	Dilution	Brand
Anti-mouse HRP	Goat	1:10000	LI-COR Biosciences, Germany
Anti-rabbit HRP	Goat	1:10000	LI-COR Biosciences, Germany

Antibodies for fluorescence-activated cell sorting (FACS)

Antibody	Fluorophore	Target species	Dilution	Brand
APC Mouse Anti-Human CD33	APC	Human	1:200	BD Pharmingen, USA
PE Mouse Anti-Human CD45	PE	Human	1:200	BD Pharmingen, USA
PE Mouse Anti-Human IgG	FITC	Human	1:200	BD Pharmingen, USA
CD33 (P67.6)	PE Cy 7	Human	1:200	BD Pharmingen, USA
CD34 (8G12)	PerCP CY 5.5	Human	1:200	BD Pharmingen, USA
CD38 (HB-7)	APC	Human	1:200	BD Pharmingen, USA
CD45 (clone 2D1)	V500-C	Human	1:200	BD Pharmingen, USA

Fluorescent stains for fluorescent microscopy

Antibody	Species	Dilution	Brand
Alexa Fluor 488 goat anti-rabbit	Goat	1:300	Invitrogen, USA
DAPI (2-(4-Amidinophenyl)-6-indolcarbamide-dihydrochloride)	N/A	1:1000	Sigma-Aldrich, USA
GS (ab178422)	Rabbit	1:100	Abcam, GB
Lamp1 rabbit polyclonal antibody	Rabbit	1:50	Proteintech, USA

2.1.7 Commercially available kits

Kit	Manufacturer
Ammonia Assay Kit - Modified Berthelot - (Colorimetric) (ab102509)	Abcam, England
CellTiter-Glo® 2.0 Cell Viability Assay	Promega, USA

CellTox™ Green Cytotoxicity Assay	Promega, USA
Nucleobond PC500 Maxi Kit	Macherey-Nagel, Germany
NucleoSpin DNA	MACHEREY-NAGEL, Germany

2.1.8 Oligonucleotides and vector maps

Plasmids

Plasmid	Source
pLentiCRISPRv2	Addgene, USA
pMD2.G	Addgene, USA
psPAX2	Addgene, USA
SIHW	Addgene, USA

CRISPR guides

Name	Sequence
CPS1 knockout antisense	AAACcattggctctggactgatgcC
CPS1 knockout sense	CACCGgcatcagtcagaccaatg
GS guide 2 antisense	AAACgcttgatgcctttatttaaC
GS guide 2 sense	CACCGttaaataaaggcatcaagc
GS guide 2b antisense	AAACgggtccgggtcttgcagcgC
GS guide 2b sense	CACCGcgctgcaagacccggaccc
GS guide 3 antisense	AAACgagtggaatttcgatggctC
GS guide 3 sense	CACCGagccatcgaaattccactc
GS guide 3b antisense	AAACtgtttcgggaccccttccgC
GS guide 3b sense	CACCGcggaaggggtcccgaaca
GS guide GPP antisense	AAACcacactggggtcactgtC
GS guide GPP sense	CACCGgacagtgagcccaagtgt
GS guide P4 antisense	AAACtccaccatgaccacctcagC
GS guide P4 sense	CACCGctgaggtggatcatggtgga
Non-target control sense	CACCGttccgggctaacaagtct
Non-target control antisense	AAACaggactgttagcccggaaC

Primers

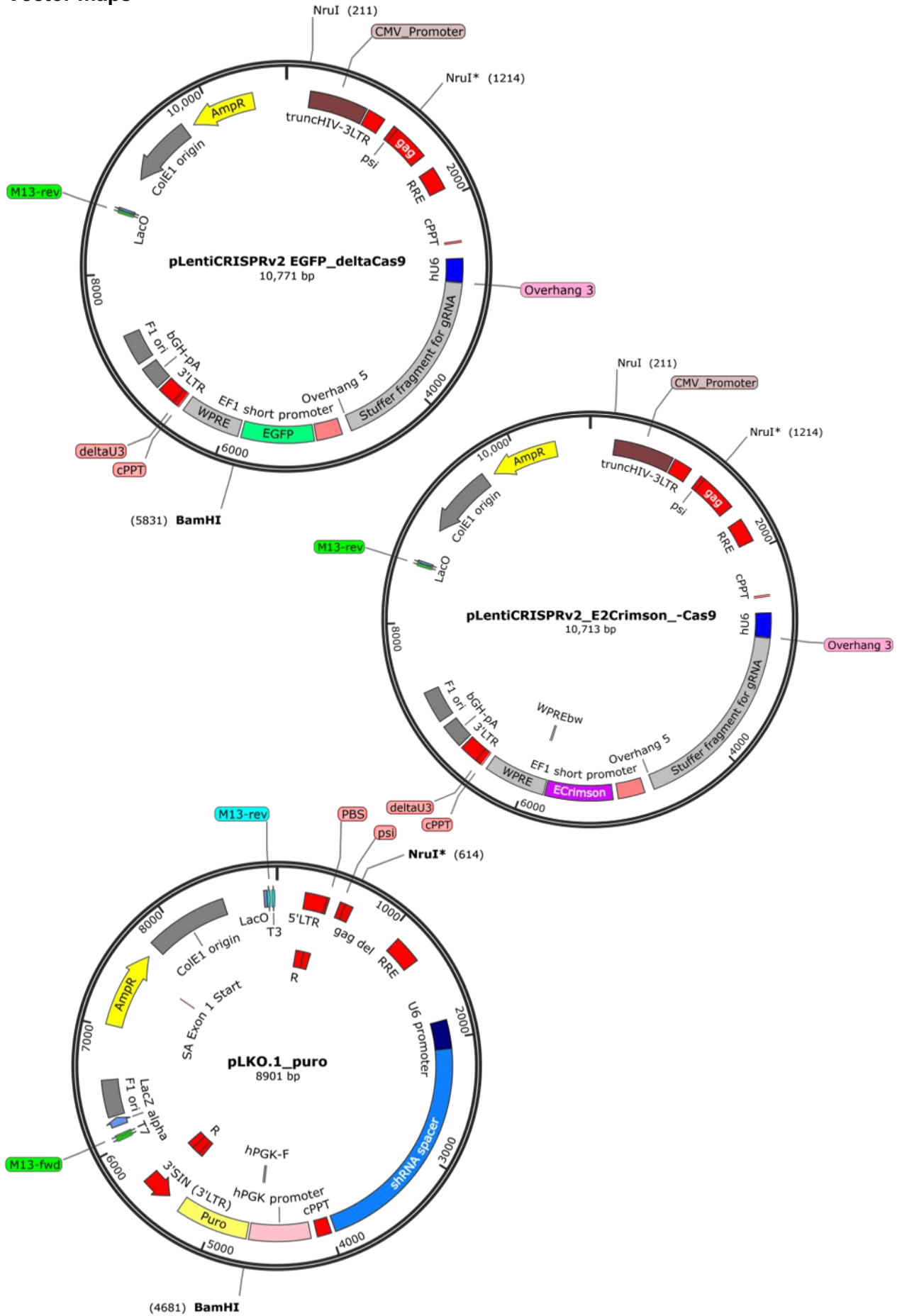
Primer	Sequence
hCPS1 antisense	AGGAACTGCCAGGTTGTTTG
hCPS1 sense	AGCAGACACCATTGGCTACC

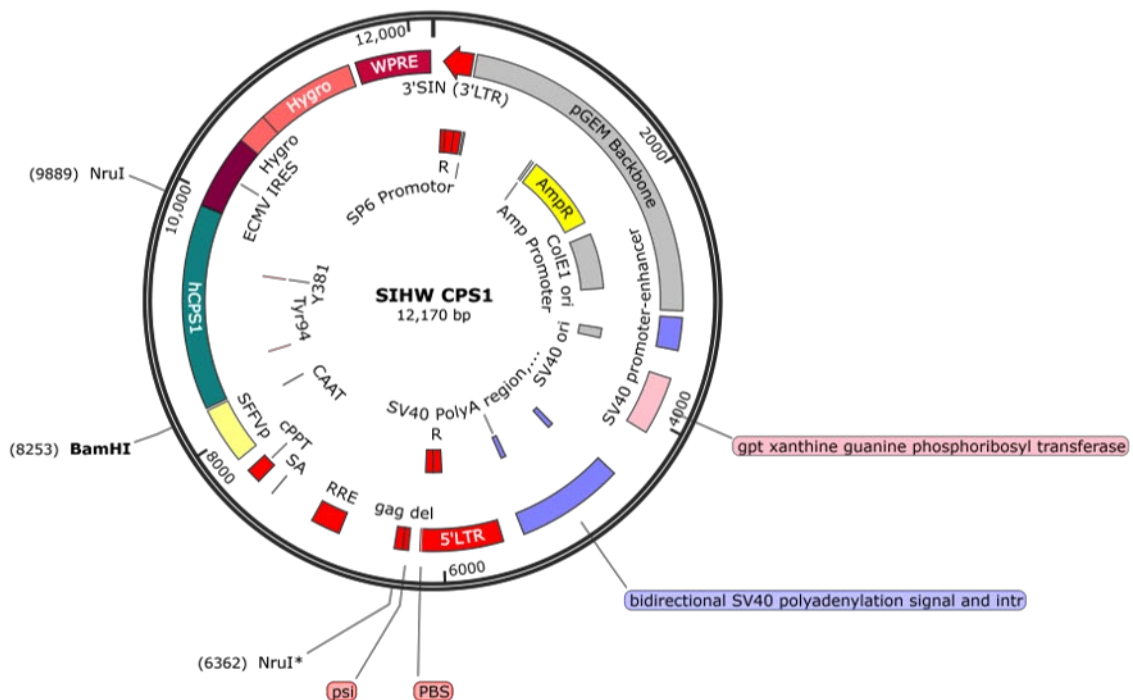
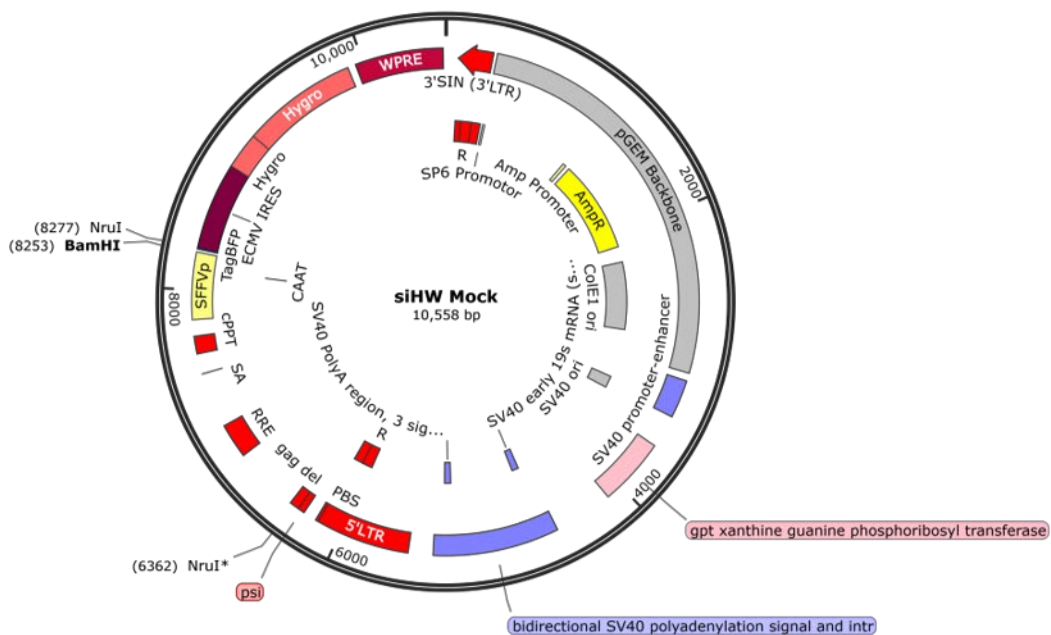
shRNA

Application	shRNA	Sequence	Target sequence	Source
GS knockdown 1	TRCN0 000343 990	5'-CCGG- AGGAGAAGAAGGGT TACTTTG-CTCGAG- CAAAGTAACCCTTCT TCTCCT-TTTTTG-3'	AGGAGAAGAAGG GTTACTTTG	Sigma-Aldrich, USA

GS	TRCN0	5'-CCGG-	TTCGATGGCTCTA	Sigma-Aldrich,
knockdown 2	000343	TTCGATGGCTCTAGT	GTACTTTA	USA
	991	ACTTTA-CTCGAG-		
		TAAAGTACTAGAGCC		
		ATCGAA-TTTTTG-3'		

Vector maps





2.1.9 Cell lines, primary AMLs, patient data and bacterial strain

Cell lines

Cell line	Cytogenetics	Culture medium	Source
HEK293T	(immortalized cell line)	DMEM, 10% (v/v) FCS, 100 U/ml penicillin, 100 µg/ml streptomycin	DSMZ, Germany
HEL	JAK2 V617F, P53 M133K	RPMI 1640, 10% (v/v) FCS, 100 U/ml penicillin, 100 µg/ml streptomycin	DSMZ, Germany
KG1	NRAS p.Gly12Asp, FGFR1OP2-FGFR1, TP53 c.672+1G>A	RPMI 1640, 10% (v/v) FCS, 100 U/ml penicillin, 100 µg/ml streptomycin	DSMZ, Germany
Molm13	FLT3-ITD, MLL-AF9 (KMT2A-MLLT3)	RPMI 1640, 10% (v/v) FCS, 100 U/ml penicillin, 100 µg/ml streptomycin	DSMZ, Germany
MV411	FLT3-ITD, MLL-AF4 (KMT2A-AFF1)	RPMI 1640, 10% (v/v) FCS, 100 U/ml penicillin, 100 µg/ml streptomycin	DSMZ, Germany
THP1	NRAS G12D, TP53 R174Fs, MLL-AF9 (KMT2A-MLLT3)	RPMI 1640, 10% (v/v) FCS, 100 U/ml penicillin, 100 µg/ml streptomycin	DSMZ, Germany

Primary AMLs

Primary AML	Genetic abnormalities	Culture medium
AML 1	CEBPA mutated	X-Vivo 10, 10% (v/v)
AML 2	FLT3-ITD, NPM1 mutated	HyClone FCS, 25 ng/ml
AML 3	FLT3-ITD, NPM1 mutated	hTPO, 50 ng/ml hSCF, 20 ng/ml hFLT3L, 20 ng/ml
AML 4	FLT3-ITD, NPM1, DNMT3A, TET2 mutated	hIL3, 100 U/ml penicillin, 100 µg/ml streptomycin
AML 5	FLT3-ITD, NPM1 mutated	
AML 6	Not known	

Patient data (for ammonium and glucose measurements in bone marrow and serum)

Category	Pa-tient	Age at diag-nosis	BM blast count (%)	Cytogenetics	Molecular genetics
<i>De novo</i> AML patients	1	73	20	Complex aberrant	DNMT3A, GATA2, IDH1, TP53
	2	83	55	45,XX -7 [20]	FLT3-ITD (Ratio 0.7), DNMT3A
	3	64	21	Complex aberrant	negative
	4	48	31	46,XX	FLT3-ITD (Ratio 0.36) NPM1, IDH1, IDH2
	5	45	20	Complex aberrant	KMT2A-PTD
	6	56	43	46,XX	NPM-1; DNMT3A
	7	70	60	46,XX del(5)[9]; 46,XX [14]	KMT2A_PTD, IDH1
	8	52	87	46,XX	FLT3-ITD (Ratio 0.72); KMT2A-PTD

	9	67	68	45,XX,der(2;6)(2pter->2q14::6p25->6q21::2q14->2q32::6q21->6qter) [4]; 46,XX [17]	CEBPA; SRSF2; U2AF1; CBFβ-MYH11 Fusion
	10	63	35		NPM1, FLT3-TKD; CEBPA
	11	75	51		NPM1, FLT3-TKD; CEBPA
AML patients in complete remission	12	76	2	46,XX	NPM1-B, FLT3-ITD (Ratio: 0.639)
	13	26	2	46,XY+8 [2]; 46,XY [20]	negative
	14	63	2	46,XX	FLT3-ITD (Ratio 0.327), NPM1, IDH2
	15	64	2	n.A.	KMT2A-PTD
	16	46	1	46,XX	NPM1, FLT3-ITD (Ratio 2.11)
	17	47	3	Not available	KMT2A(MLL)-PTD; CEPBA
	18	64	2	Complex aberrant	IDH1/2
	19	55	2	t(15/17), del(7)	PML-RARA pos., FLT3-ITD pos.
	20	21	2	Complex aberrant	negative
	21	70	4	47,XX,+8	negative
	22	29	3	Not available	negative
	23	64	2	47, XY, +21(4)/47, XY,+13(2)/46, XY (14)	BCOR, RUNX1, SRSF2
	24	65	2	46, XY	negative; recurrent: ASXL1-mutation
	25	33	1	Not available	FLT3-ITD; NPM1 A, IDH 2
	26	71	3	46,XY,t(8;21)(q22;q22)[8]9 2<4n>,XXYY,t(8;21)(q22;q22)x2[6]; 46,XY[8]	IDH2 (Ex4) VAF 39%
Relapsed AML patients	27	68	4	46,XX [20]	FLT3-ITD positive (Ratio: 0.9); NPM1
	28		7	46,XX [20]	FLT3-ITD positive (Ratio: 0.9); NPM1
	29	70	26	46,XX [11]	negative
	30	73	16	46,XX,t(3;8)(q26;q24)[20]	negative
	31		40	Complex aberrant	negative
	32	68	10	46,XX	NPM-1; DNMT3A

Bacterial strain

Name	Genotype	Source
<i>E. coli</i> (DH5α)	F- φ80lacZΔM15 Δ(lacZYA-argF)U169 recA1 endA1 hsdR17(rK-,mK+) phoA supE44 thi-1 gyrA96 relA1	Thermo Fisher Scientific, USA

2.2 Methods

2.2.1 Cell culture

2.2.1.1 Cell culture in normoxia

Cell lines were obtained from the DSMZ (Deutsche Sammlung von Mikroorganismen und Zellkulturen GmbH) and cultivated at 37°C in a humidified 5% (v/v) CO₂ incubator. Human AML cell lines (HEL, KG1, MOLM13, MV411, THP1) were cultured in RPMI 1640 medium containing 300 mg/l glutamine (unless otherwise described) (Thermo Fisher Scientific, USA) and supplemented with 10% (v/v) FCS (Sigma-Aldrich, USA), 100 U/ml penicillin and 100 µg/ml streptomycin (Thermo Fisher Scientific, USA). Cells were passaged 3 times a week. HEK 293T cells were cultured in DMEM (Thermo Fisher Scientific, USA) supplemented with 10% (v/v) FCS, 100 U/ml penicillin and 100 µg/ml streptomycin and passaged 2 to 3 times a week.

In order to obtain human primary AML cells, bone marrow mononuclear cells were purified by Ficoll-Paque™ Premium gradient centrifugation according to the manufacturer's instructions (GE Healthcare, USA). After purification, the cells were immediately stored in liquid nitrogen. The patients approved the sample collection and gave their consent according to the Declaration of Helsinki. The Ethics Committee of Frankfurt University Hospital also gave approval for the use of bone marrow aspirates (approval no. SHN-11-2016/SHN-09-2019). For experimental use primary AML cells were defrosted and cultured in X-vivo 10 medium (Lonza, Switzerland) supplemented with 10% (v/v) HyClone FCS (GE Healthcare, USA), 25 ng/ml hTPO (Peprotech, USA), 50 ng/ml hSCF (Peprotech, USA), 20 ng/ml hFLT3L (Peprotech, USA), 20 ng/ml hIL3 (Peprotech, USA), 100 U/ml penicillin and 100 µg/ml streptomycin. Cells were passaged 3 to 4 times a week.

Genetic abnormalities of AML cell lines and primary AMLs are described in section 2.1.9.

2.2.1.2 Cell culture in hypoxia

For the cultivation of cells in hypoxia, cells were transferred to a hypoxia chamber (BioSpherix Medical, USA) with 1% O₂ and 5% CO₂ levels. Cells were cultured as outlined above (section 2.2.1.1, unless otherwise described) with the exception that media was depleted of dissolved O₂ before use. O₂ depletion was achieved by equilibrating the media in the hypoxia chamber overnight (unless otherwise described). (To ensure that temperature effects of the overnight incubation of the media at 37°C in the hypoxia chamber effected both hypoxic and normoxic media to the same degree, the normoxic media bottle was also placed in the hypoxia chamber, however, only the hypoxia media bottle was opened for deoxygenation.) Prior to experiments cells were adapted to the hypoxic environment for at least 7 days unless otherwise stated.

2.2.2 Western blotting

For western blot analysis cells were harvested and washed with phosphate buffer saline (PBS; Sigma-Aldrich, USA) to remove medium components. Cells were then placed on ice and suspended in RIPA buffer (described in section 2.1.5) supplemented with 2% (v/v) EDTA-free protease inhibitor cocktail (Roche, Switzerland) and 0.5 µl/ml Pierce Universal Nuclease (Thermo Fisher Scientific, USA). After 30 minutes incubation on ice cells were incubated at 37°C for 10 minutes in order to increase the nuclease activity. This was followed by two cycles (30 seconds with 1 second intervals) of sonication on ice using the SONOPULS mini20 Ultrasonic homogenizer (Bandelin, Germany). For the removal of cell debris cell lysates were then centrifuged for 10 minutes at 15000 xg and 4°C. To determine protein concentrations the Bradford assay was applied using 5X Roti-Quant reagent (Roth, Germany). Lysates were diluted with RIPA buffer if required and prepared with 4X loading dye (Roth, Germany) following 5 minutes of incubation in a heating block heated to 95°C.

For the detection of phosphorylated proteins, SDS buffer (described in section 2.1.5) was used instead of RIPA buffer. Unlike RIPA-based lysates SDS-based lysates were prepared at room temperature. Cells were suspended in SDS buffer supplemented with 2% (v/v) protease inhibitor cocktail, 5 mM sodium fluoride (NaF; Sigma-Aldrich, USA) and 1 mM sodium orthovanadate (Na₃VO₄) to prevent dephosphorylation. This was followed by two cycles (30 seconds with 1 second intervals) of sonication and centrifugation (10 minutes, 15000 x g). To determine protein concentrations the Lowry assay was applied using DC™ Protein Assay Reagents A and B (Bio-Rad, USA). Lysates were diluted with SDS buffer if required and likewise to RIPA-based lysates prepared with 4X loading dye following 5 minutes of incubation in a heating block heated to 95°C.

For protein separation SDS polyacrylamide gel electrophoresis (SDS-PAGE) was applied. Together with 1 µl Precision Protein standard (Biorad, USA) lysates were transferred to a polyacrylamide gel consisting of a 4% acrylamide stacking gel and a 10% acrylamide separating gel and run at 150 Volts in MOPS SDS running buffer. This was followed by blotting to a 0.2 µm pore sized nitrocellulose membrane (Biorad, USA) for 2 hours at 35 Volts in pre-cooled transfer buffer (described in section 2.1.5). Membranes were then blocked for 30 minutes using milk powder-based blocking buffer (described in section 2.1.5) following primary antibody application overnight at 4°C. After primary antibody removal using TBS-T buffer (described in section 2.1.5) secondary antibodies were applied for 1 hour at room temperature. For protein visualization SuperSignal™ West Femto and PICO chemiluminescence substrates (Thermo Fisher Scientific, USA) were applied to the membrane. Chemiluminescence detection was conducted using the Odyssey® Fc Imaging system (LI-CORE, USA) and signals were analyzed and quantified by the Image Studio software (LI-CORE, USA).

All primary and secondary antibodies that were used are listed in section 2.1.6.

2.2.3 Gene editing techniques

2.2.3.1 Golden Gate assembly for target guide cloning in backbone vectors

Complementary oligonucleotides (listed in section 2.1.8) corresponding to the target guide sequence were cloned into backbone vectors (listed in section 2.1.8) using the Golden Gate assembly first described in Engler *et al.*, 2008.

In a first step 5 μ l sense and anti-sense oligonucleotides (100 μ M) were annealed in 40 μ l ddH₂O at 98°C for 5 minutes followed by 20 minutes of incubation at room temperature.

In a second step the oligo dimer was cloned into the backbone vector in the restriction- and ligation-based Golden Gate reaction shown in Table 1.

Table 1. Components and program for the Golden Gate reaction

Component	Amount
Vector	1 μ l (150 ng/ μ l)
Oligo dimers	5 μ l
10X T4 ligase buffer	2 μ l
T4 DNA ligase	1 μ l
BsmBI restriction enzyme	1 μ l
ddH ₂ O	10 μ l
Program	Step
37°C for 5 minutes	1: Restriction
16°C for 10 min	2: Ligation
Repeat step 1 - 2 10x	
37°C for 15 min	3: Elimination of empty vectors
80°C for 5 min	4: Enzyme inactivation

2.2.3.2 Transformation of competent bacteria

For the amplification of plasmid DNA through cellular replication competent *E. coli* (DH5 α) were used. For the transformation the bacterial cells were mixed with 0.1 to 2.5 μ l plasmid DNA, incubated on ice for 30 minutes and then heat-shocked for 5 minutes at 37°C. Cells were transferred back to ice for 2 minutes, plated on agar plates containing 100 μ g/ml ampicillin and incubated at 37°C overnight.

2.2.3.3 Plasmid preparation

Midiprep

For the purification of low amounts of DNA for subsequent clone validation via sequencing a Miniprep was applied. For this purpose single bacterial colonies were resuspended in 4 ml LB medium (prepared by dissolving 20 g LB broth mix in 1 liter H₂O following autoclavation) supplemented with 100 μ g/ml ampicillin and incubated overnight at 37°C. Bacterial cells were

then collected by centrifugation (15000 x g, 5 minutes) and processed with buffers provided with the Nucleobond PC500 Maxi Kit.

In a first step bacterial cells were resuspended in 100 µl S1 buffer, then lysed with 200 µl S2 buffer (5 minutes at room temperature) and neutralized in 150 µl S3 buffer. After centrifugation (15000 x g, 5 minutes) the supernatant was placed in a new Eppendorf tube, supplemented with 1 ml of 100% ethanol and centrifuged again (15000 x g, 5 minutes). The resulting DNA pellet was resuspended in 50 µl ddH₂O, sequenced using the services of SeqLab (Germany) and validated using the ApE-A plasmid editor and Clustal Omega (Multiple Sequence Alignment).

Maxiprep

For the purification of large amounts of DNA validated bacterial clones were cultured in 250 ml LB medium supplemented with 100 µg/ml ampicillin and incubated overnight at 37°C. Bacterial cells were then processed using the Nucleobond PC500 Maxi Kit (Macherey-Nagel) according to the manufacturer's instructions. This resulted in a concentrated DNA pellet free of proteins, RNA and other low-molecular-weight impurities that was reconstituted in dd H₂O to a concentration of 1 µg/µl. DNA concentrations were measured at absorption A₂₆₀ using NanoDrop 2000c spectrophotometer (Thermo Fisher Scientific, USA).

2.2.3.4 Lentivirus production

For the production of lentiviral vectors (listed in Table 3; gene and vector details provided in section 2.1.8) 11x10⁶ HEK 293T cells were seeded in 19 ml supplemented DMEM (10% (v/v) FCS, 100 U/ml penicillin, 100 µg/ml streptomycin) on 15 cm cell culture plates and incubated overnight at 37°C. When HEK 293T cells reached a confluence of around 80%, the medium was changed to 14 ml supplemented DMEM. The transfection solutions A and B (Table 2) were prepared, incubated for 5 minutes at room temperature, combined and incubated again for 20 minutes. The transfection mixture was then applied drop wise to the cells and cells were incubated at 37°C.

Table 2. Transfection mixture applied to HEK 293T cells seeded on 15 cm plates

Reagent	Amount
Solution A	
Serum free DMEM	1900 µl
Plasmid DNA	11.3 µg
Packaging Gag-Pol (psPAX2)	10.5 µg
Envelop plasmid VSV-G (pMD2.G)	5.8 µg
Solution B	
Transfection reagent polyethylenimine (PEI)	140 µl of a 1 µg/µl stock
Serum free DMEM	1760 µl

After 12 to 16 hours the medium was replaced with 14 ml supplemented RPMI (10% (v/v) FCS, 100 U/ml penicillin, 100 µg/ml streptomycin). Following 48 hours of incubation viral supernatant was collected, filtered through a 0.45 µm filter, supplemented with polybrene (hexadimethrine bromide) to a final concentration of 8 µg/ml and frozen at - 80°C.

Table 3. Lentiviral vectors

Gene editing	Vector	Marker/Resistance
GS knockout	pLentiCRISPRv2_EGFP_ΔCAS9	GFP
Non-target control	pLentiCRISPRv2_EGFP_ΔCAS9	GFP
CPS1 knockout	pLentiCRISPRv2_E2crimson_ΔCAS9	E2Crimson fluorescent protein
Non-target control	pLentiCRISPRv2_E2crimson_ΔCAS9	E2Crimson fluorescent protein
CPS1 overexpression	siHW CPS1	Hygromycin resistance
Empty vector	siHW Mock	Hygromycin resistance

2.2.3.5 Transduction of AML cell lines

For the transduction of AML cell lines with lentiviral vectors carrying a fluorescent marker, Cas9 expressing cells previously generated by PD Dr. Frank Schnütgen and colleagues (Goethe University Hospital Frankfurt, Germany) were used. Target cells were cultured in viral supernatant and supplemented RPMI (10% (v/v) FCS, 100 U/ml penicillin, 100 µg/ml streptomycin) at a density of 0.4×10^6 cells/ml. The ratio between viral supernatant and supplemented RPMI that allowed optimal transduction efficiency was tested beforehand for each batch of virus. After 48 hours of incubation at 37°C, cells were washed with PBS, reseeded in fresh supplemented RPMI and incubated for further 48 hours. Transduction efficiency was assessed by fluorescence-activated cell sorting (FACS) analysis as described in section 2.2.6.1.

The transduction of lentiviral vectors carrying a hygromycin resistance cassette was conducted at a cell density of 0.4×10^6 cells/ml in RPMI (10% (v/v) FCS, 100 U/ml penicillin, 100 µg/ml streptomycin) supplemented with 10% to 50% (v/v) viral supernatant. After 24 hours cells were washed with PBS and reseeded in RPMI (10% (v/v) FCS, 100 U/ml penicillin, 100 µg/ml streptomycin) supplemented with 400 µg/ml hygromycin B. Selection was conducted for 6 days with regular medium changes every 2 to 3 days.

2.2.3.6 CPS1 overexpression

For the overexpression of CPS1, the CPS1 cDNA coding sequence was amplified from RPMI 8226 cells in a PCR reaction using CPS1-specific primers (listed in section 2.1.8). The resulting product was cloned into a siHW vector carrying a hygromycin selection cassette using the restriction enzymes BamHI and NruI (vector map is shown in section 2.1.8). Virus production, transduction and selection was conducted as described in the sections above.

2.2.4 Growth, viability and colony assays

2.2.4.1 Cumulative growth assay

The cumulative growth assay allowed to monitor cell growth over several days. Initially, 0.2×10^6 cells/ml were plated in duplicates in 12-well cell culture plates. Every 2 or 3 three days (depending on the experiment) cells were counted using the CASY automatic cell counter (OMNI Life Science, Germany) and reseeded to the initial cell density (0.2×10^6 cells/ml) in fresh media. Unless otherwise described, cells were cultured in supplemented RPMI 1640 medium containing 300 mg/l glutamine (10% (v/v) FCS, 100 U/ml penicillin, 100 µg/ml streptomycin). For BSA rescue experiments in amino acid depleted media, cells were cultured in RPMI 1640 Medium w/o L-Glutamine, Leucine (USBiological, USA) prepared according to the manufacturer's instructions. The medium was supplemented with reduced FCS of 1% (v/v), 100 U/ml penicillin and 100 µg/ml streptomycin. Additionally, media was in parts supplemented with 5% (w/v) Bovine Serum Albumin (BSA) lyophilized powder (Sigma-Aldrich, USA), 300 mg/l L-glutamine using a 200 mM L-glutamine solution (Sigma-Aldrich, USA) and 50 mg/l L-leucine (Sigma-Aldrich, USA). The pH was adjusted to 7.4 with NaOH using a pH-meter (Hanna pH 210 (Hanna instruments, USA)). Medium was then sterilized by filtration (filter size: 0.2 µm).

For BSA rescue experiments in glucose depleted media, cells were cultured RPMI medium of either 2 g/L glucose (which is the standard glucose concentration of RPMI) or 0.5 g/L glucose (generated by mixing standard RPMI (RPMI 1640 Medium (21875034)) with RPMI 1640 medium, without glucose (111879020)). Media was in parts supplemented with 5% (w/v) BSA lyophilized powder (Sigma-Aldrich, USA). pH adjustment and sterilization were conducted as described above.

2.2.4.2 Competition growth assay

To evaluate a possible growth disadvantage of transduced cells a competition growth assay was conducted in which transduced cells competed against wildtype cells. Transduced and wildtype cells were mixed 50:50 (unless described otherwise) and cultured in supplemented RPMI (10% (v/v) FCS, 100 U/ml penicillin, 100 µg/ml streptomycin) at a cell density of 0.2×10^6 cells/ml in 12-well cell culture plates. Similar to the cumulative growth assay, cells were reseeded to the initial cell density every 2 days. The GFP-positive population of transduced cells was monitored every second day by FACS analysis as described in section 2.2.6.1.

2.2.5 ATP-based viability assay for IC₅₀ determination

To determine the half maximal inhibitory concentration (IC₅₀) of ammonium chloride (AppliChem, Germany), ethyl-isopropyl amiloride (EIPA; Tocris Bioscience, GB) and L-

methionine sulfoximine (MSO; Sigma-Aldrich, USA) the ATP-based CellTiter-Glo® 2.0 Cell Viability Assay (Promega, USA) was used. Cells were seeded in wells of flat white bottom 96-well plates (Greiner bio-one, Austria) at a density of 0.15×10^6 cells/ml (15,000 cells/well) in supplemented RPMI (10% (v/v) FCS, 100 U/ml penicillin, 100 µg/ml streptomycin) and increasing concentrations of the compound of interest. Cells were incubated for the indicated time (typically 24, 48 or 72 hours) at 37°C. After the incubation, assay plates and reagent were adjusted to room temperature and 30 µl reagent was applied to each well. Assay plates were then shaken for 2 minutes at 600 rpm using the Thermomixer Comfort (Eppendorf, Germany). Following 10 minutes of incubation at room temperature, luminescence was measured using the Infinite 200 PRO multimode plate reader (TECAN, Switzerland; 1 second flash/well) together with the i-control software (version 1.11.1.0; TECAN, Switzerland). The IC₅₀ was then determined by nonlinear regression analysis of dose response curves using GraphPad Prism 8 (GraphPad software, USA).

2.2.5.1 Colony formation assay

For the colony formation assay 5000 GS-knockout cells and respective control cells (generated in THP1 cells as described in section 2.2.11.1) were resuspended in 1 ml RPMI 1640 medium containing 300 mg/l glutamine (Thermo Fisher Scientific, USA) and supplemented with 10% (v/v) FCS (Sigma-Aldrich, USA), 100 U/ml penicillin, 100 µg/ml streptomycin (Thermo Fisher Scientific, USA) and 1 µg/ml puromycin (InvivoGen, USA). A volume of 400 µl cell solution was then added to 4 ml MethoCult H4100 (Stemcell, Canada) supplemented with IMDM medium (#36150, Stemcell, Canada), 20% (v/v) FCS (Sigma-Aldrich, USA), 100 U/ml penicillin and 100 µg/ml streptomycin (Thermo Fisher Scientific, USA). The suspensions were vortexed and in triplicates plated into 3.5 cm plates using a syringe with a blunt end needle. After 10 days colonies which were defined by a cell number ≥ 20 cells were counted.

For the replating of the cells the methylcellulose of the three triplicates was resuspended in 3 ml RPMI 1640 medium containing 300 mg/l glutamine (Thermo Fisher Scientific, USA). Cells were pelleted by centrifugation (224 x g, 5 minutes) and resuspended in 4 ml RPMI 1640 medium containing 300 mg/l glutamine (Thermo Fisher Scientific, USA). Cells were again pelleted by centrifugation (224 x g, 5 minutes). The supernatant was discarded and cells were centrifuged for another 30 seconds at 224 x g. All but 200 µl supernatant was discarded and RPMI 1640 medium containing 300 mg/l glutamine (Thermo Fisher Scientific, USA) was added to a final volume of 500 µl. The cell number of this suspension was determined and again 5000 cells were resuspended in 1 ml RPMI 1640 medium containing 300 mg/l glutamine (Thermo Fisher Scientific, USA) and supplemented with 10% (v/v) FCS (Sigma-Aldrich, USA), 100 U/ml penicillin, 100 µg/ml streptomycin (Thermo Fisher Scientific, USA) and 1 µg/ml puromycin

(InvivoGen, USA). Cells were then added to MethoCult H4100 based media and plated in triplicates as described above.

Counting the colonies and replating the colony formation assay was conducted again after 20 days and 30 days after initial setup of the colony formation assay.

2.2.6 Flow cytometry-based experiments

2.2.6.1 Fluorescence-activated cell sorting (FACS)

Prior to FACS analysis cells were washed with PBS in 75x12 mm polystyrene sample tubes (Sarstedt, Germany) and resuspended in 200 μ l PBS. Cells were then measured using the BD LSRFortessa™ flow cytometer (BD Biosciences, USA) and data was analyzed by the BD FACSDiva™ Software (BD Biosciences, USA).

Side scattered light and forward scattered light was measured and used for the determination of living cells. To further define the population of single cells a forward scatter height (FSC-H) versus forward scatter area (FSC-A) density plot was conducted. GFP-positive cells were then recorded from the single cell population using the Blue 488 nm laser (filter: 530/30). For E2crimson-positive cells the YellowGreen 561 nm laser (filter: 670/30) was used. At least 10,000 events were measured per sample.

2.2.6.2 Dextran feeding experiments

In order to draw conclusions about macropinocytic activity in AML cells, fluorescently labelled 10 kDa or 70 kDa dextran were applied to the cells. Cells were seeded in 6 cm cell culture plates at a cell density of 1.0×10^6 cells/ml in 6 ml serum free RPMI supplemented with 100 U/ml penicillin and 100 μ g/ml streptomycin. The cells were in part pre-treated for 30 minutes with different concentrations of EIPA (Tocris Bioscience, GB), IPI549 (MedChem Express, Germany) and MBQ-167 (MedChem Express, Germany) ranging from 0 μ M to 600 μ M. Following pre-treatment 0.05 mg/ml Dextran Alexa Fluor™ 555 (10,000 MW; Thermo Fisher Scientific, USA) or Dextran Oregon Green™ 488 (70,000 MW; Thermo Fisher Scientific, USA) were added to the cells as indicated. After different time points ranging from 0 to 100 minutes 2 ml of sample were removed from the plate and immediately washed twice with ice-cold PBS. Samples were then prepared and analyzed by FACS as described in section 2.2.6.1. For the detection of 10 kDa dextran-positive cells the YellowGreen 561 nm laser (filter: 610/20) was used and for the detection of 70 kDa dextran-positive cells the Blue 488 nm laser (filter: B-530/30) was used.

2.2.6.3 DQ Red BSA feeding experiments

To monitor uptake and degradation of proteins Dye Quenched (DQ) BSA was used which results in brightly fluorescent products upon hydrolysis that can be analyzed by FACS. Cell lines were seeded in 48-well plates at a cell density of 1.0×10^6 cells/ml in serum free RPMI supplemented with 100 U/ml penicillin, 100 $\mu\text{g/ml}$ streptomycin and 10 $\mu\text{g/ml}$ (0.001% (g/v)), 100 $\mu\text{g/ml}$ (0.01% (g/v)) and 300 $\mu\text{g/ml}$ (0.03% (g/v)) DQ™ Red BSA (Invitrogen, USA), respectively. Primary cells were seeded in PBS supplemented with 0.5% BSA to block unspecific binding of antibodies for immunophenotyping. The cells were in part pre-treated for 30 minutes with different concentrations of EIPA (Tocris Bioscience, GB), IPI549 (MedChem Express, Germany) and MBQ-167 (MedChem Express, Germany) ranging from 0 μM to 1000 μM . After different times points ranging from 0 to 100 minutes samples were washed twice with ice-cold PBS and prepared and analyzed by FACS as described in section 2.2.6.1. For the detection of the DQ™ Red BSA-derived fluorescent products the YellowGreen 561 nm laser (filter: 582/15) was used.

For immunophenotyping of primary AMLs, 5 μl of the following antibodies were added together with the DQ™ Red BSA for 30 minutes: CD33 (P67.6) PE Cy 7, CD34 (8G12) PerCP CY 5.5, CD38 (HB-7) APC, CD45 (clone 2D1) V500-C. All antibodies were obtained from BD Pharmingen, USA.

To monitor BSA uptake and hydrolysis in the presence of MSO and ammonium chloride cells were seeded in 24-well plates at a cell density of 0.8×10^6 cells/ml in RPMI supplemented with 100 U/ml penicillin, 100 $\mu\text{g/ml}$ streptomycin, 2% (g/v) BSA (Sigma-Aldrich, USA), 1 $\mu\text{g/ml}$ (0.0001% (g/v)) DQ™ Red BSA (Invitrogen, USA) and different concentrations of either MSO (0 to 16 mM; Sigma-Aldrich, USA) or ammonium chloride (0 to 20 mM; Sigma-Aldrich, USA). After 24 hours cells were analysed by FACS as described above.

2.2.7 Glutamine consumption assay

For the comparison of glutamine consumption rates between normoxic and chronic hypoxic growth conditions, HEL and MV411 cells were cultured in media containing 100 mg/l glutamine as described in section 2.2.1. Media were prepared from RPMI 1640 medium without glutamine (Thermo Fisher Scientific, USA) and a 200 mM L-glutamine stock solution (Sigma-Aldrich, USA) and supplemented with 10% (v/v) FCS (Sigma-Aldrich, USA), 100 U/ml penicillin and 100 $\mu\text{g/ml}$ streptomycin (Thermo Fisher Scientific, USA). At the beginning of the experiment HEL cells were seeded at a cell density of 0.1×10^6 cells/ml in both, normoxia and hypoxia. MV411 cells were seeded at a cell density of 1.2×10^6 and 0.75×10^6 cells/ml in

normoxia and hypoxia, respectively. (Cell densities were adjusted to glucose consumption rates analyzed prior to the experiment.)

After 0, 24 and 48 hours, 2 ml cell suspension of each cell line in the respective oxygen conditions was transferred to Eppendorf tubes which was conducted in triplicates. Cells and supernatant were separated by centrifugation (1500 x g, 5 minutes, 4°C) and the supernatant was transferred to a new Eppendorf tube and stored at - 80°C.

Supernatant samples were then placed on dry ice and shipped to Barcelona, Spain for further sample processing in the group of Prof. Dr. Marta Cascante at the University of Barcelona, Spain.

Here, glutamine and glutamate concentrations were determined in the cell supernatants collected at 0, 24 and 48 hours using the spectrophotometer COBAS Mira Plus Chemistry Analyzer (Horiba ABX, Japan) as described in Whitesides, 1985.

To quantify glutamine concentrations, the amino acid was first converted to glutamate through the glutaminase reaction. The glutaminase reaction was performed at 37°C for 30 minutes by agitating the samples with 125 mU/mL glutaminase (Sigma-Aldrich, USA) in 125 mM acetate (PanReac, Spain) buffer (pH 5). Glutamate concentrations were then determined by measuring the change in NADH concentration upon the GDH reaction which converts glutamate to α KG in the presence of adenosine diphosphate (ADP). The reaction was carried out at 37°C upon addition of the samples to 2.41 mM ADP (Sigma-Aldrich, USA), 3.9 mM nicotinamide adenine dinucleotide (NAD⁺; Sigma-Aldrich, USA) and 39 U/mL of GDH (Roche, Switzerland) in 0.5 M glycine (PanReac, Spain)/0.5 M hydrazine (PanReac, Spain) buffer (pH 9).

Absorbances were measured at 340 nm. Glutamine consumption rates in the samples were determined from the decrease in concentration after 24 and 48 hours compared to the initial concentration of glutamine at 0 hours, with respect to the total cell number at each time point.

2.2.8 Immunofluorescence microscopy

To visualize cellular GS under normoxic and hypoxic conditions immunofluorescence staining and microscopy was conducted. Cells were cultured as described in section 2.2.1 with the exception that medium applied to the hypoxic cells was kept at 37°C in the hypoxia chamber for several days. For immunofluorescence staining cells were suspended in PBS supplemented with 10% (v/v) FCS and fixed to Superfrost Plus microscope slides (Thermo Fisher Scientific, USA) using the Cytospin™ 4 Centrifuge (Thermo Fisher Scientific, USA; 200,000 cells/plate; 50x10 speed for 5 minutes). The cells were then fixed in 4% (w/v) paraformaldehyde (PFA) solution (described in section 2.1.5) for 10 minutes at room temperature and then washed with PBS for 5 minutes. To permeabilize and block cells PBS supplemented with 1% (w/v) BSA (Sigma-Aldrich, USA) and 0.05 mg/ml digitonin (Merck, Germany) was applied to the cells for 15 minutes and removed afterwards. Then the GS

primary antibody (ab178422; Abcam, GB) was diluted 1:100 in PBS supplemented with 1% (w/v) BSA and 0.05 mg/ml digitonin and applied to the cells for 1 hour. Cells were washed with PBS. Afterwards the secondary antibody solution was applied for 1 hour which was composed of Alexa Fluor 488 goat anti-rabbit (Invitrogen, USA) diluted 1:300 and DAPI (Sigma-Aldrich, USA) diluted 1:1000 in PBS supplemented with 1% (w/v) BSA). Cells were then mounted using 40 μ l Fluoroshield (Sigma-Aldrich, USA). Microscopic analysis was kindly conducted by Dr. Nina Kurrle using the confocal microscope LSM710 (Zeiss, Germany) of Prof. Dr. Kummer at the Institute for Anatomy and Cell Biology, Justus-Liebig-University Giessen, Germany.

To visualize dextran uptake and its inhibition through EIPA, cells were treated with dextran and EIPA as described in section 2.2.6.2. Cells were then prepared for fluorescence microscopy as described above. The primary antibody Lamp1 (Proteintech, USA) was used in a 1:50 dilution in order to stain lysosomes. The secondary antibody solution was composed of Alexa Fluor 488 goat anti-rabbit (Invitrogen, USA) diluted 1:300 and DAPI (Sigma-Aldrich, USA) diluted 1:1000 in PBS supplemented with 1% (w/v) BSA). Microscopic analysis was conducted with the help of Fabian Hahner using the confocal microscope LSM800 (Zeiss, Germany).

2.2.9 Mass spectrometry-based experiments

2.2.9.1 Intracellular tracking of ^{15}N -ammonium chloride

The intracellular tracking of ^{15}N -ammonium chloride was conducted both in the presence and absence of glutamine in the media. Cells cultured in glutamine-free media were pre-starved for 1 hour in RPMI without glutamine supplemented with 10% (v/v) FCS, 100 U/ml penicillin and 100 μ g/ml streptomycin. For this 90×10^6 cells were used at a cell density of 1×10^6 cells/ml. Following 1 hour of pre-starvation ^{15}N -ammonium chloride (Sigma-Aldrich, USA) was added to a final concentration of 5 mM and cells were incubated at 37°C. After 1, 6 and 24 hours, respectively, 10×10^6 were collected in triplicates. Cells and spent media were separated by centrifugation (224 x g, 5 minutes) and placed on ice. Cells were then resuspended in 1 ml ice-cold PBS, transferred to 1.5 ml Eppendorf tubes and centrifuged at 50000 x g at 4°C for 30 seconds. The supernatant was removed and cells were immediately placed in liquid nitrogen and stored at - 80°C. Spent media was mixed, 1.6 ml were transferred to 2 ml Eppendorf tubes and also placed in liquid nitrogen followed by storage at - 80°C.

The same was conducted with 30×10^6 cells that were cultured in glutamine-containing RPMI (10% (v/v) FCS, 100 U/ml penicillin, 100 μ g/ml streptomycin) supplemented with 5 mM ^{15}N -ammonium chloride. Here, samples were collected only after 24 hours.

^{15}N -ammonium chloride feeding as described above was conducted in HEL and THP1 cells both under normoxic and hypoxic conditions.

No-tracer control samples were prepared in normoxia in glutamine-free media using HEL cells. Cells were pre-starved as described above. After 1 hour either no or 5 mM non-labeled ammonium chloride (Sigma-Aldrich, USA) was added to the cells. Cells and supernatant were collected after 24 hours and prepared for - 80°C storage as described above.

All samples were placed on dry ice and shipped to Barcelona, Spain for further sample processing and gas chromatograph coupled to mass spectrometry (GC-MS) analysis in the group of Prof. Dr. Marta Cascante at the University of Barcelona (Department of Biochemistry and Molecular Biology, Faculty of Biology, Barcelona, Spain).

Here, cell pellets were defrosted on ice, resuspended in ice-cold methanol and transferred to 16 mm glass tubes together with 1 ml ice-cold ddH₂O. To serve as internal standard norvaline was added to each sample at a final concentration of 0.0025 mg/ml. Samples were then sonicated for 50 seconds with 5 second intervals with a titanium probe (Vibra-Cell, Sonics & Materials Inc., USA; Tune 50, Output 20). Afterwards, 2 ml ice-cold chloroform were added and the tubes were shaken for 30 minutes at 4°C and additionally mixed every 6 minutes using a vortexer. For polar and non-polar phase separation samples were then centrifuged at 4°C at 4500 x g for 15 minutes. The upper (polar) phase was transferred to a new 16 mm glass tube and dried under air flow for 2 hours. To completely dehydrate samples 50 µl dichloromethane were added and dried under continuous N₂ gas flow. For the derivatization of metabolites, samples were then mixed with 50 µl 2% (v/v) methoxamine hydrochloride in pyridine and heated for 90 minutes at 37°C on a shaker. After addition of 30 µl N-methyl-N-(tert-butyltrimethylsilyl)trifluoroacetamide (MBTSTFA) and 1% (v/v) tert-butyltrimethylchlorosilane (TBDMCS) samples were incubated at 55°C in a heating block for 1 hour. Following 5 minutes of cool-down, samples were mixed and transferred to GC-MS vials.

For the preparation of spent media, media samples were defrosted and 200 µl were transferred to 12 mm glass tubes together with 300 µl ice-cold ddH₂O and 500 µl ice-cold methanol. Similar to the cell pellet samples, 0.0025 mg/ml norvaline was added to each media sample and further processed as described above with the exception that 60 µl (not 30 µl) MBTSTFA were added. All samples were then analyzed by GC-MS analysis using a Agilent 7890A GC (Agilent Technologies, USA) equipped with a HP 5ms capillary column (Agilent Technologies, USA; reference: 19091S-433 (325°C), length: 30 m, ID: 250 µm, thickness: 0.25 µm, packaging: (5%-Phenyl)-methylpolysiloxane) connected to a Agilent 5975C MS (Agilent Technologies, USA).

To further analyze ¹⁵N-ammonium chloride treated cells by nuclear magnetic resonance (NMR), ¹⁵N-ammonium chloride treatment was repeated as described above. Processing of cell pellets and NMR analysis was then conducted by Islam Alshamleh at the Schwalbe group (Goethe University, Campus Riedberg, Frankfurt, Germany) as described in section 2.10.

2.2.9.2 Intracellular tracking of ¹⁵N-*Arthrospirulina maxima* cell extracts

GS-knockout cells together with non-target control (NTC) cells were generated in HEL as described in section 2.2.3.5. ¹⁵N-labeled and non-labeled *Arthrospirulina maxima* cell extracts obtained from Silantes (Germany) were dissolved in RPMI supplemented with 1% (v/v) FCS, 100 U/ml penicillin and 100 µg/ml streptomycin to a final concentration of 2% (w/v) by ultrasonication (for cell extract preparation see Appendix 7.1). The pH was adjusted to 7.4 with NaOH and the cell extract-containing media were then sterilized by filtration (filter size: 0.2 µm). A total of 102x10⁶ GS-knockout as well as NTC cells were resuspended in 102 ml ¹⁵N-labeled and non-labeled cell extract-containing media and incubated at 37°C for 24 hours. After incubation cells were washed with PBS, resuspended in 400 µl prechilled HPLC-grade methanol (VWR Chemicals International, USA) and mixed using a vortexer. The samples were then transferred to prechilled glass vials and 325 µl ddH₂O and 400 µl HPLC-grade chloroform (Carl Roth, Germany) were added. The different additives were mixed for 40 seconds and incubated on ice for 10 minutes to allow phase separation. For further phase separation samples were centrifuged for 10 minutes at 5000 x g and 4°C in a swingout rotor. Using a Hamilton syringe (Gilson, Germany) 400 µl of the upper (polar) layer were transferred to Eppendorf tubes, snap frozen in liquid nitrogen and stored at - 80°C. Further sample processing and NMR analysis was conducted by Islam Alshamleh at the Schwalbe group (Goethe University, Campus Riedberg, Frankfurt, Germany) as described in section 2.2.10.

2.2.10 Nuclear magnetic resonance (NMR) analysis

Prior to NMR analysis samples were dried for 4 hours using a Concentrator Plus vacuum dryer (Eppendorf, Germany). The metabolites extracts were then resuspended in 60 µl of NMR buffer (described in section 2.1.5) and sonicated for 10 minutes. Samples were then transferred to Shigemi 3 mm NMR tubes (Cortecnet, France) and measured on an AV950 MHz Bruker spectrometer equipped with a 5 mm TCI cryoprobe (Bruker, USA). 2D ¹H-¹⁵N experiments were performed at 25°C using (hsqcetf3gp) pulse program with 25% non-uniform sampling acquisition mode (25% NUS), 1024 number of scans, a TD of (2048, 110) and a spectral width of 8279 Hz. Spectral resolution was 150 Hz for the indirect dimension. Data analysis was performed in TopSpin 3.5 (Bruker, USA).

2.2.10.1 Ammonium measurements in patient samples

Ammonium measurements in patient samples were conducted in cooperation with Dr. Julius Enßle and Dr. Philipp Makowka (Goethe University Hospital Frankfurt, Germany). Peripheral blood samples and bone marrow aspirates were taken from *de novo* AML patient at the time of initial diagnosis. Immediately, the blood sample and the second milliliter of the bone marrow

aspirate were placed on ice and send to the Central Laboratory (Goethe University Hospital Frankfurt, Germany) for ammonium measurements. (The first milliliter of the bone marrow aspirate is used by the clinicians for morphological analysis of the bone marrow cells. This process is important for the diagnosis and characterization of AML.)

2.2.11 *In vivo* mouse study

2.2.11.1 Generation of GS-knockdown cells and xenotransplantation

For the generation of GS-knockdown cells, bacterial glycerol stocks containing GS-specific shRNA constructs were obtained from Merck (Germany). shRNA sequences and the vector map (pLKO.1_puro) can be found in section 2.1.8. The bacteria were cultured, plasmids were isolated by Midiprep and virus was produced as described in section 2.2.3.3. A total of 30×10^6 THP1 cells at a cell density of 0.5×10^6 cells/ml were then transduced in RPMI supplemented with 10% (v/v) FCS, 100 U/ml penicillin and 100 µg/ml streptomycin at a ratio of 1:1 with the respective virus. After 24 hours, cells were washed twice with PBS and selected for 3 days with 2 µg/ml puromycin (InvivoGen, USA). Cells were then suspended in Hanks balanced salt solution (Sigma-Aldrich, USA). In cooperation with Dr. Rahul Kumar from the Prof. Daniela Krause laboratory (Georg Speyer-House, Frankfurt, Germany) 3×10^6 cells were transplanted intravenously into non-irradiated NSG (NOD SCID gamma) mice carrying an interleukin-2 receptor knockout and being 10 to 14-weeks of age. The study was approved by the local German government (Regierungspräsidium Darmstadt, Hessen, Germany; project: Metabolismus- und Hypoxie-assoziierte Target-Gene bei der AML, FK/1117). The mice were kept and looked after in the animal facility of the Georg-Speyer-Haus, Frankfurt, Germany. Survival curve comparison was performed using the Mantel-Cox test with $p < 0.001$ significance level.

2.2.11.2 Processing of sacrificed mice

Carbon dioxide (CO₂) was used for mouse euthanasia. Blood was analysed using the ScilVet abc animal blood cell counter (ScilVet, Germany). For histological analysis parts of the lung, liver, spleen and tumour harbouring tissues as well as the pelvis, femur and tibia of the lower right leg were fixed using Roti®-Histofix 4% (Roth, Germany). For the isolation of bone marrow cells from the pelvis, femur and tibia of the lower left leg the bones were crushed, flushed with PBS containing 2% (v/v) FCS and smashed through a 40 µm nylon cell strainer (Falcon, USA) with a 5 ml plunger (Injekt, Braun, Germany). The remaining parts of the liver, spleen and tumour harbouring tissues were cut into small pieces and also flushed with PBS containing 2% (v/v) FCS and smashed through a 40 µm nylon cell strainer. Cells were then collected by centrifugation (528 rpm, 10 minutes, 4°C) and resuspended in 1 ml of erythrocyte lysis buffer

(described in section 2.1.5). Erythrocyte lysis was also applied to the remaining blood sample of about 20 μ l. The lysis reaction was stopped after 5 minutes by addition of PBS containing 2% (v/v) FCS. Cells were again collected by centrifugation (528 rpm, 10 minutes, 4°C), resuspended in PBS containing 2% (v/v) FCS and counted manually using Neubauer counting chambers (Paul Marienfeld GmbH & Co. KG, Germany). Antibodies specific to the surface markers CD33 (APC Mouse Anti-Human CD33; BD Pharmingen, USA) and CD45 (PE Mouse Anti-Human CD45; BD Pharmingen, USA) together with an IgG control (PE Mouse Anti-Human IgG; BD Pharmingen, USA) were then applied at ratio of 1:200 to 200 μ l cell suspension that contained 0.5×10^6 cells/ml. The cells were incubated at 4°C in the dark for 20 minutes and analyzed by FACS as described in section 2.2.6.1. For the detection of the IgG control and CD45-positive cells the Blue 488 nm laser (filter: 575/25) was used. For CD33-positive cells the Red 640 nm laser (filter: 670/30) was used.

3 Results

3.1 GS expression is upregulated in AML on transcriptomic and proteomic level

To assess the expression of GS on transcriptomic and proteomic level in AML, we analyzed several AML expression profiles. We visited the online database BloodSpot, which provides publicly available mRNA expression profiles in healthy and malignant haematopoietic cells. Data of 252 AML patients compared to 6 healthy donors revealed an overall significantly higher GS mRNA expression in AML cells compared to healthy hematopoietic stem and progenitor cells (HSPCs) (Figure 5 A). Higher GS mRNA expression was prevalent across all AML subtypes tested including AML harboring the translocations t(15;17), inv(16)/t(16;16), t(8; 21) and t(11q23)/MLL as well as AML with a complex karyotype. The increase in GS mRNA expression compared to the healthy counterparts ranged from 2.2-fold to 3.8-fold and was most pronounced in AML patients with a complex karyotype which belong to the highest risk group.

According to the Human Protein Atlas database, several solid cancers have high GS expression (Figure 5 C). This was shown by GS levels detected by immunohistochemistry in tissues of human solid tumors compared to healthy tissues. Human Protein Atlas-derived GS mRNA expression further revealed AML to classify among the highest GS-expressing cancer cell lines (Figure 5 D). SuperSILAC-based GS protein expression data (provided by Prof. Dr. Thomas Oellerich (Goethe University Hospital Frankfurt, Germany)) showed that this phenotype of higher GS is even stronger in the AML blasts compared to AML cell lines (NB4, MV411 and KG1) (Figure 5 B). The difference was significant for all the different genotypes including inv16 (n = 29), FLT3 (n = 12), RUNX (n = 21) and NPM1 (n = 15).

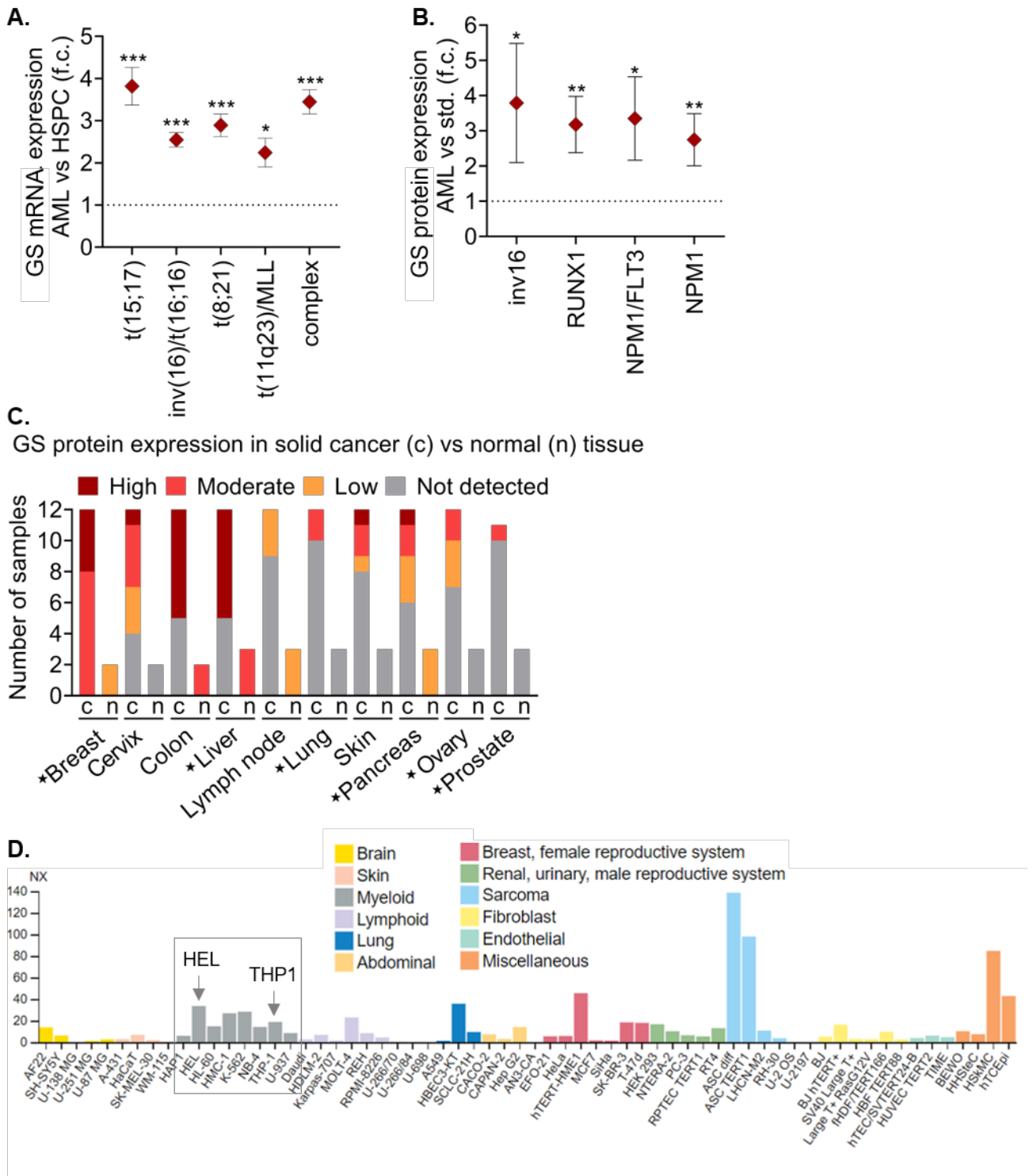


Figure 5. GS expression is upregulated in AML on transcriptomic and proteomic level

A. GS mRNA expression across different AML subtypes derived from the BloodSpot database. Primary AML blasts of 252 patients were compared to hematopoietic stem and progenitor cells (HSPCs) from 6 healthy donors. **B.** GS protein expression in primary AMLs blasts with different genetic backgrounds compared to an AML standard (std.) (consisting of NB4, MV411, KG1 cell lines) analyzed by SuperSILAC-based mass spectrometry. **C.** Human Protein Atlas-derived GS protein expression across human solid tumors compared to healthy tissues (adapted from Bott *et al.*, 2019). Stars mark cancers in which the role of GS has been investigated (for a complete list see Table 4). **D.** Human Protein Atlas-derived GS mRNA expression across different cancer cell lines.

GS = glutamine synthetase; AML = acute myeloid leukemia; f.c. = fold change; c = cancer; n = normal

To further investigate whether there is a correlation between specific AML genotypes and GS expression, we performed *in silico* analysis of The Cancer Genome Atlas (TCGA)-based GS mRNA expression profiles in AML (Figure 6 A; TCGA-based analysis was conducted by Dr. Geoffroy Andreux (University of Freiburg, Germany)). An elevation in GS expression was seen in AML cells carrying CEBPA mutations, this was however only marginal ($p = 0.0384$; Figure 6 B). The only significant difference ($p = 0.001$) was observed in RUNX1 mutated AMLs which exerted significantly lower GS compared to RUNX1 wildtype AMLs (Figure 6 C). Overall, the data suggested that with exception of RUNX1, there seems to be no correlation between AML genotypes and GS expression.

Finally, we did not observe a clinical impact of GS expression on patient survival. Clinical data from the TCGA revealed GS expression to neither predict patient survival probability in *de novo* AML patients below the age of 60 treated with cytarabine and daunorubicin (Figure 6 D) nor in AML patients overall (Figure 6 E).

In summary, the analysis of GS expression profiles in AML unveiled higher levels of GS on transcriptomic and proteomic level in AML cells compared to their healthy counterparts or an AML standard. However, there seems to be no significant correlation between high GS expression and common AML gene mutations or overall survival.

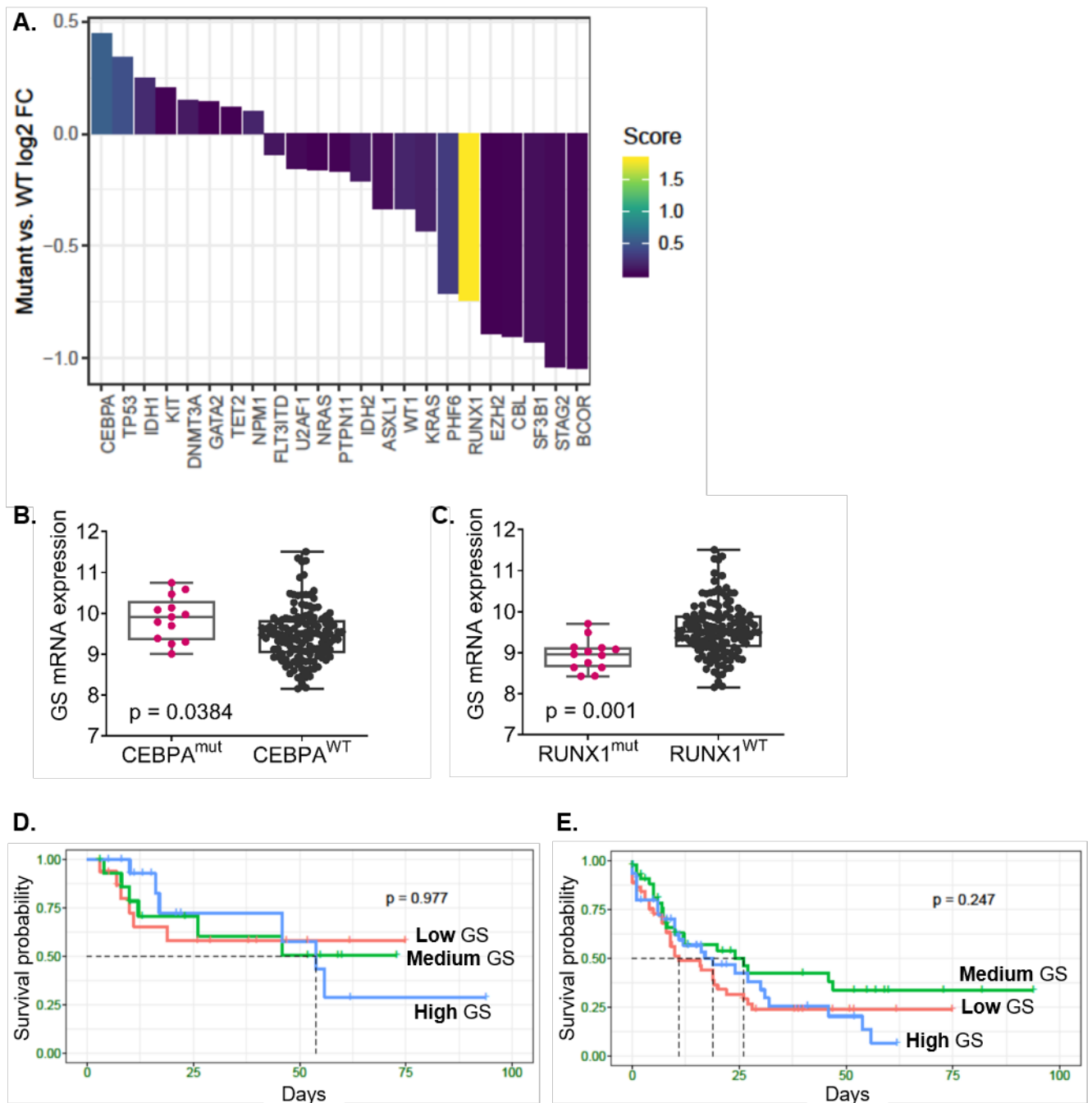


Figure 6. GS expression in AML with different genetic mutations and GS-based patient survival

A. The Cancer Genome Atlas (TCGA)-based GS mRNA expression in AML blasts with specific gene mutations compared to the wildtype. **B./C.** TCGA-based scatter dot-plots representing the levels of GS mRNA expression in CEBPA (**B.**) and RUNX1 (**C.**) mutant versus wildtype cells of AML patients. Significance was determined by unpaired t-test. **D./E.** TCGA-based Kaplan Meier curves divided into low, medium and high GS mRNA expression for *de novo* AML patients below 60 years treated with cytarabine and daunorubicin (**D.**) and all AML patients grouped together (**E.**). P value refers to a log-rank (Mantel–Cox) test. GS = glutamine synthetase; WT = wildtype; FC = fold change; mut = mutated

3.2 Genetic deletion of GS reduces AML cell growth

Having shown that AML cells compared to healthy HSPCs express high levels of GS on transcriptomic and proteomic levels, we were interested to know whether a lack of GS would affect AML growth. We were further interested to understand the impact of oxygen availability on GS dependency and carried out investigations under both normoxic (21% O₂) and chronic hypoxic conditions (1% O₂, adapted > 7 days).

To deplete GS in Cas9-positive cells and to induce a GFP expression marker for tracking, we applied the clustered regularly interspaced short palindromic repeats (CRISPR)/Cas9 gene editing technique. Six single guide RNAs (sgRNAs) were designed targeting different regions of the GS expressing *GLUL* gene as well as *GLUL* pseudogenes: guide 2 targeting the second exon of *GLUL* and pseudogene 4 (Ge2), guide 2b targeting the second exon of *GLUL* alone (Ge2b), guide 3 and 3b targeting the third exon of *GLUL* (Ge3, Ge3b), guide P4 targeting *GLUL* pseudogene 4 (GP4) and guide GPP co-targeting the second exon and pseudogenes 3 and 4 of *GLUL*.

The resulting GFP-positive cell populations were screened for GS expression via immunoblotting and showed various degrees of GS knockout efficiencies (Figure 7 A). Guide GPP proved most successful in depleting the cells of GS. Similar degrees of depletion were obtained in cells expressing guides 2b, 3 and 3b with exception of guide 2 which only achieved minor reductions in GS protein levels. As expected, guide GP4 targeting *GLUL* pseudogene 4 showed only minimal reduction in GS expression level.

Both under normoxia and hypoxia, GS deficiencies in HEL cells led to a significant decrease in cellular growth correlating with the degree of GS depletion with few exceptions under hypoxic growth conditions (Figure 7 B). GS depletion using the GPP sgRNA slowed down growth by 80% in normoxia and by 50% in hypoxia (where cells independently of GS grow at a slower rate). A similar growth disadvantage was also observed in other AML cell lines (MOLM13, MV411 and THP1; Figure 7 C, D).

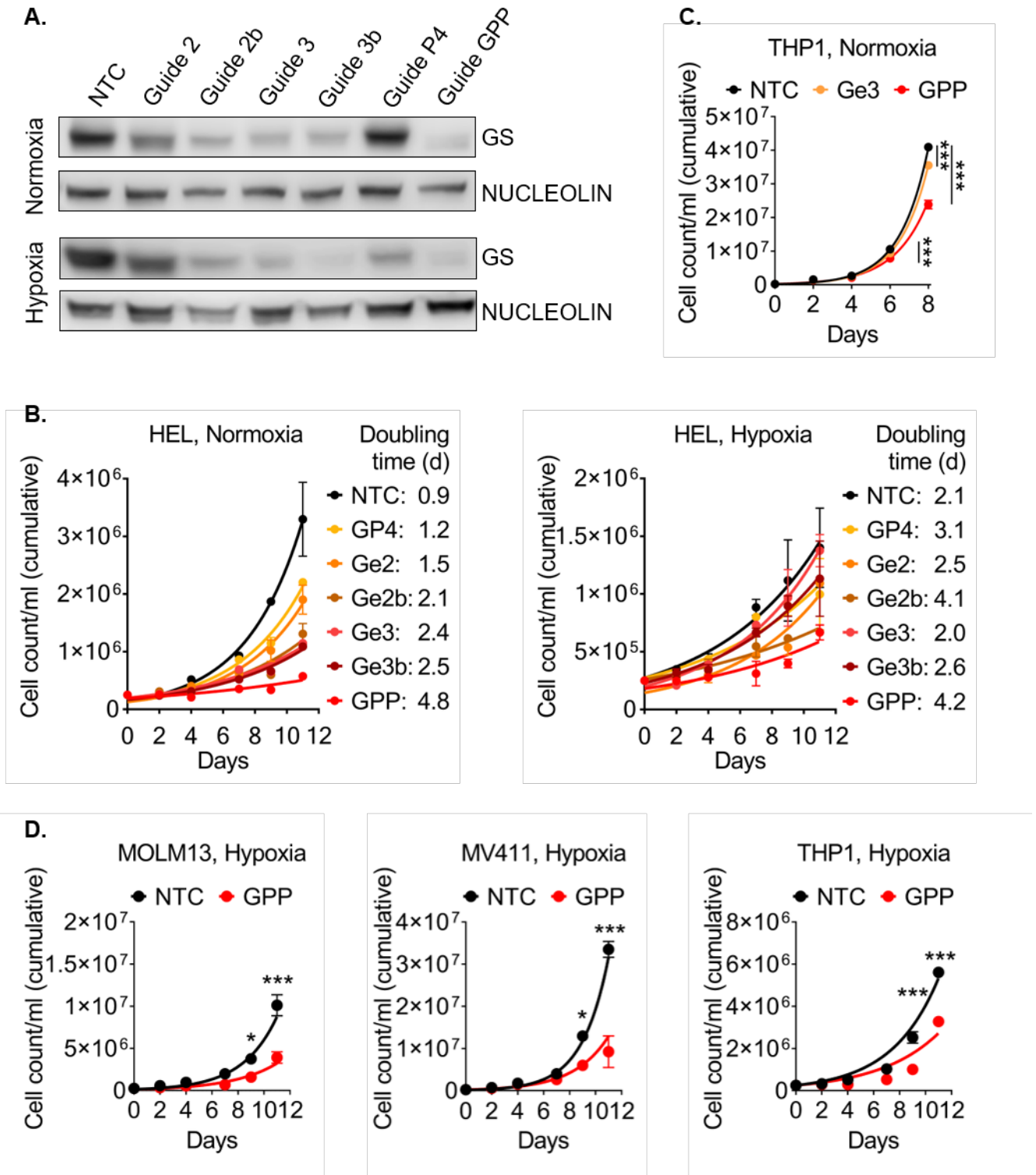


Figure 7. Genetic deletion of GS reduces AML cell growth

A. Western blot of GS levels upon GS knockout in HEL-Cas9 cells using different sgRNAs targeting human *GLUL* compared to NTC control. **B.** Cumulative growth assay of HEL cells showing reduced proliferation capacity upon GS depletion under normoxia as well as hypoxia. Cells were cultured in 100 mg/l glutamine-containing full medium. **C./D.** Cumulative growth assay in different AML cell lines upon GS knockout under normoxic and hypoxic conditions. Cells were cultured in 300 mg/l glutamine-containing medium. Error bars indicate mean \pm s.e.m. Statistical significance was determined by 2way ANOVA; * P ,0.033, *** P ,<0.0001. GS = glutamine synthetase; NTC = non-target control; Ge3 = Guide 3; d = days

To further examine the importance of GS to leukemia growth *in vivo*, GS knockdown was generated in THP1 cells using two different GS-targeting shRNAs (GS KD 1 and GS KD 2) (Figure 8 A). *In vitro*, shRNA-mediated GS depletion led to a significantly decreased cell growth (Figure 8 B) and significantly reduced the cellular capacity to form colonies (Figure 8 C). Consistent with these results, mice injected with GS KD 1 and GS KD 2 cells (n = 8 per group) showed a significant delay in disease progression and had a prolonged overall survival (49.5 and 47 days, respectively, compared to 33 days in the NTC mice) (Figure 8 D) (one GS KD 2 and one NTC mouse died early on day 4 and 6 post-transplantation before leukemia onset).

Analysis of CD45-positive cells isolated from the femur further revealed significantly decreased AML bone marrow infiltration in mice injected with GS deficient cells (Figure 8 E). Decreased AML infiltration was also found in the liver and the spleen of GS-knockdown mice, however, did not reach statistical significance. Additionally, GS deficiency reduced the number of tumors which in NTC mice were most often located at the sides of the lymph nodes or present in the form of sarcomas (Figure 8 F). Heavily infiltrated and swollen lymph nodes as well as sarcomas were found in every NTC mice by the time of death. In contrast, only 2 out of 15 GS-knockdown mice developed infiltrated lymph nodes and only 7 out of 15 mice developed sarcomas.

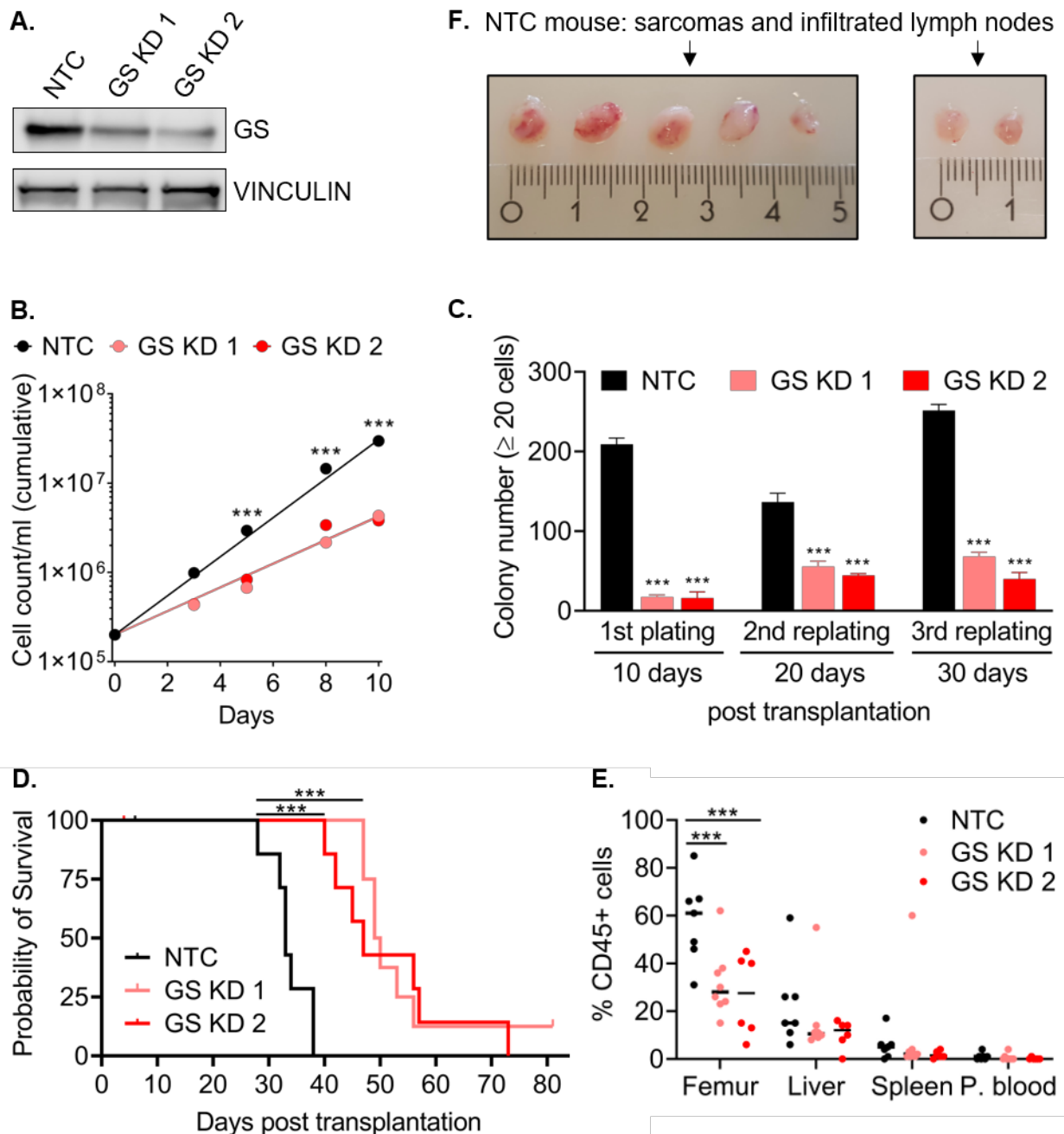


Figure 8. GS knockdown reduces AML cell growth and colony formation and impairs leukemia progression *in vivo*

A. Western blot of GS protein levels in THP1 cells transduced with two different GS-shRNAs compared to a NTC. **B.** Cumulative growth curve of reduced cellular proliferation in THP1 cells upon GS knockdown. **C.** GS knockdown impaired colony formation capacity in a serial replating colony formation assay (replated every 10 days up to day 30). Experiments in (**B.**) and (**C.**) were performed with 300 mg/l glutamine-containing medium. Error bars indicate mean \pm s.e.m. Statistical significance was determined by 2way ANOVA; ***P,0.0002. **D.** Kaplan Meier curves showing prolonged overall survival of Non-irradiated NSG (NOD SCID gamma) mice transplanted with GS-knockdown THP1 compared to a NTC (n = 8 per group). Survival curve comparison was performed using a Mantel-Cox test, p<0.001. **E.** FACS analysis of CD45⁺ cell ratios in different organs of the mice upon scarification. Statistical significance was determined by 2way ANOVA; ***P,0.0002. **F.** Sarcomas and lymph nodes carrying > 90% CD45-positive cells were isolated from a NTC mouse at the time of death (day 38). GS = glutamine synthetase; NTC = non-target control; KD = knockdown; P. = peripheral

3.3 The role of GS in glutamine synthesis

Previous *in vitro* and *in vivo* experiments established that GS expression is important for proliferation and leukemogenicity of AML cell line models. Next, we were interested in understanding the functional role of GS in AML. Since GS has two defined biological functions, namely glutamine production and ammonium detoxification, we experimentally evaluated which of these functions mediate GS importance in AML.

Earlier experiments showed that GS function is important for AML growth even under standard culturing conditions where sufficient amounts of glutamine are present. To further evaluate whether GS is necessary for AML metabolism as a provider of glutamine, we starved AML cells from glutamine and compared their growth properties with and without GS. For this purpose, we performed a competitive growth assay between GFP-positive GS-knockout cells (GPP cells) and GFP-negative control cells (mixed in 1:1 ratio) under varying glutamine concentrations (17% (50 mg/l), 33% (100 mg/l), 100% (300 mg/l) and 200% (600 mg/l) of standard glutamine media concentration). We tracked the proportion of GFP-positive cells as an indicator of proliferation over a period of 16 days. As expected, NTC control cells showed no growth disadvantage under different glutamine concentrations. Surprisingly, different glutamine concentrations did not affect the dependency of the GS-knockout cells on GS (Figure 9 A). We observed the same degree of growth disadvantage upon GS-knockout in 100 mg/l, 300 mg/l and 600 mg/l glutamine. Only a reduction of glutamine to 50 mg/ml increased the growth disadvantage upon GS knockout, however, not within the first 10 days.

These results show that under prolonged glutamine starvation GS can be important for glutamine provision, however, they exclude that GS function as glutamine provider is the cause for GS knockout-mediated growth deficiency under standard culturing conditions.

We were further interested, how the different glutamine concentrations affected overall growth of the AML cells. Therefore, we performed cell counting in parallel to FACS measurements during the competitive growth assay. From the cell counts and the FACS analysis, we determined the cumulative growth of the GFP-positive NTC and GPP cells. Despite large variances in glutamine availability, the NTC cells showed the same growth behavior independent of extracellular glutamine concentrations (Figure 9 B). Similarly, glutamine restriction did not impact GS-knockout cells and only a minor growth disadvantage was observed at a glutamine concentration of 50 mg/ml on day 16. Again, these data provide some hint that glutamine availability (to a large extent) is not decisive for the growth of GS-knockout cells.

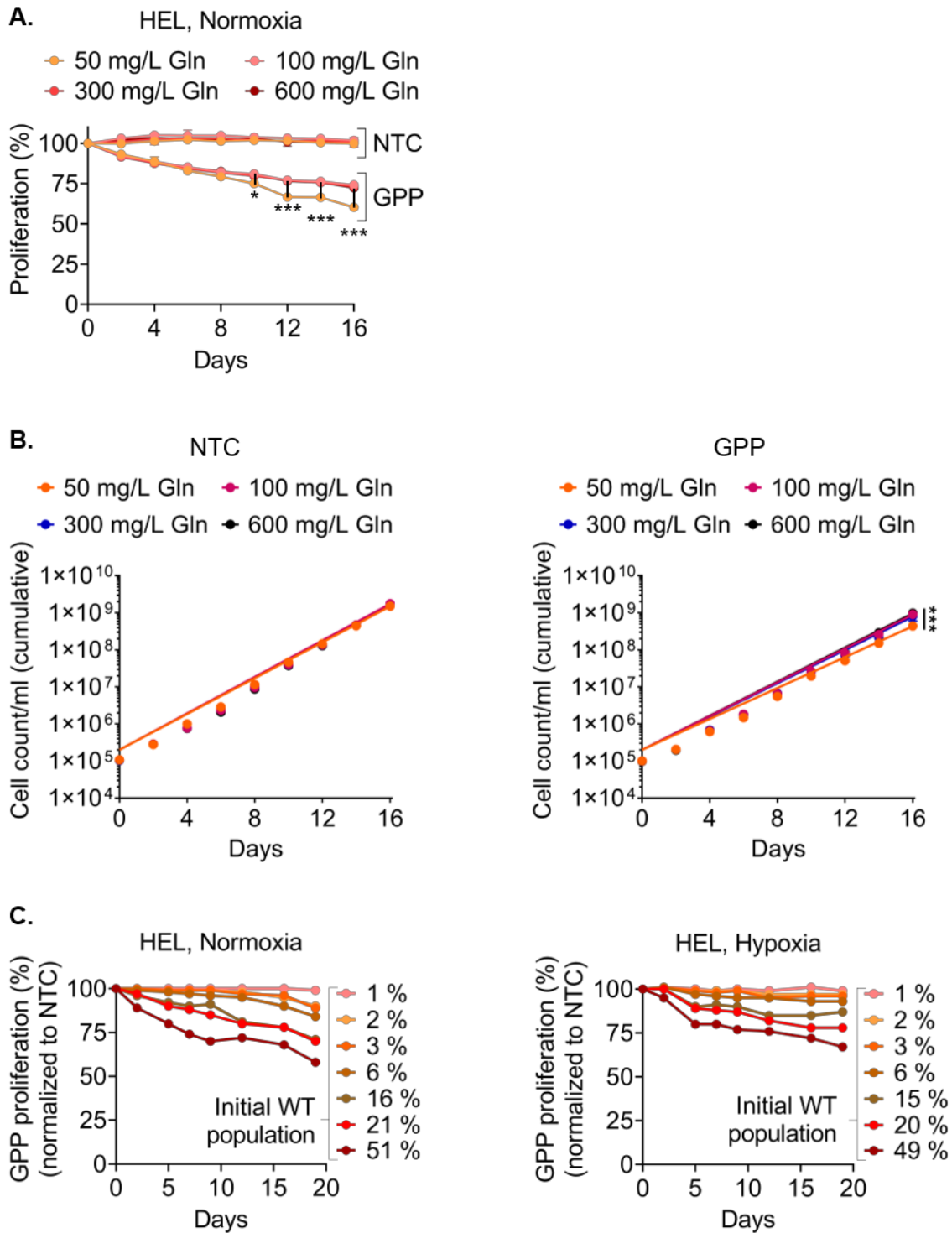


Figure 9. AML growth dependency on GS is independent of glutamine availability

A. Impact of glutamine availability on GS-negative cell growth as determined by the competitive growth assay. **B.** Cumulative growth curves of NTC and GPP populations as determined from cell counts and FACS analysis shown in **A.** **C.** Competitive growth assays of GS knockout cells in co-cultures with varying mixing ratios of WT cells under normoxic and hypoxic conditions. Medium contained 300 mg/l glutamine. Error bars indicate mean \pm s.e.m. Statistical significance was determined by 2way ANOVA; *P,0.0185, ***P,<0.0001.

GS = glutamine synthetase; NTC = non-target control; Gln = glutamine; WT = wildtype

To exclude the possibility that the control GS-positive cells in the competitive assay rescued the GS-negative cells by producing and providing them with glutamine (and therefore undermining their sensitivity to external glutamine restriction), we repeated the competitive growth assay with limited GS-positive population ratios (1% to 50% of the co-culture (Figure 9 C). Interestingly, GS-positive control cells still overgrew the GS-knockout cells in a correlative manner with the proportion of the initial GS-positive population. Similarly, we observed a similar trend when we performed the experiment under hypoxic conditions, albeit the overgrowth was slower due to the reduced growth rate under hypoxia. These results rule out the possibility that GS-positive cells support the growth of GS-negative cells.

Altogether, these experiments establish that GS knockout results in a competitive growth disadvantage, even in the presence of excess amounts of glutamine. Thus, it seems likely that besides its function in glutamine synthesis, GS fulfills a different function in AML cells that is important for their growth.

3.4 The role of GS in ammonium detoxification

GS catalyzes the amination of glutamate to yield glutamine. In this reaction, ATP and glutamate bind to the active sites of GS and induce a conformational shift upon glutamate phosphorylation. This allows binding of ammonium and its transfer to glutamate. Hence, the functional role of GS in AML might not primarily serve the production of glutamine but rather the detoxification of ammonium ions.

To investigate the relevance of GS in ammonium detoxification we first determined the sensitivity of GS-negative cells towards extracellular ammonium that was added in the form of ammonium chloride. We demonstrated that all AML cell lines tested were significantly more sensitive towards ammonium chloride upon GS depletion (Figure 10 A). Ammonium chloride IC_{50} values revealed GS-negative AML cells to tolerate about 30% to 60% less ammonium chloride than GS-positive cells. Similarly, we evaluated cellular proliferation under increasing concentrations of ammonium chloride for extended periods of time (96 hours) and observed a stronger toxicity of the GS knockout in the presence of ammonium ions (Figure 10 B).

These observations suggest that GS-negative cells are less capable of detoxifying ammonium. Hence, we assessed whether GS-negative GPP cells and Ge3 cells (which were generated with guides targeting different regions of *GLUL*) accumulated more ammonium in the media than GS-positive cells. Indeed, ammonium levels in the extracellular medium were significantly higher for GS-negative Ge3 and GPP cells compared to control cells (with higher levels observed in GPP cells compared to Ge3 cells considering their stronger GS knockout (for knockout efficiencies see Figure 7 A)).

Altogether, these findings indicate that the functional relevance of GS in AML cells is linked to the role of GS in ammonium detoxification.

The increased sensitivity towards ammonium and the increased ammonium accumulation in GS-knockout cells (Figure 10) suggest an important role of GS in ammonium detoxification. Therefore, we aimed at understanding the cellular response to extracellular ammonium and the exact role of GS in this process.

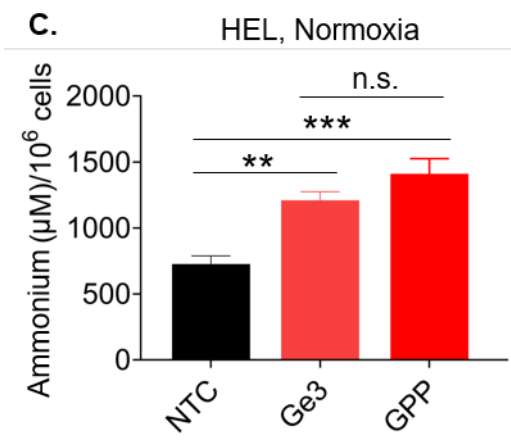
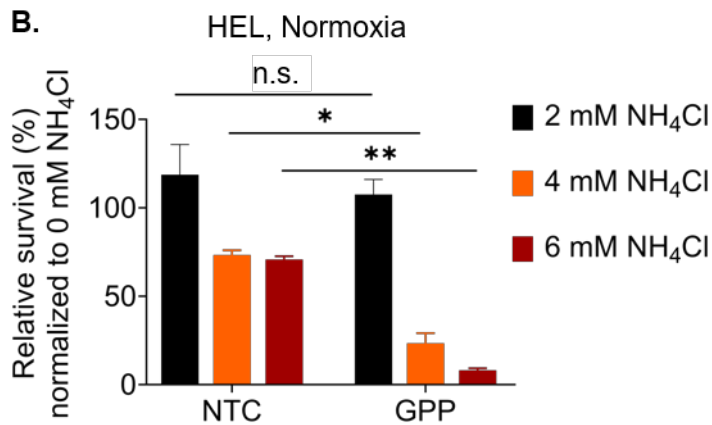
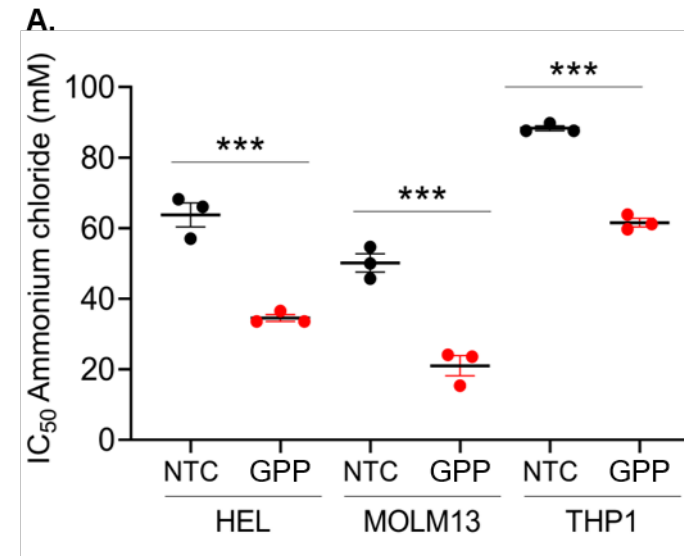


Figure 10. GS depletion in AML leads to an increased sensitivity towards ammonium and increased accumulation

A. Ammonium chloride (NH₄Cl) IC₅₀ determination in GS-positive NTC and GS-negative GPP cells in multiple AML cell lines. IC_{50s} were determined after 24 hours from ATP-based cell viability assays. Statistical significance was determined by 1way ANOVA; ***P,<0.0001. **B.** Cellular sensitivity to ammonium chloride in GS-negative GPP cells compared to NTC cells after 96 hours. Statistical significance was determined by 2way ANOVA; *P,0.0152, **P,0.0050. **C.** Ammonium accumulation determined after 72 hours in extracellular medium. Statistical significance was determined by 1way ANOVA; **P,0.0072, ***P,0.0003. All error bars indicate mean ± s.e.m.

GS = glutamine synthetase; NTC = non-target control; n.s. = not significant; Ge3 = Guide 3

To this end, we supplemented the cells with ^{15}N -labelled ammonium chloride ($^{15}\text{N-NH}_4\text{Cl}$) and performed GC-MS to assess whether *de novo* glutamine contains the ^{15}N -labelled NH group originating from exogenous $^{15}\text{N-NH}_4\text{Cl}$. To verify that GS-mediated ammonium detoxification occurs independent of oxygen and glutamine availability, we conducted the analysis in normoxia and hypoxia and in the presence and absence of glutamine.

In preliminary experiments we identified 5 mM as optimal ammonium chloride concentration that allows high intracellular ammonium levels without affecting cell viability (Figure 11 A). Hence, 5 mM $^{15}\text{N-NH}_4\text{Cl}$ was applied to the cells and the metabolic tracing analysis using GC-MS was performed.

As expected, a pronounced ^{15}N labeling of glutamine was observed (Figure 11 B). The presence of ^{15}N -glutamine under normoxia and hypoxia and varying glutamine availability verified GS-mediated ^{15}N -ammonium scavenging to occur independent of oxygen and glutamine conditions.

Next to ^{15}N -glutamine, large quantities of ^{15}N -glutamate (catalyzed by glutamate dehydrogenase (GDH); Figure 12) were detected in HEL and THP1 cells (Figure 11 C). After 24 hours 25 to 50% of glutamine and glutamate carried a ^{15}N label in HEL. The high amount of ^{15}N labeling in these amino acids implied that GS- and GDH-mediated reactions are essential in the detoxification of ammonium.

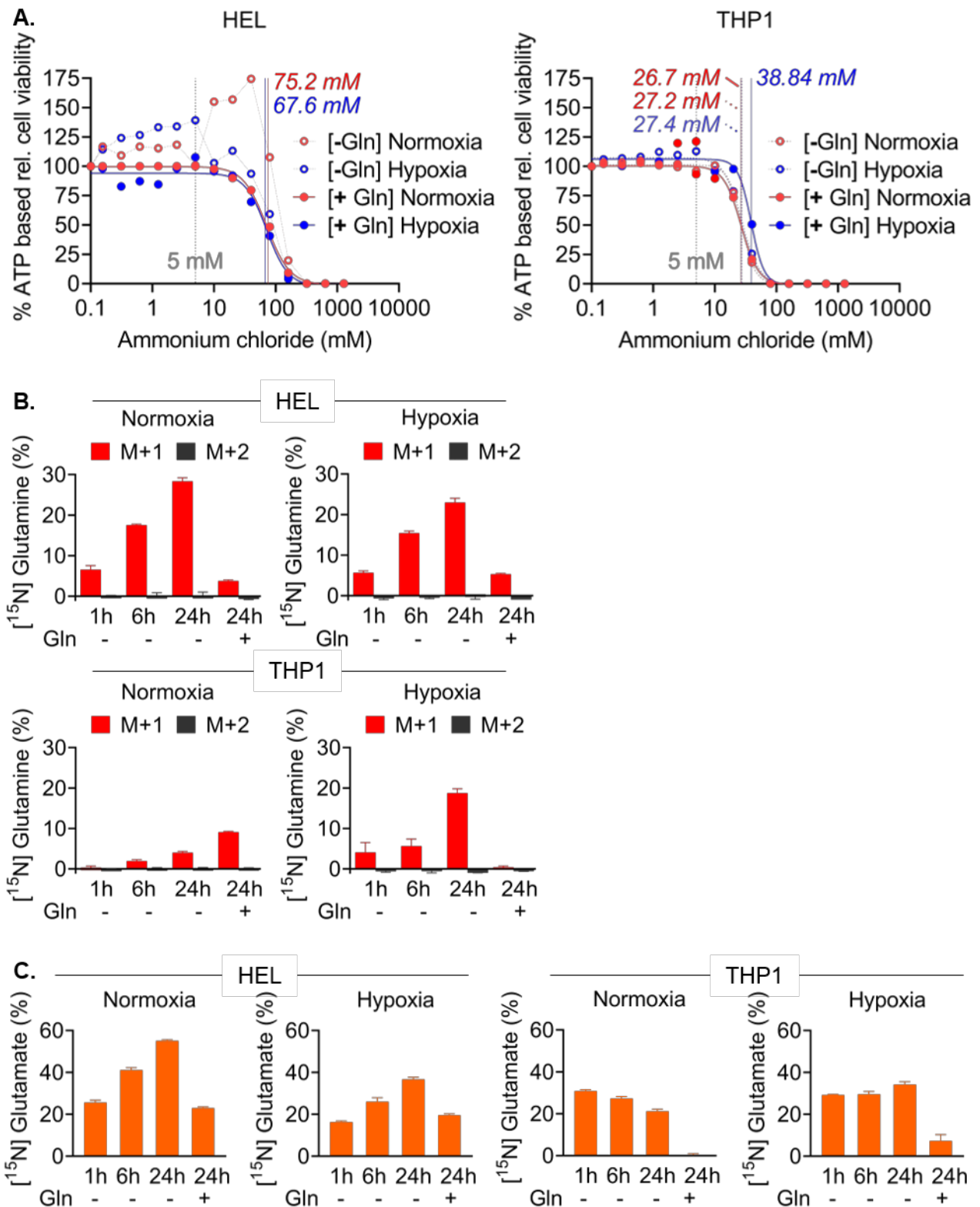


Figure 11. Addition of ¹⁵N-ammonium chloride results in the formation of ¹⁵N-glutamine and ¹⁵N-glutamate

A. IC₅₀ determination of ammonium chloride in THP1 and HEL cells (measured by ATP-based cell viability assays). **B./C.** Relative abundance of ¹⁵N-glutamine (**B.**) and ¹⁵N-glutamate (**C.**) in HEL and THP1 cells after treatment with 5 mM ¹⁵N-ammonium chloride. Values are means ± SD; n = 3 per condition.

Gln = glutamine; ATP = adenosine triphosphate; rel. = relative

Interestingly, the GDH-derived ^{15}N -glutamate did not serve as substrate for GS which would have resulted in double-labeled glutamine at both NH groups (one ^{15}N at the alpha carbon (^{15}N -ammonium-derived) and another ^{15}N at the delta carbon (^{15}N -glutamate-derived)). This was revealed by further analysis of atom specific label incorporation using NMR spectroscopy (Figure 13) (as GC-MS measurements are limited to showing mass increase but not ^{15}N label positioning).

(To determine ^{15}N label positioning of ^{15}N -glutamine by NMR spectroscopy, ^1H - ^{15}N HSQC NMR reference spectra for glutamate and glutamine were first recorded individually to assign the exact signal position (chemical shift) of each of the two ^{15}N signals observed (corresponding to the two amino groups) (Figure 13 A, B). Next, NMR spectra were recorded from HEL cells fed with ^{15}N - NH_4Cl (Figure 13 C). This showed that the ^{15}N label was exclusively present at the side chain NH_2 group of glutamine (added by GS activity; see Figure 12).)

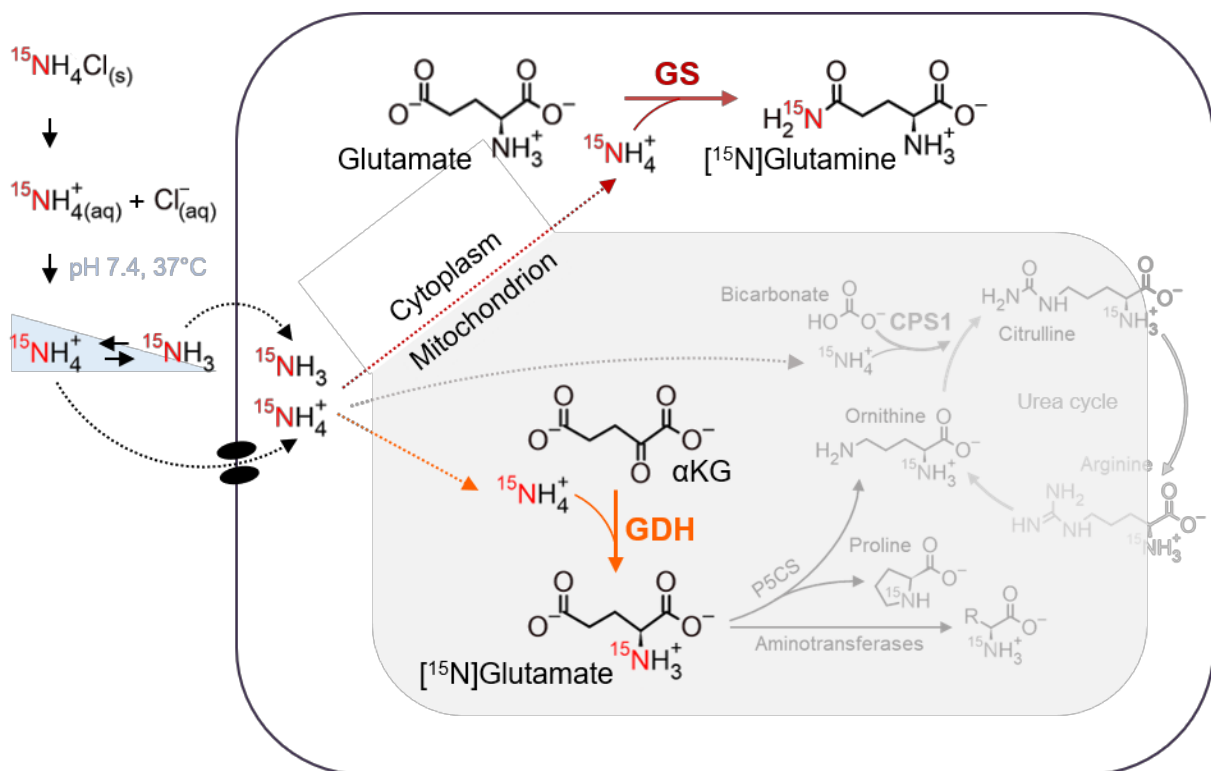


Figure 12. Predicted ^{15}N distribution after ^{15}N -ammonium chloride treatment

Schematic of predicted ^{15}N distribution in the cytoplasm (white) and the mitochondria (grey) after ^{15}N -ammonium chloride treatment. Under physiological conditions (pH 7.4, 37°C) the majority of ^{15}N -ammonium (ca. 98%) is present in its ionic form NH_4^+ . Unlike NH_3 , NH_4^+ requires energy-driven or carrier-mediated cell uptake. The fate of NH_4^+ is likely dictated by its cellular location: cytoplasmic NH_4^+ is assimilated by GS and mitochondrial NH_4^+ is assimilated by GDH. (^{15}N labelling was further observed in several amino acids and urea cycle intermediates.)

GS = glutamine synthetase; GDH = glutamate dehydrogenase; P5CS = pyrroline-5-carboxylate synthase; R = 'functional group of the possible amino acids aspartate, alanine, leucine, isoleucine and methionine'; s = solid; aq = aqueous

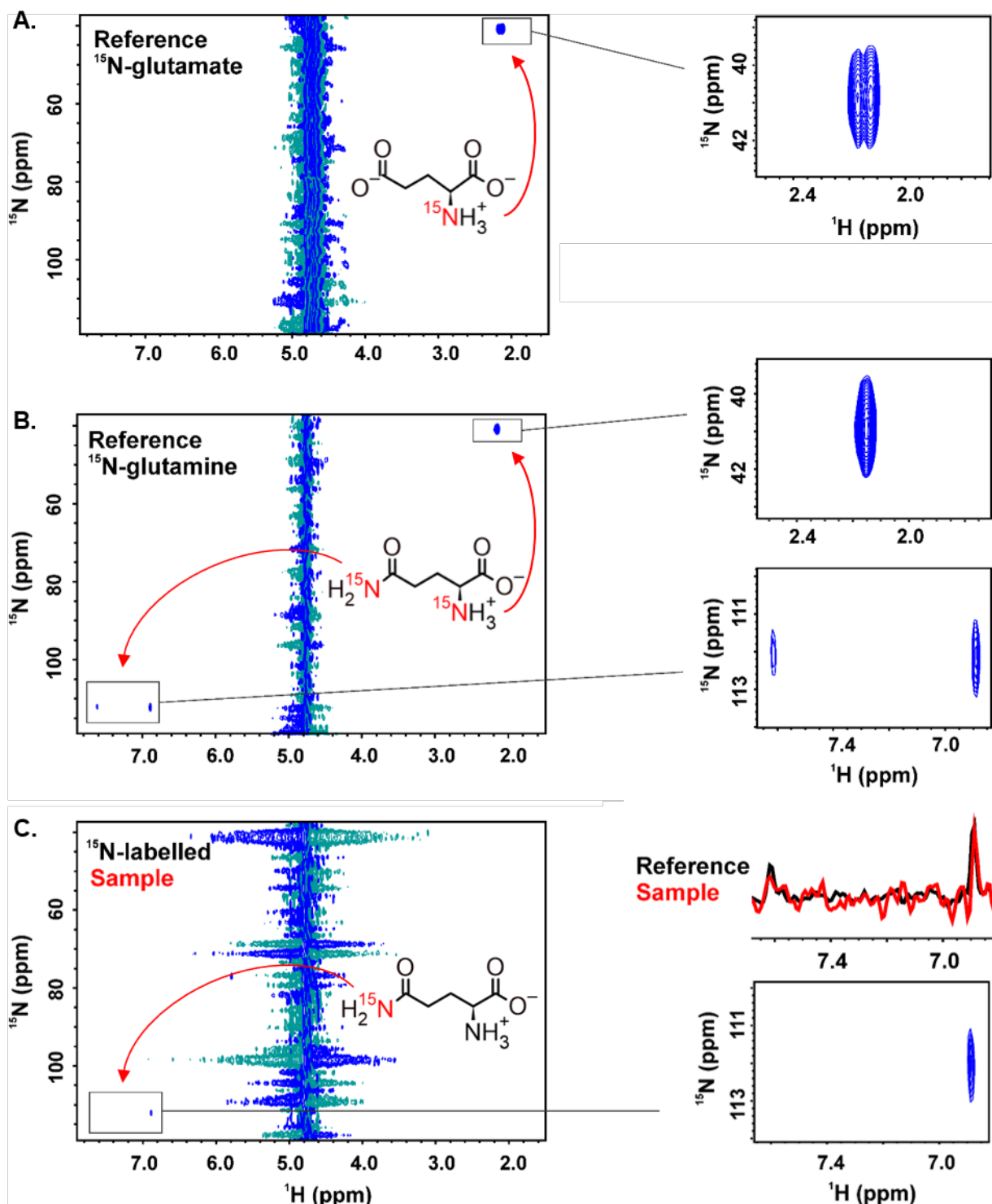


Figure 13. NMR analysis reveals ^{15}N -glutamine to be exclusively labeled at the side chain NH_2 group

2D ^1H - ^{15}N HSQC NMR spectra of **A.** ^{15}N -glutamate and **B.** ^{15}N -glutamine reference samples dissolved in NMR buffer. Peak assignment is shown for each of the amino groups. **C.** 2D ^1H - ^{15}N HSQC NMR spectrum of HEL cells fed with ^{15}N -ammonium chloride. 1D projections overlay from the 2D spectra of reference glutamine and the cell sample are shown for the side chain amino group signals. The spectra were recorded on a AV950 MHz Bruker spectrometer using the pulse program hsqcetf3gp (number of points: 2048 /128; number of scans: 8 for the reference spectra and 512 for the media sample; temperature: 25°C)

NMR = nuclear magnetic resonance

Since GS is located in the cytoplasm and GDH is located in the mitochondria, it is likely that newly synthesized ^{15}N -glutamate did not serve as substrate for GS due to its cellular compartmentalization. Instead, GDH-derived ^{15}N -glutamate was further metabolized by aminotransferases and pyrroline-5-carboxylate synthase (P5CS) (see Figure 12) as shown by the presence of several ^{15}N -labeled amino acids and urea cycle intermediates (both extracellularly and intracellularly; Figure 14, Figure 15).

Altogether, these findings verified the role of GS in the removal of ammonium and further revealed ammonium scavenging to be dictated by its cellular location with GS-mediated detoxification taking place in the cytoplasm and GDH-mediated detoxification taking place in the mitochondria.

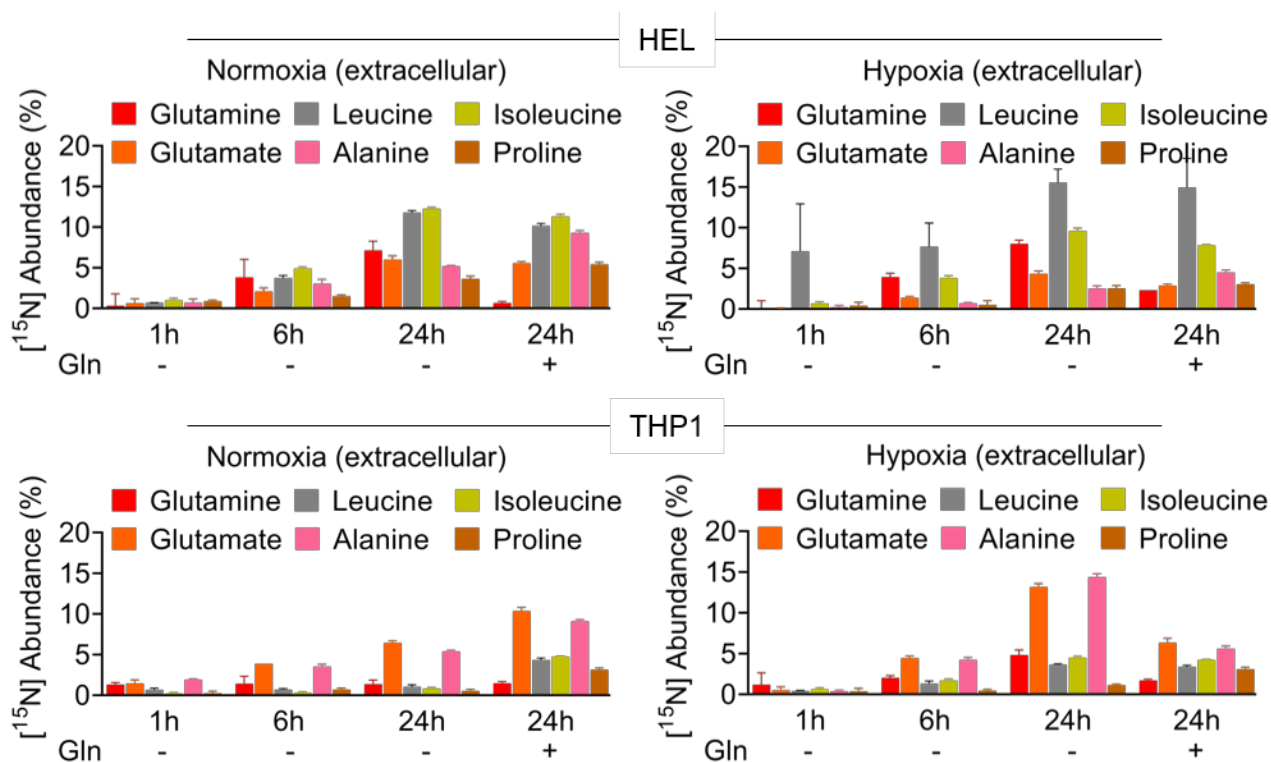


Figure 14. ^{15}N Ammonium derivatives are also present extracellularly

Relative abundance of ^{15}N amino acids in spent media of HEL and THP1 after treatment with 5 mM ^{15}N ammonium chloride. Values are means \pm SD; n = 3 per condition.

Gln = glutamine

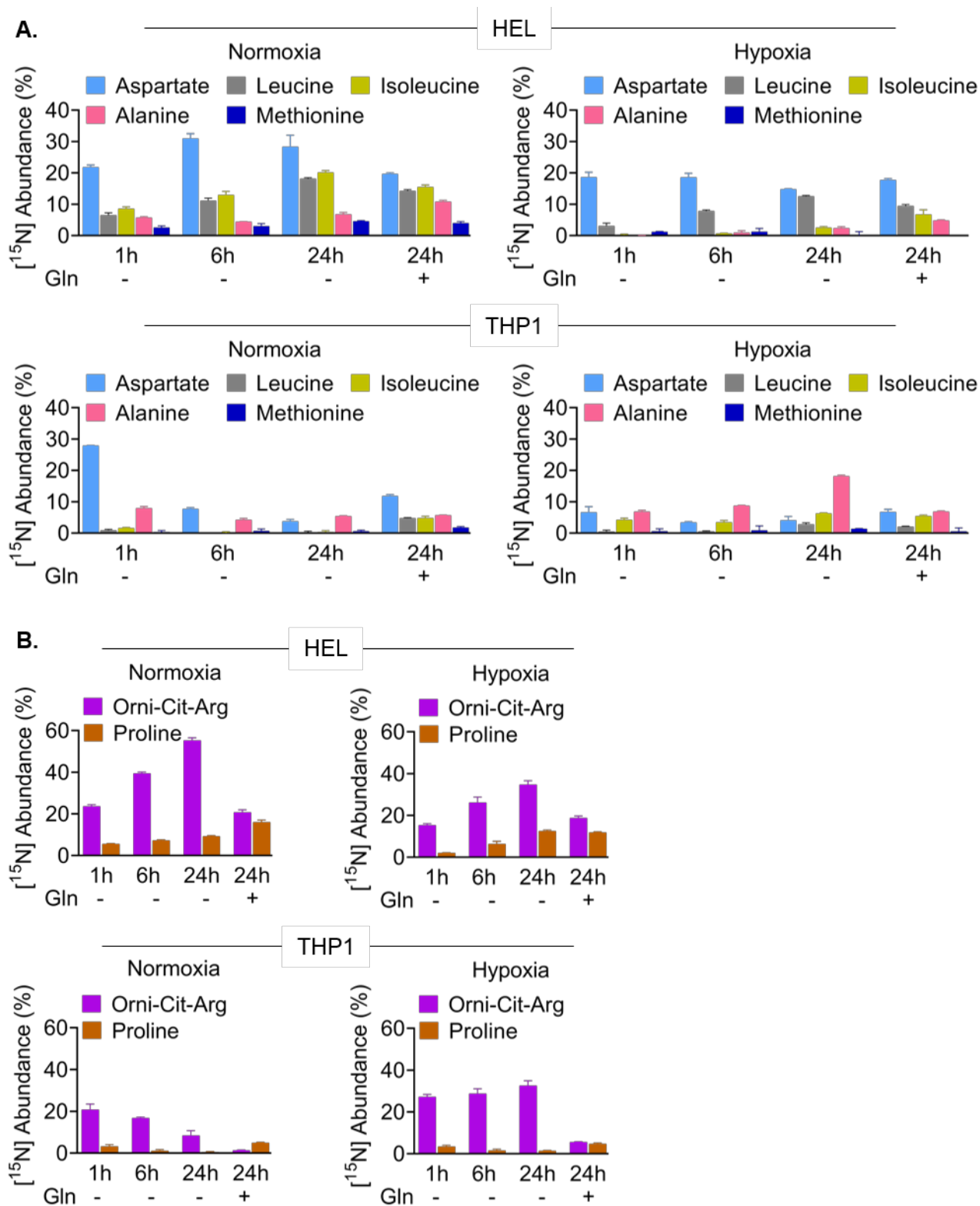


Figure 15. GDH-derived glutamate is used for the generation of amino acids

Relative abundance of **A.** [^{15}N]amino acids and **B.** Urea cycle intermediates in cell pellets of HEL and THP1 after treatment with 5 mM [^{15}N]ammonium chloride. Values are means \pm SD; n = 3 per condition.

Gln = glutamine; Orni = ornithine; Cit = citrulline; Arg = arginine

3.5 Endocytic protein uptake and catabolism contribute to amino acid metabolism

Next to *de novo* synthesis or uptake of free amino acids, cells can acquire amino acids such as glutamine through endocytosis-driven protein uptake and subsequent protein degradation. A form of endocytosis through which proteins can enter the cell is macropinocytosis. The following experiments aimed at examining whether macropinocytosis or other endocytic processes drive protein uptake in AML and whether extracellular proteins contribute to AML amino acid metabolism.

First, we assessed macropinocytic activities in AML cells. We used fluorophore-conjugated dextrans (10 and 70 kDa) which are large sugar molecules that can only be internalized through the actions of an endocytic process like macropinocytosis.

All tested AML cell lines (HEL, MOLM13, THP1) showed a linear uptake of 10 kDa dextran which reached a plateau after 80 minutes (Figure 16 A). The B-ALL cell line TMD5 served as negative control and showed almost no dextran uptake.

Next, we assessed the effects of macropinocytosis inhibition on dextran uptake using ethylisopropyl amiloride (EIPA) and immunofluorescent imaging. EIPA inhibits the Na^+/H^+ exchanger located in the plasma membrane to which macropinocytosis, in contrast to other types of endocytosis, is uniquely susceptible. Within 40 minutes, dextran significantly accumulated in the cells and colocalized with lysosomes, the first entry point of internalized macropinosomes (Figure 16 B). Upon treatment with 75 μM EIPA, dextran uptake was considerably reduced showing a successful inhibition of macropinocytosis (Figure 16 B, C).

Using DQ-BSA that releases fluorescent products upon hydrolysis, it was further shown that AML cell lines (HEL, MOLM13, MV411, THP1) internalize and degrade the most abundant protein of human blood plasma – albumin (Figure 16 D). On the other hand, the B-ALL cell line TMD5, showed significantly less DQ-BSA proteolysis. The addition of DQ-BSA further revealed the uptake and degradation of extracellular protein to occur at a rapid pace, more rapidly than dextran uptake. The strongest accumulation of hydrolyzed DQ-BSA took place within the first 5 minutes. This was observed among all the different cell lines (Figure 16 D). While MV411 and MOLM13 cells were less efficient in accumulating dextran compared to HEL cells, their efficiency in DQ-BSA uptake exceeded or equaled that of HEL cells (Figure 16 A, D).

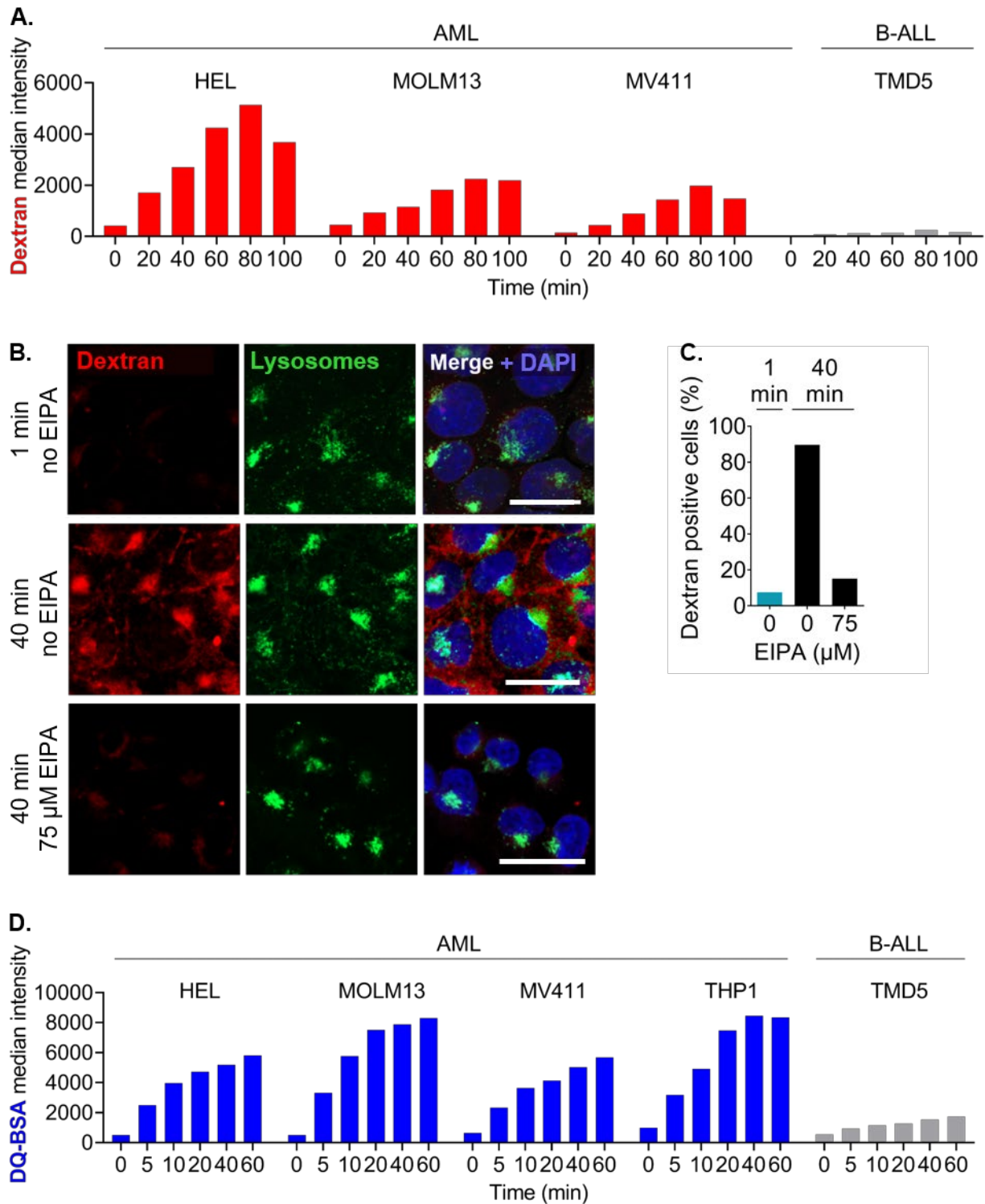


Figure 16. AML cell lines conduct macropinocytosis and catabolize extracellular proteins

A. Uptake of fluorescent 10 kDa dextran (50 $\mu\text{g}/\text{ml}$) by different AML cell lines in medium with 1% serum. A B-ALL cell line served as negative control. **B.** Immunofluorescent images of 10 kDa dextran uptake in medium with 1% serum \pm EIPA, pretreated for 30 minutes. Lysosomes (Lamp-1 staining) and nuclei (DAPI staining) were stained. Scale bar, 20 μm . **D.** Quantification of dextran positive cells shown in **B.** **D.** Proteolysis of DQ-BSA (10 $\mu\text{g}/\text{ml}$) by different AML cell lines in medium with 1% serum. A B-ALL cell line served as negative control. All experiments were carried out in normoxia. AML = acute myeloid leukemia; ALL = B-cell acute lymphoblastic leukemia; EIPA = ethyl-isopropyl amiloride; DAPI = 4',6-Diamidino-2-phenylindol; DQ-BSA = dye quenched-bovine serum albumin

To further analyze the mechanism underlying dextran and DQ-BSA uptake, the effects of different macropinocytosis inhibitors were tested. The addition of increasing concentrations of EIPA significantly reduced the uptake of dextran, however, showed only a minor inhibitory effect on DQ-BSA uptake and proteolysis (Figure 16 E). Further, we tested IPI549, an inhibitor of the PI3 kinase (PI3K) which is involved in membrane ruffle extension and macropinosome formation during macropinocytosis. In contrast to EIPA, IPI549 inhibited dextran and DQ-BSA to an equal degree (Figure 16 F). Finally, MBQ-167, (inhibits Cdc42 and Rac which are also important for membrane ruffling and macropinosome formation) showed to be more successful in inhibiting the uptake and catabolism of DQ-BSA (65% compared to 35% for dextran) (Figure 16 G).

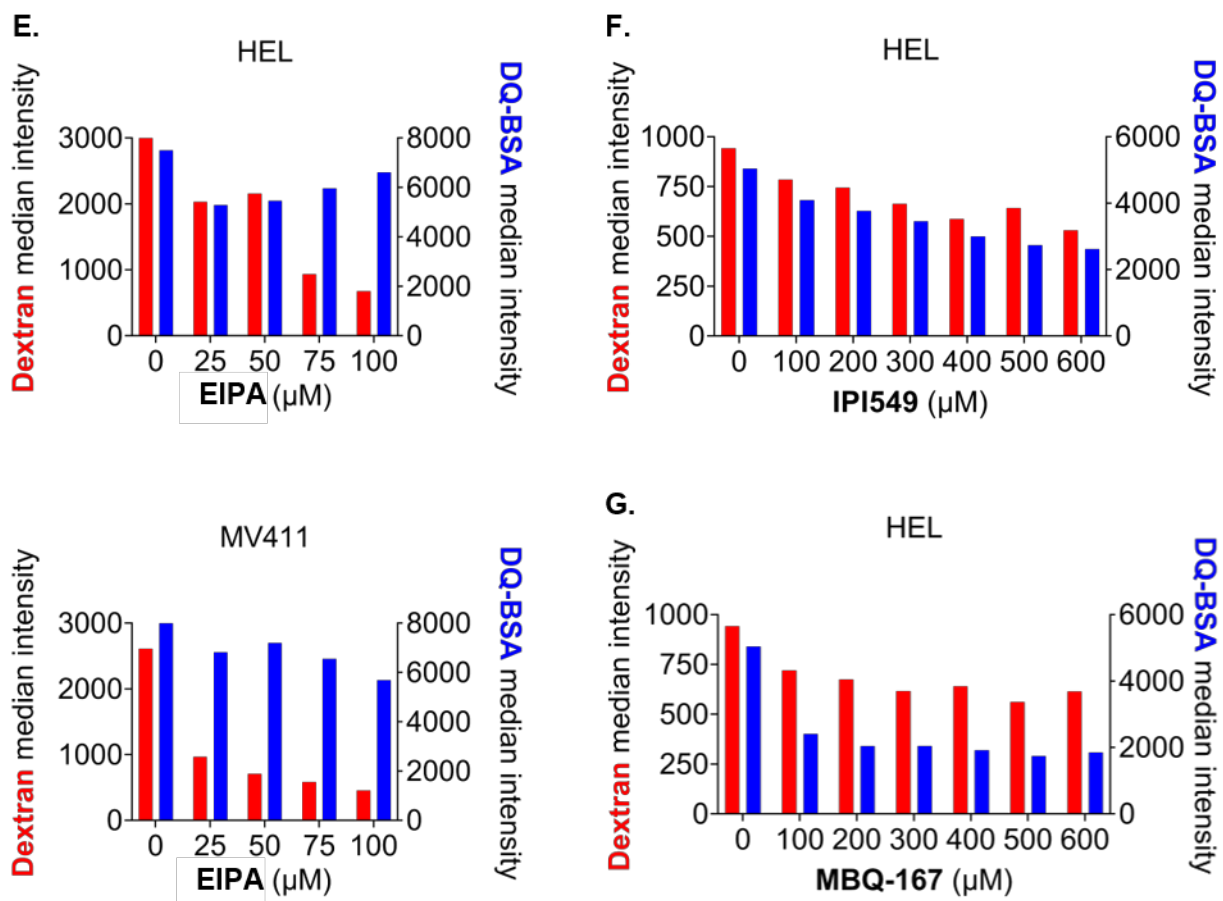
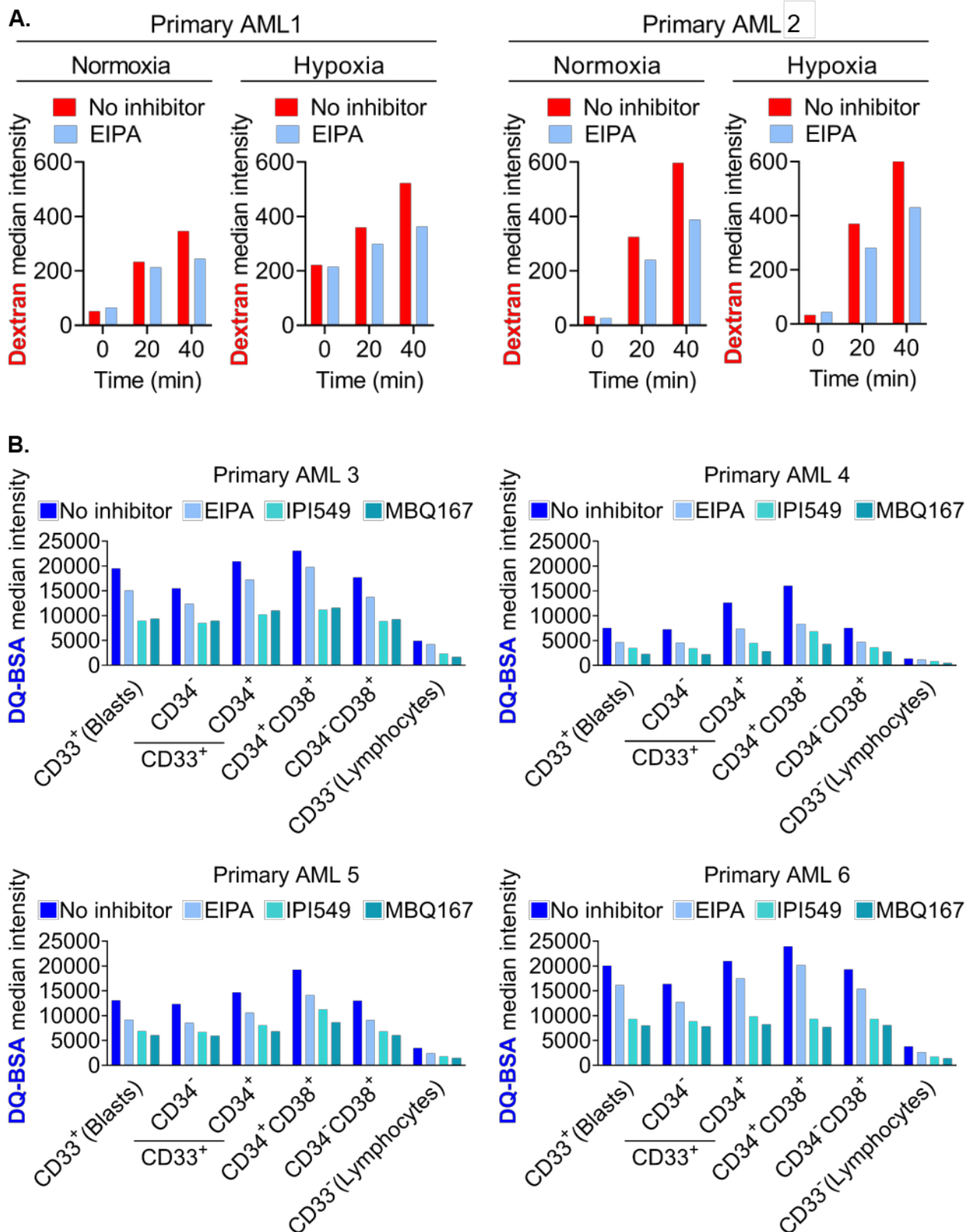


Figure 16. continued. AML cell lines conduct macropinocytosis and catabolize extracellular proteins

The effects of macropinocytosis inhibitors EIPA (E.), IPI549 (F.) and MBQ-167 (G.) on the uptake of fluorescent dextran and the uptake and proteolysis of DQ-BSA. Cells treated with EIPA were pretreated for 3 hours prior to 10 kDa dextran and DQ-BSA addition over 60 minutes. Cells treated with IPI549 and MBQ-167 were pretreated for 30 minutes prior to 70 kDa dextran and DQ-BSA addition over 60 minutes. All experiments were carried out in normoxia.

EIPA = ethyl-isopropyl amiloride; DQ-BSA = dye quenched-bovine serum albumin

Next, we validated the cell line findings in primary patient-derived AML blasts and confirmed their macropinocytic activity and the catabolism of extracellular serum protein. Primary AML blasts took up dextran in a timely manner which could partly be inhibited through the addition of EIPA (Figure 17 A). This was observed under both normoxic and hypoxic conditions. Primary AML blasts also took up and hydrolyzed DQ-BSA (Figure 17 B). Staining for CD33, CD34, C38 and CD117 markers further revealed immunophenotype-specific differences in DQ-BSA uptake/hydrolysis among subgroups of CD33⁺ AML blasts, CD34⁺CD38⁺ and CD34⁻CD38⁺ populations and the small population of CD33⁻ lymphocytes. In all tested primary AMLs, the CD33⁺ blast population showed a significantly higher accumulation of proteolyzed DQ-BSA than the CD33⁻ lymphocyte population. What was also consistent was that CD34⁺CD38⁺ population followed by CD33⁺CD34⁺ population showed the highest DQ-BSA uptake/hydrolysis activity. As observed for the AML cell lines, DQ-BSA uptake/hydrolysis in primary AMLs was inhibited only to a small degree by EIPA and more significantly inhibited by IPI549 and MBQ-167.



A. Uptake of fluorescent 10 kDa dextran by primary AMLs in serum depleted medium \pm EIPA (75 μ M), pretreated for 30 minutes. **B.** Proteolysis of DQ-BSA by immunophenotype-specific subgroups of primary AML samples. DQ-BSA was added for 30 minutes. Proteolysis was tracked under normoxic conditions in PBS supplemented with 0.5% BSA \pm EIPA (150 μ M), IPI549 (1000 μ M) and MBQ-167 (1000 μ M), pretreated for 30 minutes. AML = acute myeloid leukemia; EIPA = ethyl-isopropyl amiloride; DQ-BSA = dye quenched-bovine serum albumin

Next, we aimed to assess whether serum proteins are catabolized and metabolically used by the AML cells as a source of amino acids. For this purpose, we conducted growth experiments under varying glucose concentrations with or without the supplementation of BSA (at physiological levels (5%)). Cells that experienced reduced glucose availability (0.5 g/l instead of 2 g/l) and no metabolic substitution in the form BSA were unable to proliferate (Figure 18 A). In the presence of BSA however, cellular growth under glucose deficiency (0.5 g/l) was rescued and was similar to that under standard glucose levels (2 g/l). Also, cells under standard glucose conditions showed a further growth advantage upon BSA supplementation. These findings confirmed the metabolic utilization of BSA by AML cells.

Furthermore, it was tested whether BSA supplementation could also rescue cells lacking growth essential amino acids such as leucine and glutamine. For this purpose, cells were grown in amino acid-deficient media. As expected, in the absence of leucine cellular proliferation was markedly reduced and in the absence of glutamine cells did not survive at all (Figure 18 B). Strikingly, BSA addition rescued the effects of individual leucine and glutamine deprivation and furthermore, it alleviated the effects of their combinatorial deprivation. Even under full amino acid conditions, the addition of BSA increased cellular growth significantly.

To further evaluate to which extent extracellular proteins can provide essential amino acids for metabolic use, we assessed the impact of BSA supplementation on the cellular activation of mTOR in amino acid-deficient media. mTOR is a central regulator of cellular growth that, upon activation, drives proliferation by promoting anabolic processes like protein synthesis whilst inhibiting catabolic processes (Kim and Guan, 2019). Activation of mTOR occurs when extracellular stimuli including levels of glucose, growth factors and amino acids abundance signal favorable growth conditions (Figure 18 D). Since amino acids are essential for protein synthesis and a source of energy and carbon for multiple metabolic processes, mTOR activation is tightly bound to amino acid availability. When mTOR is active, downstream products such as p70S6K and 4EBP1 get phosphorylated. Expectedly, leucine and glutamine deprivation caused a deactivation of mTOR (p70S6K dephosphorylation), however, BSA supplementation reactivated mTOR (p70S6K phosphorylation) (Figure 18 C). mTOR activation was even more pronounced in amino acid-deficient media supplemented with BSA compared to full media without BSA. Most pronounced however was mTOR activation in full media additionally supplemented with BSA.

In summary, these observations demonstrate that AML cells take up and catabolize proteins and metabolically utilize the resulting amino acids to support cellular growth.

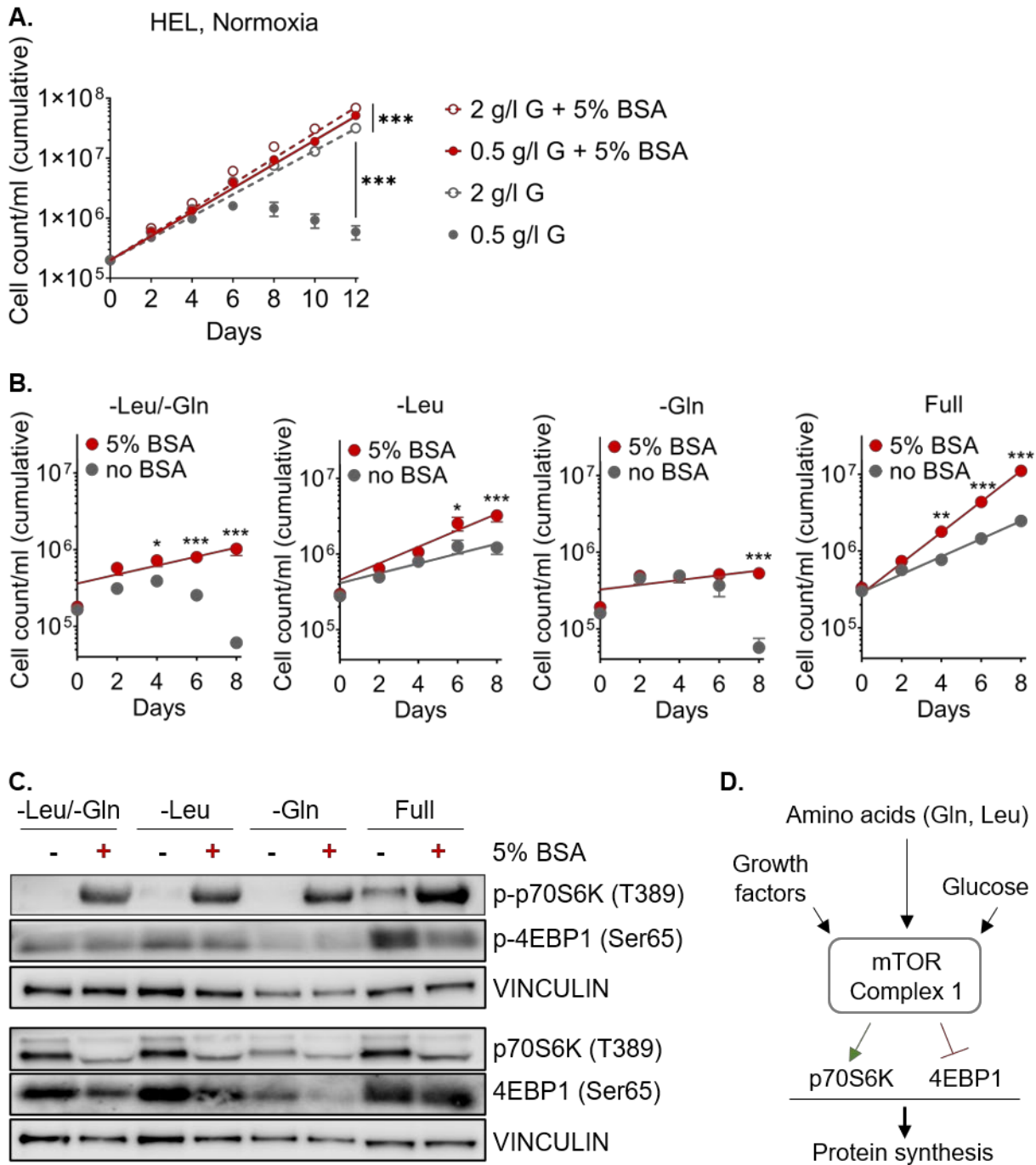


Figure 18. Extracellular albumin is taken up and metabolically utilized

A. Cellular proliferation in 1% serum-containing medium with standard (2 g/l) versus reduced (0.5 g/l) glucose concentrations supplemented with or without 5% BSA. **B.** Cellular proliferation in 1% serum-containing medium lacking essential amino acids and supplemented with or without 5% BSA. Experiment was conducted on HEL cells in normoxia. **C.** Immunoblotting of cell lysates taken from **B.** on day 8 demonstrating the (re-)activation of mTORC1 in the presence of serum protein shown by activated (phosphorylated) p70S6K. **D.** Schematic illustration of regulatory mechanisms of mTORC1. Error bars indicate mean \pm s.e.m. Statistical significance was determined by 2way ANOVA; *P,0.0243, **P,0.0065, ***P,<0.0001

G = glucose; BSA = bovine serum albumin; Leu = leucine; Gln = glutamine; p = phosphorylated; mTORC1 = mechanistic target of rapamycin complex 1; p70S6K = 70 kDa ribosomal protein S6 kinase; 4EBP1 = translation initiation factor 4E-binding protein 1

3.6 GS-mediated ammonium detoxification is important for protein-derived amino acid metabolism

The findings on the breakdown of proteins and the further deamination of the resulting amino acids in AML cells anticipate an active release of ammonium. This led us to draw a connection between protein catabolism and the previous findings on GS role in ammonium detoxification. To investigate this hypothesis, we first measured ammonium levels in bone marrow and peripheral blood samples from AML patients (Figure 19). Ammonium levels in the bone marrow of *de novo* AML patients were overall significantly higher than those in the peripheral blood where the blast count is typically lower (Figure 19 A, D). In contrast, this elevation in ammonium levels in the bone marrow was no longer observed in AML patients that had reached complete remission ($n = 15$; Figure 19 B). Whether ammonium levels in the bone marrow again increase following relapse cannot be concluded from this data and more patient data is required (current cohort: $n = 6$; Figure 19 C). Nevertheless, these data support our hypothesis of increased ammonium production in AML cells which might be linked to an increased protein turnover.

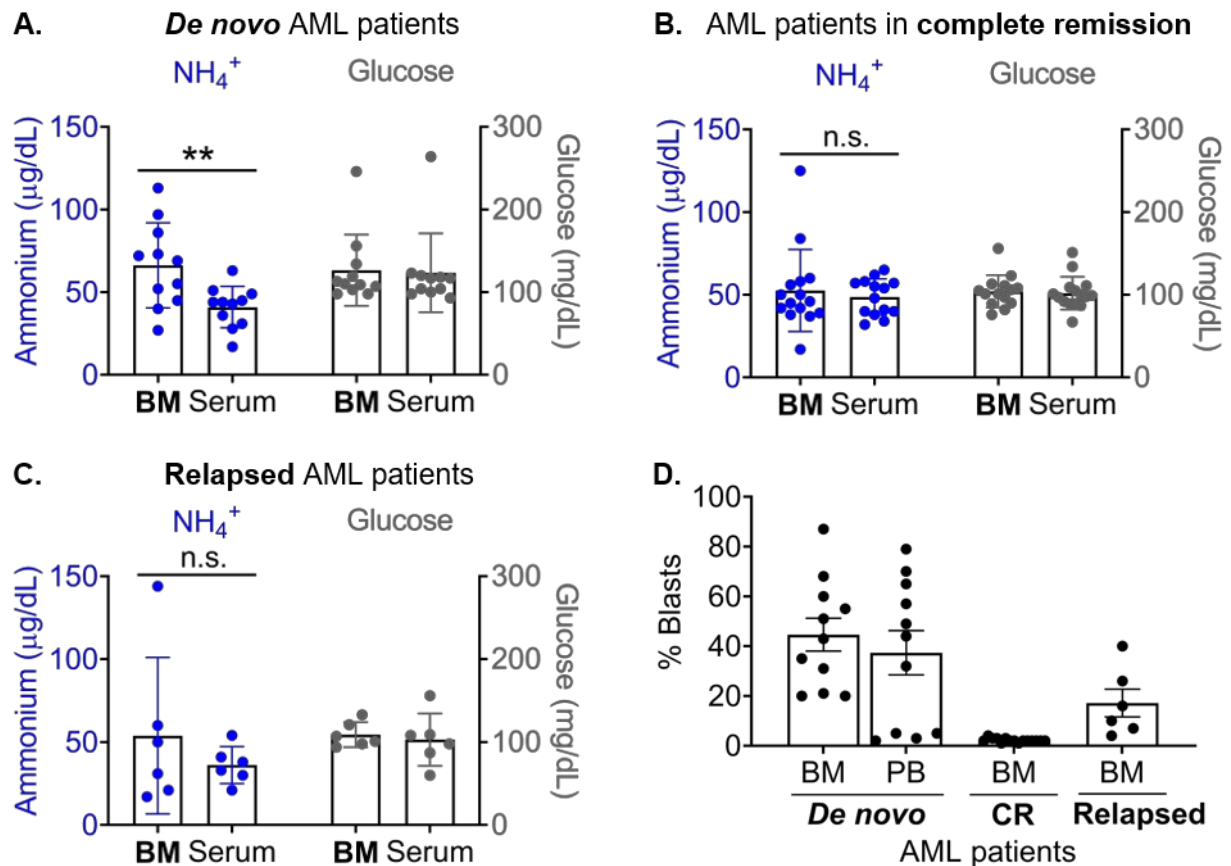


Figure 19. Elevated ammonium levels in AML bone marrow

Grouped ammonium and glucose levels in **A.** *de novo* AML patients ($n = 11$), **B.** AML patients in complete remission ($n = 15$) and **C.** relapsed AML patients ($n = 6$). Bone marrow and peripheral blood samples were withdrawn from AML patients where ammonium and glucose levels were measured immediately. Error bars indicate mean \pm s.e.m. Statistical significance was determined by paired t test; $**P, 0.0087$. **D.** Percentage of blasts in the bone marrow and peripheral blood of AML patients shown in **A.- C.** taken at the time of ammonium measurement. AML = acute myeloid leukemia; BM = bone marrow; n.s. = not significant; PB = Peripheral blood; CR = complete remission

To establish the link and the interdependence between GS and protein catabolism, we assessed the impact of GS inhibition on extracellular protein uptake and proteolysis. Therefore, DQ-BSA uptake and proteolysis was tested in the presence of L-methionine sulfoxamine (MSO), a GS-specific inhibitor (Ronzio and Meister, 1967). Interestingly, increasing concentrations of the GS inhibitor (0 - 16 mM) caused decreasing uptake and proteolysis of DQ-BSA (Figure 20 A). Likewise, increasing concentrations of ammonium chloride (0 - 20 mM) significantly decreased DQ-BSA uptake and proteolysis (Figure 20 B). Importantly, this blockade was not due to decreased cell viability or toxicity (as measured by Cell Titer Glo and CellTox Green assays), and therefore, it can be suggested that GS functionality is a prerequisite for the activation of protein catabolism.

If GS deficient cells were indeed less able to utilize BSA compared to GS expressing cells, then GS expressing cells should overgrow GS deficient cells at a faster rate in a competition assay when provided with BSA (given earlier results on the growth boosting effect of BSA). To test this, HEL NTC, Ge3 and GPP cells were each mixed in 1:1 ratio with HEL wildtype cells and cultured in 1% serum supplemented media, both in the presence and absence of 5% BSA (Figure 20 C). Expectedly, the results showed an additional significant reduction in the ability of the GS-deficient GPP cells to compete against the GS expressing cells in the presence of 5% BSA. Similar results were found for GS-deficient Ge3 cells, which due to less efficient GS depletion were overgrown at a slower rate (for GS knockout efficiencies see Figure 7 A). The same results were reflected by NTC, Ge3 and GPP specific growth curves that could be determined from the FACS data and the cell counts that were taken every second day (Figure 20 D). The growth of the NTC population slightly increased in the presence of 5% BSA, while the addition of protein had the opposite effect on the growth of both Ge3 and GPP populations.

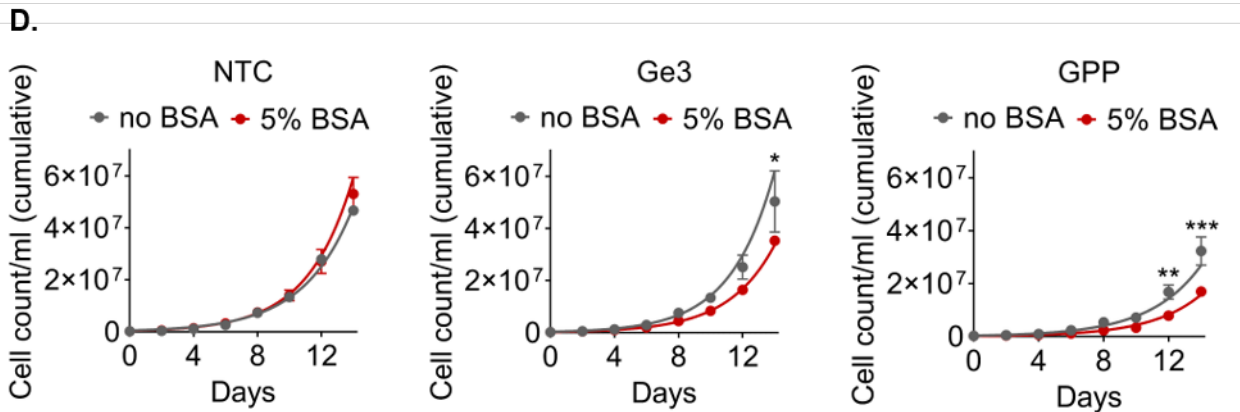
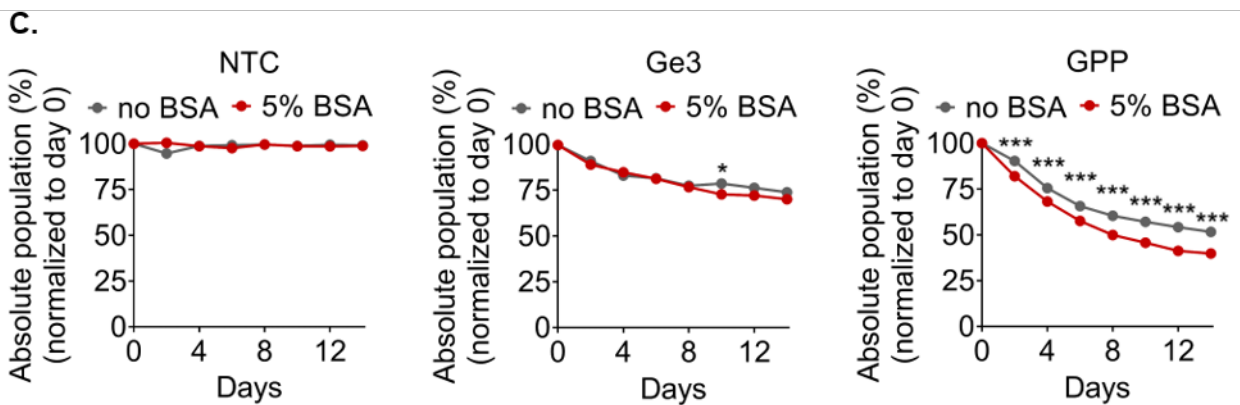
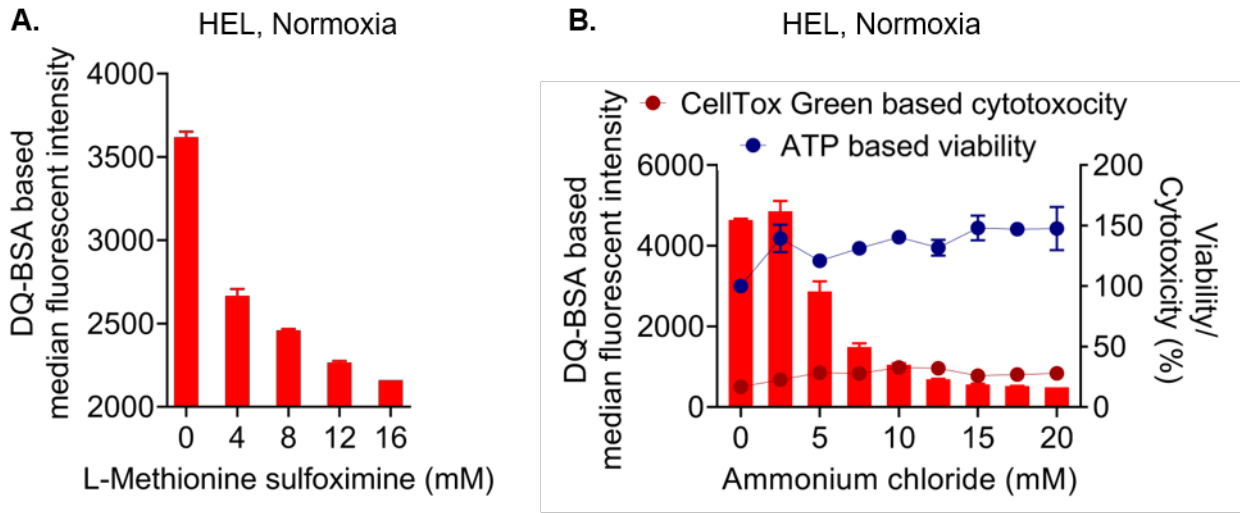


Figure 20. GS is essential for BSA proteolysis

A. Impact of L-methionine sulfoximine (pretreated for 6 days) on the uptake and proteolysis of DQ-BSA (1 $\mu\text{g/ml}$) after 24 hours. **B.** Impact of ammonium chloride on the uptake and proteolysis of DQ-BSA (1 $\mu\text{g/ml}$), on cell viability (based on ATP) and cytotoxicity (based on Cell Tox Green assay) after 24 hours. **C.** Impact of BSA supplementation (5%) on GS-negative cell growth as determined by the competition growth assay in normoxia. **D.** Cumulative growth curves of NTC, Ge3 and GPP populations in the presence and absence of 5% BSA as determined from cell counts and FACS analysis shown in **C.**

Error bars indicate mean \pm s.e.m. Statistical significance was determined by 2way ANOVA; *P,0.0404 (C.), *P,0.0352 (D.), **P,0.0700, ***P,<0.0001.

DQ-BSA = dye quenched-bovine serum albumin; Ge3 = Guide 3

To gain further insights into the specific role of GS in the utilization of protein, mechanistical studies were performed to elucidate GS involvement in the removal of ammonium. For this purpose, ¹⁵N-labeled amino acids (in the form of *Arthrospirulina maxima* cell extracts) were added to both NTC and GPP cells and NMR experiments were performed to assess site-specific ammonium incorporation into glutamine (Figure 21 A). (The ¹⁵N-labeled amino acids did not contain ¹⁵N-labeled glutamine (for cell extract preparation see Appendix 7.1)). Indeed, GS-expressing NTC cells generated ¹⁵N-labeled glutamine (on the side chain amino group) upon the addition of ¹⁵N-labeled amino acids by incorporating amino acid-derived ¹⁵N-ammonium into glutamate (Figure 21 B). In contrast, this side chain ¹⁵N-labeled glutamine was not detected in the GS-depleted GPP cells (Figure 21 C, D). The presence of ¹⁵N-labeled α amino groups in both NTC and GPP cells further revealed that the labeled amino acids had been imported into the cells independent of GS expression and that therefore it was not a lack of amino acid uptake that led to the absence of ¹⁵N-labeled glutamine in the GS-depleted cells.

Altogether, these findings confirm the active role of GS in detoxifying ammonium produced during the breakdown of amino acids and hence during the utilization of proteins. It would be further interesting to also confirm this observation using ¹⁵N- and ¹³C-labeled proteins were to be used it could be additionally traced through NMR-based metabolic flux analysis whether deaminated protein-derived amino acids enter the TCA cycle or are used for other metabolic processes.

It would have further been of interest to measure the difference in the intracellular ¹⁵N-labeled ammonium between the control and GS-knockout cells to assess whether GS-knockout cells indeed display an increase in ammonium levels, however, NMR was not suitable to detect ammonium due to the rapid exchange of the NH₄⁺ protons.

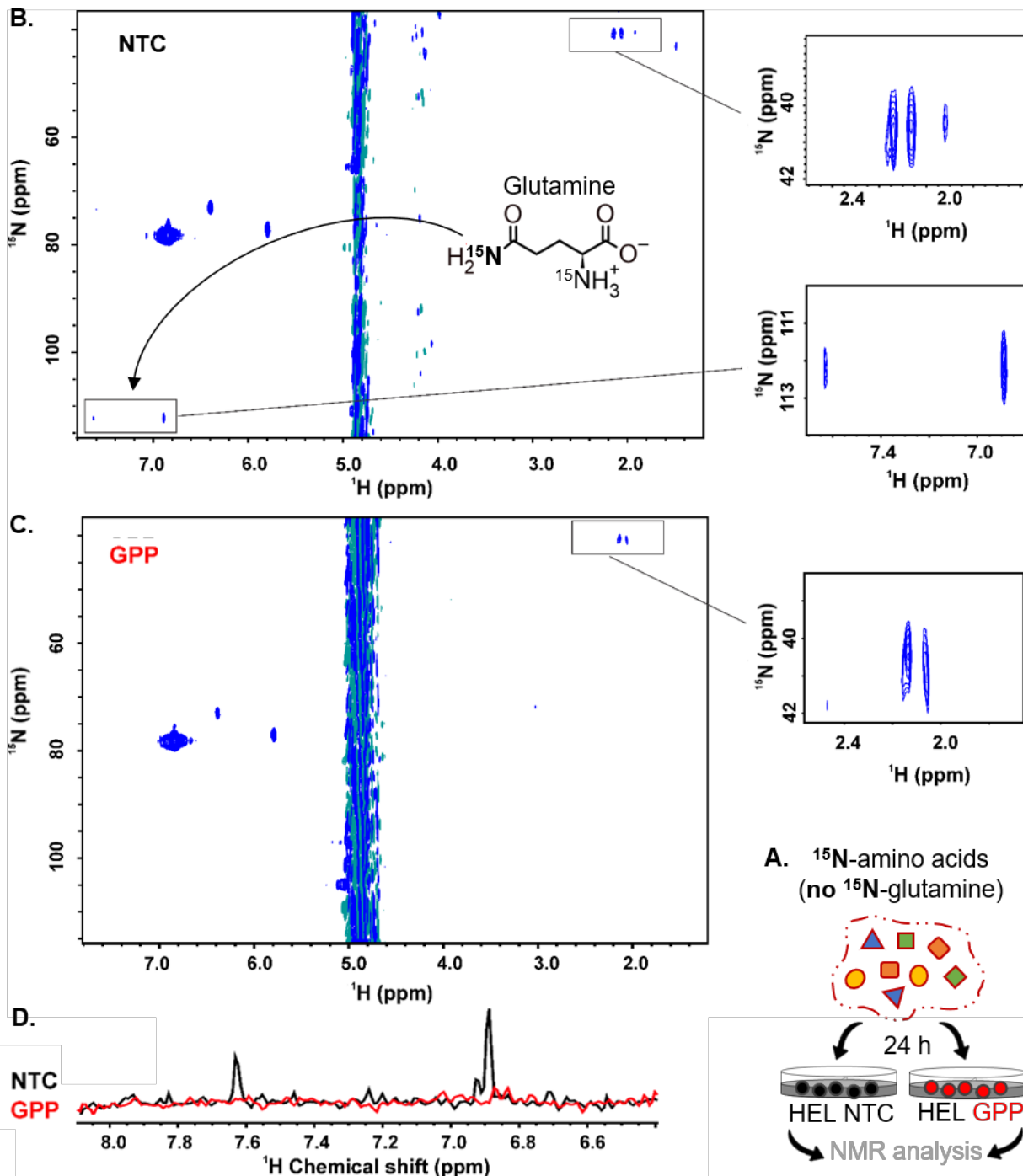


Figure 21. Ammonium released during the breakdown of ^{15}N -labeled hydrolysates is scavenged by GS

A. Schematic of feeding experiment in HEL NTC and GPP cells with 2% ^{15}N -labeled *Arthrospirulina maxima* hydrolysates containing ^{15}N -labeled amino acids (but not ^{15}N -labeled glutamine). The experiment was conducted in normoxia over 24 hours ($n = 2$). **B./C.** 2D ^1H - ^{15}N HSQC NMR spectra of HEL NTC cells (**B.**) and GPP cells (**C.**) fed with 2% ^{15}N -labeled *Arthrospirulina maxima* hydrolysates as described in **A.** (The respective spectrum is representative for both duplicates.) For peak assignment, refer to Figure 13. **D.** Overlay of 1D projections of the glutamine side chain amino group signals from the 2D NMR spectra shown in **B./C.** NMR spectra were recorded on a AV950 MHz Bruker spectrometer using the pulse program hsqcetf3gp (number of points: 2048 /110; number of scans: 1024; acquisition mode: non-uniform sampling (25%); temperature: 25°C)

NMR = nuclear magnetic resonance; NTC = non-target control; h = hours

3.7 The adaptive role of the urea cycle/arginine biogenesis pathway upon GS deletion

The results presented in section 3.2 confirmed both sgRNA- and shRNA-mediated GS deficiency to significantly reduce the growth of AML cells (Figure 7, Figure 8). Nevertheless, after prolonged periods post-transduction (> 3 months), this growth disadvantage diminished (Figure 22 A). We confirmed that these adapted GPP cells did not lose their GS knockout (Figure 22 B). This implicated cellular adaptation to GS deficiency to have had taken place in the adapted GPP cells and prompted investigations into the process that had induced the adaptation. In order to examine differences between the adapted NTC and GPP cells, a wide array of metabolites was analyzed in a mass spectrometry Metabolon study. No differences were observed in the intracellular glutamine, glutamate and α KG levels (Figure 23 D, E). Nevertheless, a significant upregulation of urea cycle/arginine biosynthesis metabolites was found in the adapted GPP cells including ornithine, citrulline and arginine (Figure 23 B, C).

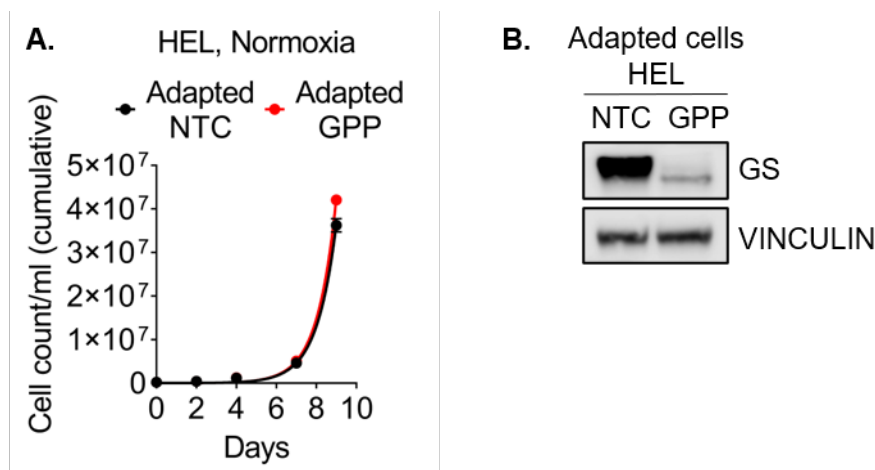


Figure 22. After long-term culturing GS-knockout cells adapt and resume a normal growth behaviour

A. Cumulative growth curves of adapted HEL cells (> 3 months adaption) under normoxic conditions in 300 mg/l glutamine containing medium. Error bars indicate mean \pm s.e.m. **B.** Western blot confirmation of GS knockout in adapted GPP cells shown in **A.**. GS = glutamine synthetase; NTC = non-target control

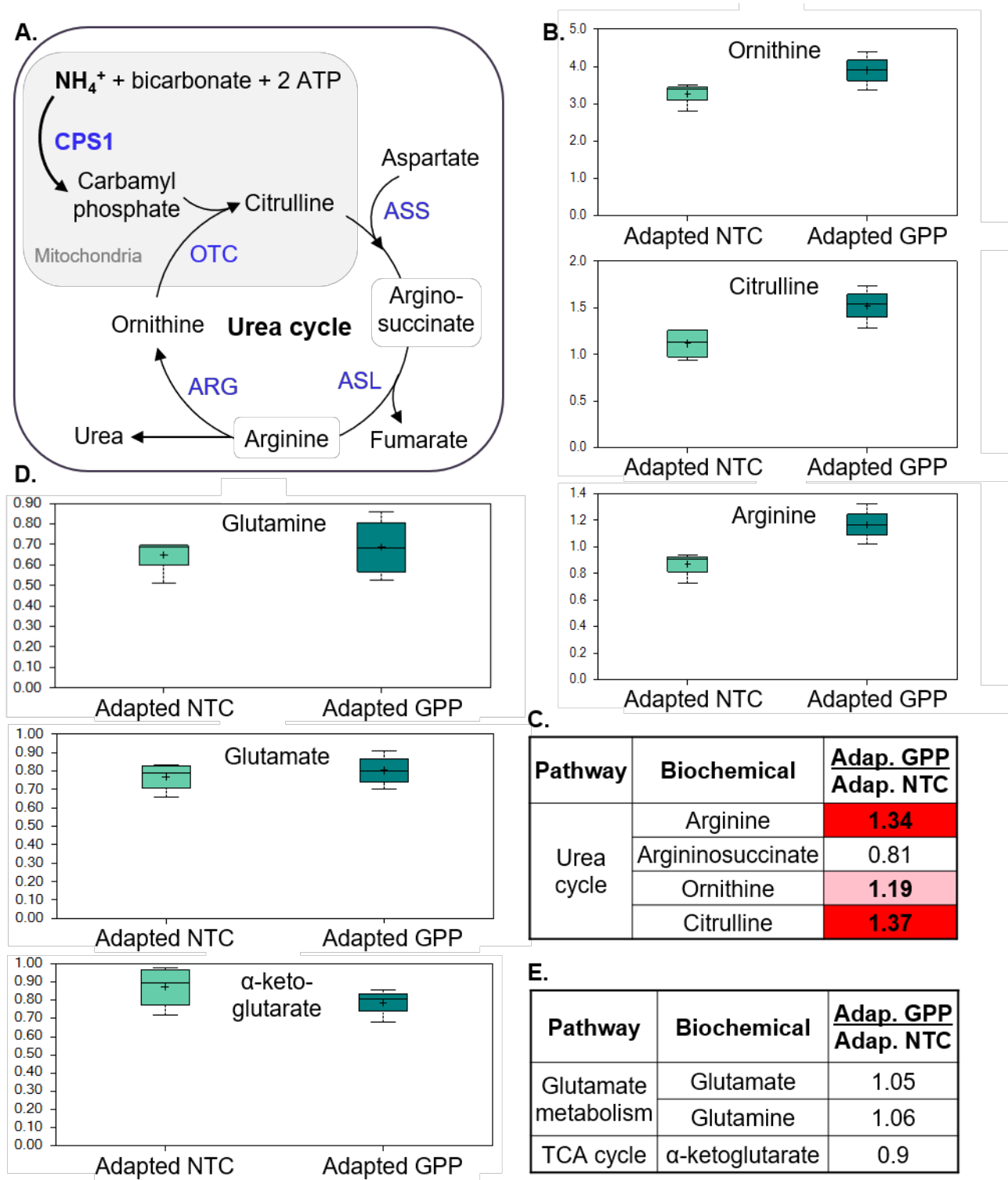


Figure 23. Adapted GS-knockout cells exert high urea cycle/arginine biogenesis activity

A. Urea cycle, active predominantly in the liver, is an important pathway for the removal of ammonium. **B.-E.** Metabolon analysis was conducted on long-term cultured (> 3 months) adapted THP1 NTC and GPP cells in 300 mg/l glutamine containing medium in hypoxia (n = 4). Indicated are median values of the intensity with minimum and maximum of distribution. Statistical significance (red) was determined by Welch's unequal variances t-test; p≤0.05 **B./C.** Urea cycle intermediates including ornithine, citrulline and arginine are upregulated in adapted THP1 GPP cells compared to the NTC cells. **D./E.** Glutamine, glutamate and α-ketoglutarate levels are unchanged in adapted THP1 NTC and GPP cells. ATP = adenosine triphosphate; CPS1 = carbamoyl phosphate synthetase 1; OTC = ornithine transcarbamoylase; ASS = argininosuccinate synthetase; ASL = argininosuccinate lyase; ARG = arginase

Since the urea cycle (which largely overlaps with the arginine biosynthesis pathway (shown in Figure 23 A)) represents an alternative route of ammonium scavenging, upregulated urea cycle intermediates in the adapted GPP cells hinted towards an increased ammonium turnover through urea cycle enzymes. CPS1 is the gatekeeper enzyme of the urea cycle which binds ammonium to bicarbonate in an ATP-dependent reaction (Figure 23 A). To further investigate its compensatory role in ammonium scavenging shortly upon GS knockout (< 2 weeks) as well as after adaptation, we performed a CRISPR Cas9 knockout with sgRNA targeting CPS1 (Figure 24 A). Additionally, we also overexpressed CPS1 in a different setting. Indeed, a knockout of CPS1 in adapted NTC and GPP cells as well as in freshly transfected NTC and GPP cells significantly decreased the tolerability towards ammonium (Figure 24 B). Strikingly, the adapted GPP^{NTC} cells exerted a different phenotype. They were significantly less sensitive towards ammonium compared to their corresponding adapted control. CPS1 knockout in the adapted GPP cells decreased their ammonium sensitivity however, to a level that similar to the adapted control cells (without GPP or CPS1 knockout). In contrast to the CPS1 knockout, CPS1 overexpression in freshly transfected NTC and GPP cells did not significantly change the tolerability towards ammonium.

Next, cumulative growth assays were conducted to evaluate whether the change in ammonium sensitivity upon changes in CPS1 expression would influence cellular growth. However, neither CPS1 knockout nor CPS1 overexpression affected the growth of freshly transfected cells, neither that of NTC cells nor that of GPP cells (Figure 24 C). A slight change in growth was observed upon CPS1 knockout in the adapted cells, however, this affected adapted NTC and GPP cells equally.

Altogether, the observation of decreased ammonium tolerance upon CPS1 knockout, especially in the adapted cells, suggests that CPS1 plays a role in the adaptation process. Nevertheless, the data remains inconclusive considering that no rescue effect was observed upon CPS1 overexpression. Further investigation is needed to address this aspect and to understand the driving mechanism behind the increased ammonium tolerance in adapted GS-knockout cells.

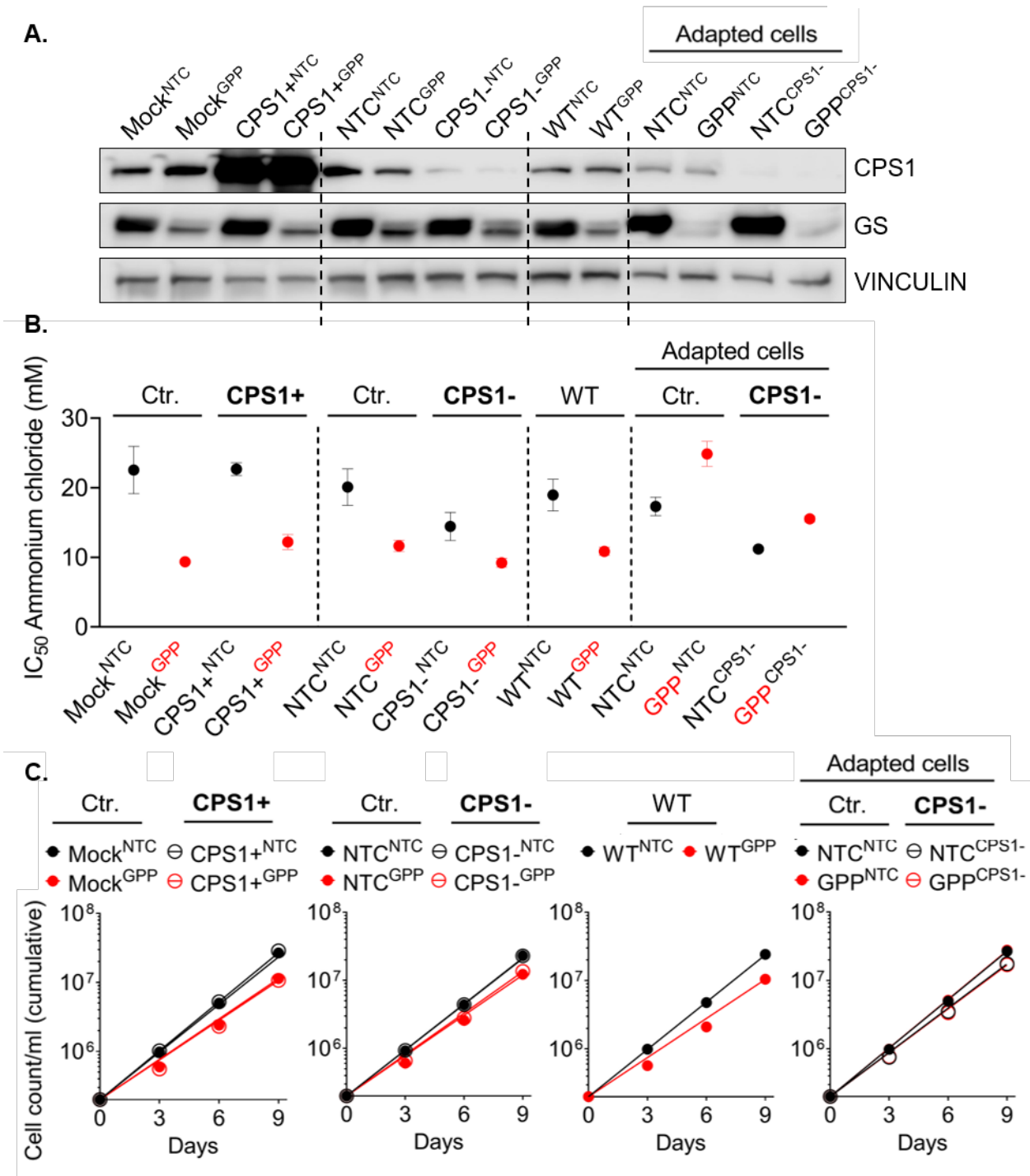


Figure 24. CPS1 overexpression does not rescue GS knockout-induced growth disadvantage

A. CPS1-overexpressing, CPS1-knockout and the respective control HEL cells were additionally transfected with NTC sgRNA and GPP sgRNA, as were wildtype cells. Previously generated and long-term cultured NTC and GPP cells (termed 'adapted' cells) were transfected with a sgRNA targeting CPS1 and a control sgRNA. **B.** Ammonium chloride IC_{50} determination in cells generated in **A.** IC_{50} s were determined after 72 hours from ATP-based cell viability assays. Statistical significance was determined by 1way ANOVA; $***P, < 0.0001$. **C.** Cumulative growth curves of cells generated in **A.** as determined from cell counts. Error bars indicate mean \pm s.e.m. CPS1 = carbamoyl phosphate synthetase 1; CPS1+ = CPS1 overexpression; CPS1- = CPS1 knockout; GS = glutamine synthetase; NTC = non-target control; WT = wildtype; ctr. = control

4 Discussion

4.1 The function of GS is relevant for the metabolism of endocytosed proteins

AML cells have a metabolic dependency for the amino acid glutamine (reviewed in Kreitz *et al.*, 2019). Several regulators of glutamine metabolism including glutaminase and the high-affinity glutamine transporter SLC1A5 have been identified as important metabolic players in AML (Bromley-Dulfano *et al.*, 2013; Willems *et al.*, 2013; Matre *et al.*, 2016). GS, the only enzyme capable of *de novo* glutamine synthesis, however, has gained little attention in AML research (or leukemia research in general). Here, we showed that AML cells require GS for cellular growth *in vitro* (Figure 7) and that GS depletion impairs leukemia progression *in vivo* (Figure 8). Interestingly, we found that AML cells depend on GS even in the presence of excess amounts of glutamine (Figure 9). This is in contrast to most solid cancers where the dependency on GS has been shown to be limited to conditions of glutamine starvation and where GS hence serves primarily the provision of glutamine (Kung, Marks and Chi, 2011; Bott *et al.*, 2015, 2019; Tardito *et al.*, 2015; Issaq *et al.*, 2019; for an overview of GS functions in different cancer types see Table 4). Functional studies revealed that the prime function of GS in AML instead serves the detoxification of ammonium (Figure 10).

To fulfill the requirements for amino acids including glutamine, we could show that AML cells endocytose extracellular proteins which provide amino acids upon protein catabolism (Figure 18). Endocytosis of proteins and their subsequent metabolism create large amounts of ammonium ions, making their removal an important task for leukemia maintenance. Here, we revealed that GS fulfills this role in AML by detoxifying ammonium released upon protein and amino acid breakdown (Figure 21) and that GS is hence required for the metabolism of endocytosed proteins.

In cancer, the removal of ammonium upon protein and amino acid catabolism has not been investigated, although several malignancies have been identified to feed on extracellular proteins especially under nutrient starvation (reviewed in Commisso, 2019). However, there are some hints that point towards a potential link between GS and protein catabolism also in other tumors.

The cancer most studied in regard to catabolism of endocytosed proteins is pancreatic cancer (Commisso *et al.*, 2013; Kamphorst *et al.*, 2015; Davidson *et al.*, 2017). Interestingly, GS expression is consistently elevated in human pancreatic cancer and in several pancreatic ductal carcinoma (PDAC) mouse models (Bott *et al.*, 2019). Deletion of GS in the PDAC mouse model derived cell line KPC revealed that these cells depend on GS for cellular growth. This

however accounted only for conditions of glutamine starvation. Under these conditions, GS was shown to mediate ammonium detoxification.

As protein catabolism in pancreatic cancer cells was only shown under glutamine starvation (Commisso *et al.*, 2013) and glutamine starvation was identified to drive protein uptake in PDAC cells (Lee *et al.*, 2019), the role of GS in ammonium detoxification during endocytosed protein catabolism might only be important when the PDAC cells lack glutamine and switch to extracellular protein metabolism. It would be of interest to test the dependency of pancreatic cancer cells on GS in the presence and absence of extracellular proteins under glutamine starvation. This would reveal whether the dependency on GS is linked to protein catabolism as we show here for AML.

Similar to pancreatic cancer, also non-small cell lung cancer (NSCLC) relies on extracellular proteins under nutrient starvation (Hodakoski *et al.*, 2019). Interestingly, also in NSCLC GS is highly expressed (Yuneva *et al.*, 2012). Similar to what we observed for AML, GS depletion blocks NSCLC cell growth even under glutamine sufficient conditions (Zhao *et al.*, 2019). Therefore, GS seems to serve a different role in NSCLC rather than as glutamine provider. In light of the fact that NSCLC cells catabolize extracellular proteins, it can be speculated that, similar to AML, NSCLC cells require GS for ammonium detoxification to metabolize endocytosed proteins.

Another potential link between protein catabolism and GS could be observed in HeLa cells (Albrecht *et al.*, 2020). Here, it was shown that glycogen synthase kinase 3 inhibition induces macropinocytosis and metabolization of extracellular proteins. Extracellular protein catabolism led to significantly increased intracellular glutamine levels while levels of glutamate slightly decreased. This might indicate that also here GS is active in removing the protein-derived ammonium which would explain the increase in glutamine while the substrate of GS, glutamate, was slightly decreased.

The importance of GS has been shown not only in malignant cell proliferation, but also in embryonic development. GS deficiency was shown to be embryonically fatal at early stages of development (He *et al.*, 2007). Studies on mouse embryos showed that when embryos transition from the uterine tube to the harsher uterine environment, they catabolize amino acids to produce energy, and that is where GS importance lies: detoxifying the resulting ammonium. As congenital GS deficiency in humans is extremely rare (only four cases have been reported so far (reviewed in Spodenkiewicz *et al.*, 2016; Ünal *et al.*, 2018)), it is likely that GS fulfills a similar function in human embryogenesis.

In summary, GS serves various functions in different malignancies and our study was the first to identify the functional relevance of GS in the scavenging of protein and amino acid-derived ammonium. While there are some indications that GS plays a similar role in other malignancies and cells that feed on extracellular proteins, further research is necessary to confirm this.

Table 4. Expression and functional role of GS in different types of cancer

Cancer type	GS expression	Functional role	Reference
AML	High upon L-asparaginase treatment	Resistance towards L-asparaginase in some AML	Willems <i>et al.</i> , 2013
ALL	High upon glucocorticoid treatment	Possibly ammonium scavenging	Dyczynski <i>et al.</i> , 2018
Brain	High expression associated with lower overall survival ¹ ; Varies among tumors, did not predict overall survival ²	Nucleotide biosynthesis especially under glutamine starvation ²	¹ Rosati <i>et al.</i> , 2013 ² Tardito <i>et al.</i> , 2015
Breast	Lineage-specific: high in luminal and low in basal cells ¹ ; High expression associated with large tumor size and lower overall survival ²	Luminal cells provide glutamine to basal cells ¹ p38 MAPK and ERK1/ERK2 signaling pathway activation ²	¹ Kung <i>et al.</i> , 2011 ² Wang <i>et al.</i> , 2017 ³ Spinelli <i>et al.</i> , 2017
Liver	Overall high ^{1,2,3} ; High expression associated with lower overall survival ⁵	Not significantly involved in ammonium recycling ³ Mediating autophagy ⁴ Mediating epithelial-mesenchymal transition and promoting metastasis ⁵	¹ Christa <i>et al.</i> , 1994 ² Long <i>et al.</i> , 2010 ³ Long <i>et al.</i> , 2011 ⁴ Sohn <i>et al.</i> , 2018 ⁵ Liu <i>et al.</i> , 2019
Lung	High in gefitinib-sensitive cells	Mediating increased glutamine anabolism, sensitizing cells to gefitinib	Wang <i>et al.</i> , 2018
Ovary	High in low-invasive tumors, high expression associated with better overall survival ¹ ; High in aggressive tumors ² ; Varies among tumors, high expression associated with lower overall survival ³	Glutamine anabolism ¹ Possibly ammonium scavenging ² p38 MAPK signaling pathway activation ³	¹ Yang <i>et al.</i> , 2014 ² Kitajima <i>et al.</i> , 2017 ³ Fan <i>et al.</i> , 2018
Pancreas	Overall high	Nucleotide biosynthesis under glutamine starvation	Bott <i>et al.</i> , 2019
Prostate	Overall high		Shi <i>et al.</i> , 2014
Sarcoma		Resistance towards L-asparaginase ¹ Nucleotide biosynthesis and mitochondrial bioenergetics under glutamine starvation ²	¹ Tardito <i>et al.</i> , 2007 ² Issaq <i>et al.</i> , 2019
Myc-driven	Tissue-specific: low in liver and high in lung tumours ¹ ; High in varies Myc-upregulated cancer cells ²	Nucleotide/protein biosynthesis and amino acid uptake ²	¹ Yuneva <i>et al.</i> , 2012 ² Bott <i>et al.</i> , 2015

GS = glutamine synthetase; AML = acute myeloid synthetase; ALL = acute lymphoid leukemia

4.2 The adaptive role of the urea cycle/arginine biogenesis pathway upon GS deletion

In the current work we further observed a common feature of cancer cells - metabolic reprogramming. After prolonged culturing of the GPP GS-knockout cells (> 3 months), the cells underwent metabolic reprogramming and adapted to the loss of GS. Tumor cells frequently undergo metabolic adaptation to adapt to intracellular and extracellular changes and to enable continuous growth (Vander Heiden and Deberardinis, 2017). Several studies have described how metabolic rewiring can lead to drug resistance in AML (Gallipoli *et al.*, 2018; van Gastel *et al.*, 2020; reviewed in Knoechel and Aster, 2015 and Vidal *et al.*, 2018). Here, we observed that the adapted GPP cell population resumed a growth behavior similar to that of the control cells (Figure 22 A) without losing GS knockout (Figure 22 B) or having compensated by importing higher glutamine levels (Figure 23 D). These findings suggest that adapted GS-knockout cells acquired an alternative route of ammonium detoxification.

In human cells, two other enzymes exist next to GS that bind and hence detoxify ammonium: GDH and CPS1/2. Analysis of the fate of ¹⁵N-ammonium in wildtype AML revealed ammonium detoxification to also occur through the reductive amination of α KG catalyzed by GDH (Figure 11 C, see Figure 12 for the GDH reaction), an enzyme found upregulated in many AML subtypes (Matre *et al.*, 2016). GDH is of bidirectional nature and occupies a pivotal role between carbon and nitrogen metabolism (Friday *et al.*, 2012). In AML, like in many other cancers, GDH has been described to be of a significance in carbon metabolism, specifically in the process of glutaminolysis and TCA anaplerosis (Matre *et al.*, 2016; Plaitakis *et al.*, 2017). The current data showed GDH to largely catalyze the opposite direction synthesizing glutamate from α KG and ammonium. It might have been the supraphysiological concentrations of ammonium and the need to maintain pH homeostasis that drove the GDH reaction towards glutamate production and hence nitrogen metabolism rather than carbon metabolism. Nevertheless, it demonstrated that GDH, next to GS, can also play a pivotal role in ammonium detoxification in AML. However, we observed no contribution of CPS1 to ammonium detoxification in AML cells. (The urea cycle intermediate arginine was not labeled and the relative abundance of ¹⁵N-ornithine/citrulline resembled almost exactly that of GDH-derived ¹⁵N-glutamate (Figure 11, Figure 15).)

Since GS is typically located in the cytoplasm (Labow *et al.*, 2001) and GDH is dominantly located in the mitochondria (Mastorodemos *et al.*, 2009; Plaitakis *et al.*, 2017), ammonium detoxification in wildtype AML cells is most likely dictated by the location of ammonium inside the cell. This notion was supported by the finding that ¹⁵N-ammonium and exclusively non-labeled glutamate were the substrates for GS-derived ¹⁵N-glutamine, although, GDH-derived ¹⁵N-glutamate was vastly present in the cell (Figure 11, Figure 13).

Nevertheless, the picture was different for adapted GS-knockout cells. These cells relied on a compensatory role of the urea cycle/arginine biogenesis pathway in ammonium removal, which we confirmed in the Metabolon analysis (higher urea intermediates levels in adapted GPP cells; Figure 23 B, C). The upregulation of urea cycle intermediates in the adapted GPP cells suggested that upon the loss of GS, ammonium was shuffled into the urea cycle/arginine biogenesis pathway through the activity of CPS1. These findings are novel since no role of the urea cycle/arginine biosynthesis enzymes in ammonium scavenging has been described before in AML.

Here, a knockout of CPS1 showed its contribution to ammonium removal in AML. Deletion of CPS1 decreased ammonium tolerability most significantly in the adapted GPP cells (Figure 24 B) confirming that CPS1 contributes to a greater extent to ammonium detoxification in GS depleted cells and hence possibly causes the observed adaptation. An upregulation of CPS1 on protein level was however not detected in the adapted GPP cells (Figure 24 A). Unlike a knockout of CPS1, an overexpression of the enzyme did not change the tolerability towards ammonium in the cells (Figure 24 B). Likewise, CPS1 overexpression did not affect cell growth of the GPP cells and hence failed to rescue the GS deficient GPP cells (Figure 24 C). It is possible that a CPS1 overexpression alone cannot rescue cells due to a lack of activity of the other urea cycle enzymes such as ASS1 which is expressed at very low levels in AML (Miraki-Moud *et al.*, 2015; Mussai *et al.*, 2015). Nevertheless, we excluded that this failure to rescue is due to the mitochondrial localization of CPS1, and hence its inability to scavenge cytosolic ammonium. We overexpressed CPS1 in the cytosol through the deletion of the N-terminal mitochondrial signal sequence and still saw no rescue effect on GPP cells (data not shown).

In summary, our data demonstrate the urea cycle/arginine biogenesis pathway and specifically CPS1 to compensate for the loss of GS in adapted GPP cells and to serve as alternative ammonium scavenger. Nevertheless, the data remain inconclusive. Further experiments should evaluate whether adapted GPP cells indeed no longer show an increased ammonium secretion. Additional factors, possibly involving other components of the urea cycle, should be studied for their role in the adaptation mechanism of the GPP cells.

4.3 AML cells conduct macropinocytosis and metabolize protein-derived amino acids

Macropinocytosis is an ancient process that evolved more than 1.5 billion years ago in ancestral organisms like amoebozoans and opisthokonts as a means of nutrient uptake (King and Kay, 2019). For the first time in 2013, it was shown that also Ras-driven pancreatic cancer cells conduct the energetically costly process of macropinocytosis (Commisso *et al.*, 2013). Upon the macropinocytosis-driven uptake of extracellular fluid, cancer cells internalize large quantities of nutrients mostly in the form of protein, but also lipids and nucleotides, which they feed into metabolic processes (for reviews on the role of macropinocytosis in cancer see Palm, 2019 and Zhang and Commisso, 2019). Multiple publications have followed since, revealing macropinocytosis to be a common route of nutrient supply across solid tumors transformed by oncogenic Ras or Src, including bladder (Redelman-Sidi *et al.*, 2013), prostate (Kim *et al.*, 2018) and lung cancers (Hodakoski *et al.*, 2019b). Oncogenic Ras triggers constitutive macropinocytosis activity by stimulating processes that lead to actin polymerization and membrane ruffling including Rac, Cdc42, PI3K, and Raf/Erk activation (Recouvreux and Commisso, 2017b). Likewise, also oncogenic Src reorganizes the actin cytoskeleton resulting in constitutive macropinocytosis activation in a PI3K dependent manner.

While macropinocytosis in cancer cells is a relatively novel field of research, it has long been known to be conducted by innate immune cells that adapted the ancient process as a means of improved immune defense (Canton, 2018). Unlike in cancer cells, the primary role of macropinocytosis in dendritic cells and macrophages is not to satisfy their metabolic needs but to scan their environment for indicators of infection. In this regard macropinocytosis mediates non-specific uptake of soluble antigens for improved antigen presentation in dendritic cells (Liu and Roche, 2015) and allows pathogen and danger-associated molecule uptake in macrophages (Doodnauth *et al.*, 2019). The metabolic use of macropinocytically internalized nutrients in those cells has gained far less attention. In general, little is known about the role of macropinocytosis in supplying nutrients to non-transformed cells which normally rely on membrane transporters for the uptake of nutrients. A recent advance in this regard has been a study by Charpentier *et al.*, 2020 on T lymphocytes that showed activation of T cells to lead to a rapid increase of macropinocytically-driven protein uptake for mTORC1 activation. The Ras independent cells were macropinocytically active even under replete amino acid conditions revealing a metabolic role of macropinocytosis also in the realm of non-transformed cells.

This study is the first to reveal that also AML cells conduct macropinocytosis (Figure 16, Figure 17). Since AML cells are malignant precursors of cells programmed to conduct constitutive macropinocytosis such as dendritic cells and macrophages, it is not surprising to observe this

mechanism also in the leukemic cells. Whether macropinocytic activities of AML cells are based on AML cells being derivatives of functional immune cells or whether it is a process that is further driven upon leukemia development has yet to be assessed.

The current study further demonstrated that malignant myeloid precursors rapidly take up and hydrolyze serum proteins (Figure 16, Figure 17). Whether AML cells internalize the protein by macropinocytosis-driven processes alone or additionally by receptor-mediated protein endocytosis is currently under investigation. What gave reason to speculate receptor-mediated protein uptake to take place were the differential responses to macropinocytosis inhibitors and a more rapid uptake and hydrolysis of DQ-BSA compared to dextran (Figure 16).

Uptake of serum protein was shown to serve the cells metabolically (Figure 18). The endocytosed proteins were found to serve as alternative fuel for glucose and to provide essential amino acids under amino acid depletion. Similar to AML, macropinocytically active non-small lung cancer cell lines were also found to sustain growth under glucose deficiency by metabolizing extracellular protein (Hodakoski *et al.*, 2019). ¹³C-metabolic flux analysis in lung cancer cells revealed that in order to maintain survival in the absence of glucose, protein-derived amino acids were used to generate gluconeogenic and TCA cycle intermediates. It is likely that AML cells utilize the extracellular proteins for the same anabolic processes as shown for the lung cancer cells.

The current study demonstrated that protein-derived amino acids also maintain leukemic growth when essential amino acids are absent (Figure 18 B). The derived amino acids, next to possibly serving as source for new protein synthesis, were found to sustain mTORC1 activity. Sustaining mTORC1 activity in AML cells has been shown to be an important driver of leukemogenesis (Shen *et al.*, 2016). Similar to many solid malignancies, mTOR is aberrantly activated in the majority of AMLs where its inhibition has shown success in suppressing leukemic growth (Carneiro *et al.*, 2015; Tabe *et al.*, 2017; Nepstad *et al.*, 2020). A number of internal stimuli have been identified to lead to mTOR activation in AML including oncogenic Lyn kinase, high levels of Rheb and Raptor or increased activity of ERK, WNT or HIF-1 (Visnjic *et al.*, 2018). Next to internal stimuli, mTOR is highly reliant on external stimuli including the presence of amino acids such as glutamine and leucine. This dependency is also true for AML cells as demonstrated by Willems *et al.*, 2013 that, similar to the current study (Figure 18 C), showed the depletion of glutamine to lead to mTORC1 inhibition and cell death. Data collected in this study revealed that in addition to external amino acids also endocytosed proteins activate mTORC1 and sustain its activity during amino acid deplete conditions.

Ammonium concentrations measured in the bone marrow and the peripheral blood of AML patients indicated protein catabolism to not only be a metabolic characteristic of *in vitro* but also *in vivo* AML cells. This became apparent by the significantly increased ammonium levels

in the highly blast-infiltrated bone marrow of *de novo* AML patients while patients in complete remission showed no difference in bone marrow and peripheral blood ammonium levels (Figure 19 A, B). Also former studies have taken an interest in blood ammonium levels of leukemia patients and revealed high ammonium contents in venous blood to be consistent across patients with both myeloid and lymphoid leukemias compared to healthy donors (Rezzonico *et al.*, 1968 and publications referenced within). Since ammonium primarily results from the breakdown of amino acids, it is possible that the increased ammonium burden observed in AML patients here and elsewhere is the result of increased degradation of protein-derived amino acids. Degradation of amino acids and the resulting carbon backbones might in turn be used to feed metabolic processes such as the TCA cycle.

What could also be an indicator of increased protein catabolism in AML cells are reduced serum albumin levels that are frequently observed in AML patients where the condition known as hypoalbuminemia correlates with a poor prognosis (Khan *et al.*, 2011; Komrokji *et al.*, 2012; Sevindik *et al.*, 2015; Wang *et al.*, 2020). Whether protein catabolism in AML cells or other macropinocytically active cancers takes place at a rate that contributes to hypoalbuminemia remains to be addressed. Further *in vivo* studies are required to fully assess the degree of protein catabolism and its impact on blood ammonium and albumin levels in AML patients. It would be of interest to observe possible changes in blood ammonium and albumin in mice during the onset of AML. To also shed some light on the degree to which AML cells conduct macropinocytosis *in vivo*, fluorescent-labelled dextran could be injected into AML mice models with subsequent analysis of dextran uptake in the blasts. A similar study has been conducted on pancreatic tumors in mice showing that cancer cells readily take up dextran which is inhibited upon EIPA treatment (Seglen, 1978; Davidson *et al.*, 2017). Additionally, EIPA treatment in AML mice models could provide insights into the necessity of conducting macropinocytosis for AML cells.

In conclusion, endocytosis-driven protein uptake and subsequent protein degradation seems to add to the metabolic plasticity of AML cells by driving cell growth and important metabolic signaling pathways even under conditions of amino acid or glucose shortage.

5 Conclusion

The present study is the first that describes the metabolic dependency of AML on GS. We presented concrete evidence of the importance of GS for the detoxification of ammonium that is mainly generated during amino acid catabolism. GS was found to be upregulated in AML cells and this correlated with high ammonium levels detected in AML bone marrow. Further work revealed an adaptation mechanism towards GS-knockout-mediated growth-inhibition. This involved the urea cycle/arginine biosynthesis pathway which represents an alternative ammonium scavenging route.

The functional role of GS in ammonium scavenging was linked to the catabolism of endocytosed proteins which contribute to the cellular amino acid pool and thus to ammonium generation.

Examining protein uptake in AML demonstrated protein endocytosis and metabolization to contribute to AML survival and mTOR activation, especially in the absence of essential metabolites. Future studies are needed to further confirm the link between protein-derived amino acid catabolism and ammonium removal through GS.

This dependency of AML cells on GS-mediated ammonium detoxification positions GS as a potential therapeutic target in AML. Further preclinical studies are needed to assess the toxicity of GS inhibition on healthy cells prior to considering developing GS inhibitors.

6 References

- Abdul-Aziz, A. M. *et al.* (2018) 'HIF1 α drives chemokine factor pro-tumoral signaling pathways in acute myeloid leukemia', *Oncogene*, 37, pp. 2676–2686. doi: 10.1038/s41388-018-0151-1.
- Albrecht, L. V. *et al.* (2020) 'GSK3 Inhibits Macropinocytosis and Lysosomal Activity through the Wnt Destruction Complex Machinery', *Cell Reports*, 32(4). doi: 10.1016/j.celrep.2020.107973.
- Ast, T. and Mootha, V. K. (2019) 'Oxygen and mammalian cell culture: are we repeating the experiment of Dr. Ox?', *Nature Metabolism*. Nature Publishing Group, 1(9), pp. 858–860. doi: 10.1038/s42255-019-0105-0.
- Bertout, J. A., Patel, S. A. and Simon, M. C. (2008) 'The impact of O₂ availability on human cancer', *Nature Reviews Cancer*, 8(12), pp. 967–975. Available at: <https://www.ncbi.nlm.nih.gov/pmc/articles/PMC3140692/pdf/nihms-311210.pdf> (Accessed: 9 January 2018).
- von dem Borne, P. A. *et al.* (2016) 'Effectivity of a strategy in elderly AML patients to reach allogeneic stem cell transplantation using intensive chemotherapy: Long-term survival is dependent on complete remission after first induction therapy', *Leukemia Research*. Elsevier Ltd, 46, pp. 45–50. doi: 10.1016/j.leukres.2016.03.010.
- Bott, A. J. *et al.* (2015) 'Oncogenic Myc Induces Expression of Glutamine Synthetase through Promoter Demethylation', *Cell Metabolism*. Cell Press, 22(6), pp. 1068–1077. doi: 10.1016/J.CMET.2015.09.025.
- Bott, A. J. *et al.* (2019) 'Glutamine Anabolism Plays a Critical Role in Pancreatic Cancer by Coupling Carbon and Nitrogen Metabolism', *Cell Reports*. Elsevier B.V., 29(5), pp. 1287-1298.e6. doi: 10.1016/j.celrep.2019.09.056.
- Bromley-Dulfano, S. *et al.* (2013) 'Antitumor Activity Of The Glutaminase Inhibitor CB-839 In Hematological Malignances', *Blood*, 122(21). Available at: <http://www.bloodjournal.org/content/122/21/4226> (Accessed: 22 November 2018).
- Canton, J. (2018) 'Macropinocytosis: New insights into its underappreciated role in innate immune cell surveillance', *Frontiers in Immunology*. Frontiers Media S.A. doi: 10.3389/fimmu.2018.02286.
- Carneiro, B. A. *et al.* (2015) 'Targeting mTOR signaling pathways and related negative feedback loops for the treatment of acute myeloid leukemia Targeting mTOR signaling pathways and related negative feedback loops for the treatment of acute myeloid leukemia'. doi: 10.1080/15384047.2015.1026510.
- Castegna, A. and Menga, A. (2018) 'Glutamine Synthetase: Localization Dictates Outcome.', *Genes*. Multidisciplinary Digital Publishing Institute (MDPI), 9(2). doi: 10.3390/genes9020108.

- Castro, I., Sampaio-Marques, B. and Ludovico, P. (2019) 'Targeting Metabolic Reprogramming in Acute Myeloid Leukemia', *Cells*. Multidisciplinary Digital Publishing Institute, 8(9), p. 967. doi: 10.3390/cells8090967.
- Chapuis, N. *et al.* (2019) 'Rationale for targeting deregulated metabolic pathways as a therapeutic strategy in acute myeloid leukemia', *Frontiers in Oncology*. Frontiers Media S.A., 9(MAY), p. 405. doi: 10.3389/fonc.2019.00405.
- Charpentier, J. C. *et al.* (2020) 'Macropinocytosis drives T cell growth by sustaining the activation of mTORC1', *Nature Communications*. Nature Research, 11(1), pp. 1–9. doi: 10.1038/s41467-019-13997-3.
- Chen, K. T. J. *et al.* (2019) 'Recent Treatment Advances and the Role of Nanotechnology, Combination Products, and Immunotherapy in Changing the Therapeutic Landscape of Acute Myeloid Leukemia', *Pharmaceutical Research*. Springer New York LLC. doi: 10.1007/s11095-019-2654-z.
- Chen, S. J., Shen, Y. and Chen, Z. (2013) 'A panoramic view of acute myeloid leukemia', *Nature Genetics*. Nat Genet, pp. 586–587. doi: 10.1038/ng.2651.
- Chen, W.-L. *et al.* (2014) 'A distinct glucose metabolism signature of acute myeloid leukemia with prognostic value.', *Blood*. American Society of Hematology, 124(10), pp. 1645–54. doi: 10.1182/blood-2014-02-554204.
- Christa, L. *et al.* (1994) *Overexpression of Glutamine Synthetase in Human Primary Liver Cancer*. Available at: [https://www.gastrojournal.org/article/0016-5085\(94\)90024-8/pdf](https://www.gastrojournal.org/article/0016-5085(94)90024-8/pdf) (Accessed: 18 July 2019).
- Coltella, N. *et al.* (2015) 'Synergistic leukemia eradication by combined treatment with retinoic acid and HIF inhibition by EZN-2208 (PEG-SN38) in preclinical models of PML-RAR α and PLZF-RAR α -driven leukemia', *Clinical Cancer Research*. American Association for Cancer Research Inc., 21(16), pp. 3685–3694. doi: 10.1158/1078-0432.CCR-14-3022.
- Commisso, C. *et al.* (2013) 'Macropinocytosis of protein is an amino acid supply route in Ras-transformed cells', *Nature*, 497. doi: 10.1038/nature12138.
- Commisso, C. (2019) 'The pervasiveness of macropinocytosis in oncological malignancies', *Philosophical Transactions of the Royal Society B: Biological Sciences*. The Royal Society, 374(1765), p. 20180153. doi: 10.1098/rstb.2018.0153.
- Cooper, A. J. L. *et al.* (1979) 'The Metabolic Fate of ^{13}N -labeled Ammonia in Rat Brain', *The Journal of Biological Chemistry*, 254(12), pp. 4982–4992. doi: 10.1016/S0021-9258(18)50550-0.
- Cruzat, V. *et al.* (2018) 'Glutamine: Metabolism and Immune Function, Supplementation and Clinical Translation', *Nutrients*. Multidisciplinary Digital Publishing Institute (MDPI), 10(11). doi:

10.3390/NU10111564.

Davidson, S. M. *et al.* (2017) 'Direct evidence for cancer-cell-autonomous extracellular protein catabolism in pancreatic tumors', *Nature Medicine*, 23(2). doi: 10.1038/nm.4256.

Deynoux, M. *et al.* (2016) 'Hypoxia and hypoxia-inducible factors in leukemias', *Frontiers in Oncology*. Frontiers Media S.A., p. 41. doi: 10.3389/fonc.2016.00041.

Dharampuriya, P. R. *et al.* (2017) 'Tracking the origin, development, and differentiation of hematopoietic stem cells', *Current Opinion in Cell Biology*. Elsevier Ltd, pp. 108–115. doi: 10.1016/j.ceb.2018.01.002.

Doodnauth, S. A., Grinstein, S. and Maxson, M. E. (2019) 'Constitutive and stimulated macropinocytosis in macrophages: Roles in immunity and in the pathogenesis of atherosclerosis', *Philosophical Transactions of the Royal Society B: Biological Sciences*. Royal Society Publishing. doi: 10.1098/rstb.2018.0147.

Dyczynski, M. *et al.* (2018) 'Metabolic reprogramming of acute lymphoblastic leukemia cells in response to glucocorticoid treatment', *Cell Death and Disease*. Nature Publishing Group, 9(9). doi: 10.1038/s41419-018-0625-7.

Egami, Y. *et al.* (2014) 'Small GTPases and phosphoinositides in the regulatory mechanisms of macropinosome formation and maturation', *Frontiers in Physiology*. Frontiers, 5, p. 374. doi: 10.3389/fphys.2014.00374.

Eisenberg, D. *et al.* (2000) 'Structure–function relationships of glutamine synthetases', *Biochimica et Biophysica Acta (BBA) - Protein Structure and Molecular Enzymology*, 1477(1–2), pp. 122–145. doi: 10.1016/S0167-4838(99)00270-8.

Emadi, Ashkan (2015) 'Exploiting AML vulnerability: glutamine dependency'. *Blood*, 126 (11), pp. 1269–1270. doi: 10.1182/blood-2015-07-659508.

Engler, C., Kandzia, R. and Marillonnet, S. (2008) 'A One Pot, One Step, Precision Cloning Method with High Throughput Capability', *PLoS ONE*. Edited by H. A. El-Shemy. Public Library of Science, 3(11), p. e3647. doi: 10.1371/journal.pone.0003647.

Estey, E. *et al.* (2017) 'Diagnosis and management of AML in adults: 2017 ELN recommendations from an international expert panel'. doi: 10.1182/blood-2016-08.

Fan, S. *et al.* (2018) 'High expression of glutamate-ammonia ligase is associated with unfavorable prognosis in patients with ovarian cancer', *Journal of Cellular Biochemistry*. John Wiley & Sons, Ltd, 119(7), pp. 6008–6015. doi: 10.1002/jcb.26797.

Farber, S. and Diamond, L. (1948) 'Temporary remissions in acute leukemia in children produced by folic acid antagonist, 4-aminopteroyl-glutamic acid', *The New England journal of medicine*. N Engl J Med, 238(23), pp. 787–793. doi: 10.1056/NEJM194806032382301.

Forte, D. *et al.* (2019) 'Updates on the hematologic tumor microenvironment and its therapeutic

targeting', *Haematologica*. Ferrata Storti Foundation, pp. 1928–1934. doi: 10.3324/haematol.2018.195396.

Friday, E. *et al.* (2012) 'Role of Glutamate Dehydrogenase in Cancer Growth and Homeostasis', in *Dehydrogenases*. InTech. doi: 10.5772/48606.

Fuhrmann, D. C. *et al.* (2013) 'Chronic hypoxia alters mitochondrial composition in human macrophages', *Biochimica et Biophysica Acta - Proteins and Proteomics*. Elsevier, 1834(12), pp. 2750–2760. doi: 10.1016/j.bbapap.2013.09.023.

Fuhrmann, D. C. *et al.* (2019) 'Chronic Hypoxia Enhances β -Oxidation-Dependent Electron Transport via Electron Transferring Flavoproteins', *Cells*. MDPI AG, 8(2), p. 172. doi: 10.3390/cells8020172.

Gala, J. L. *et al.* (1994) 'High expression of bcl-2 is the rule in acute lymphoblastic leukemia, except in Burkitt subtype at presentation, and is not correlated with the prognosis', *Annals of Hematology*. Springer-Verlag, 69(1), pp. 17–24. doi: 10.1007/BF01757343.

Gallipoli, P. *et al.* (2018) 'Glutaminolysis is a metabolic dependency in FLT3 ITD acute myeloid leukemia unmasked by FLT3 tyrosine kinase inhibition', *Blood*. American Society of Hematology, 131(15), pp. 1639–1653. doi: 10.1182/blood-2017-12-820035.

Ganapathy-Kanniappan, S. (2018) 'Molecular intricacies of aerobic glycolysis in cancer: current insights into the classic metabolic phenotype', *Critical Reviews in Biochemistry and Molecular Biology*. Taylor and Francis Ltd, pp. 667–682. doi: 10.1080/10409238.2018.1556578.

van Gastel, N. *et al.* (2019) 'The Distinctive Metabolic Environment of the Bone Marrow Niche Drives Leukemia Chemoresistance', *Blood*. American Society of Hematology, 134(Supplement_1), pp. 3725–3725. doi: 10.1182/blood-2019-124789.

van Gastel, N. *et al.* (2020) 'Induction of a Timed Metabolic Collapse to Overcome Cancer Chemoresistance', *Cell Metabolism*. Elsevier Inc., 32(3), pp. 391-403.e6. doi: 10.1016/j.cmet.2020.07.009.

Gregory, M. A. *et al.* (2018) 'Targeting glutamine metabolism and redox state for leukemia therapy', *bioRxiv*. Cold Spring Harbor Laboratory, p. 303529. doi: 10.1101/303529.

Gregory, M. A. *et al.* (2019) 'Targeting Glutamine Metabolism and Redox State for Leukemia Therapy.', *Clinical cancer research : an official journal of the American Association for Cancer Research*. American Association for Cancer Research, 25(13), pp. 4079–4090. doi: 10.1158/1078-0432.CCR-18-3223.

Grimwade, D., Ivey, A. and Huntly, B. J. P. (2016) 'Molecular landscape of acute myeloid leukemia in younger adults and its clinical relevance.', *Blood*. American Society of Hematology, 127(1), pp. 29–41. doi: 10.1182/blood-2015-07-604496.

- Grimwade, D., Ivey, A. and Huntly, B. J. P. (2016) 'Molecular landscape of acute myeloid leukemia in younger adults and its clinical relevance', *Blood*, 127(1), pp. 29–41. doi: 10.1182/blood-2015-07-604496.
- Hakvoort, T. B. M. *et al.* (2017) 'Pivotal role of glutamine synthetase in ammonia detoxification', *Hepatology*. John Wiley & Sons, Ltd, 65(1), pp. 281–293. doi: 10.1002/hep.28852.
- Han, Y. *et al.* (2016) 'The progress of angiogenic factors in the development of leukemias', *Intractable and Rare Diseases Research*. International Advancement Center for Medicine and Health Research, pp. 6–16. doi: 10.5582/irdr.2015.01048.
- Hanada, M. *et al.* (1993) 'bcl-2 Gene hypomethylation and high-level expression in B-cell chronic lymphocytic leukemia', *Blood*, 82(6), pp. 1820–1828. doi: 10.1182/blood.v82.6.1820.1820.
- He, Y. *et al.* (2007) 'Glutamine synthetase is essential in early mouse embryogenesis', *Developmental Dynamics*. John Wiley & Sons, Ltd, 236(7), pp. 1865–1875. doi: 10.1002/dvdy.21185.
- He, Y. *et al.* (2010) 'Glutamine synthetase in muscle is required for glutamine production during fasting and extrahepatic ammonia detoxification.', *The Journal of biological chemistry*, 285(13), pp. 9516–9524. doi: 10.1074/jbc.M109.092429.
- Vander Heiden, M. G. and DeBerardinis, R. J. (2017) 'Understanding the Intersections between Metabolism and Cancer Biology', *Cell*, 168, pp. 657–669. doi: 10.1016/j.cell.2016.12.039.
- Hodakoski, C. *et al.* (2019) 'Rac-Mediated Macropinocytosis of Extracellular Protein Promotes Glucose Independence in Non-Small Cell Lung Cancer.', *Cancers*, 11(37), pp. 1–18. doi: 10.3390/cancers11010037.
- Hodakoski, C. *et al.* (2019) 'Rac-Mediated Macropinocytosis of Extracellular Protein Promotes Glucose Independence in Non-Small Cell Lung Cancer.', *Cancers*. Multidisciplinary Digital Publishing Institute (MDPI), 11(1). doi: 10.3390/cancers11010037.
- Hou, K. K. *et al.* (2013) 'Mechanisms of nanoparticle-mediated siRNA transfection by melittin-derived peptides', *ACS Nano*. NIH Public Access, 7(10), pp. 8605–8615. doi: 10.1021/nn403311c.
- Irigoyen, M., García-Ruiz, J. C. and Berra, E. (2017) 'The hypoxia signalling pathway in haematological malignancies', *Oncotarget*. Impact Journals, LLC, 8(22), pp. 36832–36844. doi: 10.18632/oncotarget.15981.
- Issaq, S. H. *et al.* (2019) 'Glutamine synthetase is necessary for sarcoma adaptation to glutamine deprivation and tumor growth', *Oncogenesis*. Nature Publishing Group, 8(3), p. 20. doi: 10.1038/s41389-019-0129-z.
- Jacque, N. *et al.* (2015) 'Targeting glutaminolysis has antileukemic activity in acute myeloid

- leukemia and synergizes with BCL-2 inhibition.', *Blood*. American Society of Hematology, 126(11), pp. 1346–56. doi: 10.1182/blood-2015-01-621870.
- Jiang, Y. and Nakada, D. (2016) 'Cell intrinsic and extrinsic regulation of leukemia cell metabolism', *International Journal of Hematology*. Springer Tokyo, pp. 607–616. doi: 10.1007/s12185-016-1958-6.
- Jonas, B. A. and Pollyea, D. A. (2019) 'How we use venetoclax with hypomethylating agents for the treatment of newly diagnosed patients with acute myeloid leukemia', *Leukemia*. Springer Nature, 33(12), pp. 2795–2804. doi: 10.1038/s41375-019-0612-8.
- Ju, H. Q. *et al.* (2017) 'ITD mutation in FLT3 tyrosine kinase promotes Warburg effect and renders therapeutic sensitivity to glycolytic inhibition', *Leukemia*. Nature Publishing Group, 31(10), pp. 2143–2150. doi: 10.1038/leu.2017.45.
- Juliusson, G. *et al.* (2009) 'Age and acute myeloid leukemia: Real world data on decision to treat and outcomes from the Swedish Acute Leukemia Registry', *Blood*. American Society of Hematology, 113(18), pp. 4179–4187. doi: 10.1182/blood-2008-07-172007.
- Kamphorst, J. J. *et al.* (2015) 'Human pancreatic cancer tumors are nutrient poor and tumor cells actively scavenge extracellular protein.', *Cancer research*. NIH Public Access, 75(3), pp. 544–53. doi: 10.1158/0008-5472.CAN-14-2211.
- Kawada, H. *et al.* (2013) 'High Concentrations of L-Ascorbic Acid Specifically Inhibit the Growth of Human Leukemic Cells via Downregulation of HIF-1 α Transcription', *PLoS ONE*. PLoS One, 8(4). doi: 10.1371/journal.pone.0062717.
- Khan, A. M. *et al.* (2011) 'Albumin Is a Prognostic Factor for Overall Survival in Newly Diagnosed Patients with Acute Myeloid Leukemia (AML)', *Blood*, 118(21). Available at: <http://www.bloodjournal.org/content/118/21/4253> (Accessed: 18 July 2018).
- Khwaja, A. *et al.* (2016) 'Acute myeloid leukaemia', *Nature Reviews Disease Primers*. Nature Publishing Group, 2(1), p. 16010. doi: 10.1038/nrdp.2016.10.
- Kim, J. and Guan, K. L. (2019) 'mTOR as a central hub of nutrient signalling and cell growth', *Nature Cell Biology*. Nature Publishing Group, pp. 63–71. doi: 10.1038/s41556-018-0205-1.
- Kim, S. M. *et al.* (2018) 'PTEN Deficiency and AMPK Activation Promote Nutrient Scavenging and Anabolism in Prostate Cancer Cells'. doi: 10.1158/2159-8290.CD-17-1215.
- King, J. S. and Kay, R. R. (2019) 'The origins and evolution of macropinocytosis', *Philosophical Transactions of the Royal Society B: Biological Sciences*. Royal Society Publishing. doi: 10.1098/rstb.2018.0158.
- Kitajima, S. *et al.* (2017) 'Hypoxia-inducible factor-1 α promotes cell survival during ammonia stress response in ovarian cancer stem-like cells', *Oncotarget*. Impact Journals LLC, 8(70), pp. 114481–114494. doi: 10.18632/oncotarget.23010.

- Knoechel, B. and Aster, J. C. (2015) 'Metabolic Mechanisms of Drug Resistance in Leukemia', *Cell Metabolism*. Cell Press, 22(5), pp. 759–760. doi: 10.1016/J.CMET.2015.10.005.
- Koh, M. Y. and Powis, G. (2012) 'Passing the baton: The HIF switch', *Trends in Biochemical Sciences*. NIH Public Access, pp. 364–372. doi: 10.1016/j.tibs.2012.06.004.
- Komrokji, R. S. *et al.* (2009) 'Albumin Is a Prognostic Factor for Response and Overall Survival in Relapsed or Refractory Acute Myeloid Leukemia (AML).', *Blood*. American Society of Hematology, 114(22), pp. 4685–4685. doi: 10.1182/blood.v114.22.4685.4685.
- Komrokji, R. S. *et al.* (2012) 'Hypoalbuminemia is an independent prognostic factor for overall survival in myelodysplastic syndromes', *American Journal of Hematology*. John Wiley & Sons, Ltd, 87(11), pp. 1006–1009. doi: 10.1002/ajh.23303.
- De Kouchkovsky, I. and Abdul-Hay, M. (2016) "Acute myeloid leukemia: a comprehensive review and 2016 update", *Blood Cancer Journal*, 6. doi: 10.1038/bcj.2016.50.
- Kreitz, J. *et al.* (2019) 'Metabolic Plasticity of Acute Myeloid Leukemia', *Cells*. Multidisciplinary Digital Publishing Institute, 8(8), p. 805. doi: 10.3390/cells8080805.
- Kung, H.-N., Marks, J. R. and Chi, J.-T. (2011) 'Glutamine synthetase is a genetic determinant of cell type-specific glutamine independence in breast epithelia.', *PLoS genetics*. Public Library of Science, 7(8), p. e1002229. doi: 10.1371/journal.pgen.1002229.
- Labow, B. I., Souba, W. W. and Abcouwer, S. F. (2001) 'Mechanisms Governing the Expression of the Enzymes of Glutamine Metabolism—Glutaminase and Glutamine Synthetase', *The Journal of Nutrition*. Oxford University Press (OUP), 131(9), pp. 2467S-2474S. doi: 10.1093/jn/131.9.2467s.
- Lagadinou, E. D. *et al.* (2013) 'BCL-2 inhibition targets oxidative phosphorylation and selectively eradicates quiescent human leukemia stem cells', *Cell Stem Cell*, 12(3), pp. 329–341. doi: 10.1016/j.stem.2012.12.013.
- Liu, P. *et al.* (2019) 'Glutamine synthetase promotes tumor invasion in hepatocellular carcinoma through mediating epithelial–mesenchymal transition', *Hepatology Research*, 50(2), pp. 246–257. doi: 10.1111/hepr.13433.
- Liu, X. and Gong, Y. (2019) 'Isocitrate dehydrogenase inhibitors in acute myeloid leukemia', *Biomarker Research*. BioMed Central Ltd. doi: 10.1186/s40364-019-0173-z.
- Liu, Z. and Roche, P. A. (2015) 'Macropinocytosis in phagocytes: regulation of MHC class-II-restricted antigen presentation in dendritic cells', *Frontiers in Physiology*. Frontiers Research Foundation, 6(JAN), p. 1. doi: 10.3389/fphys.2015.00001.
- Long, J. *et al.* (2010) 'Glutamine synthetase as an early marker for hepatocellular carcinoma based on proteomic analysis of resected small hepatocellular carcinomas.', *Hepatobiliary & pancreatic diseases international: HBPD INT*, 9(3), pp. 296–305. Available at:

<http://www.ncbi.nlm.nih.gov/pubmed/20525558> (Accessed: 6 November 2019).

Long, J. *et al.* (2011) 'Expression level of glutamine synthetase is increased in hepatocellular carcinoma and liver tissue with cirrhosis and chronic hepatitis B.', *Hepatology international*. Springer, 5(2), pp. 698–706. doi: 10.1007/s12072-010-9230-2.

Majmundar, A. J., Wong, W. J. and Simon, M. C. (2010) 'Hypoxia-Inducible Factors and the Response to Hypoxic Stress', *Molecular Cell*, 40, pp. 294–309. doi: 10.1016/j.molcel.2010.09.022.

Martignoles, J.-A., Delhommeau, F. and Hirsch, P. (2018) 'Genetic Hierarchy of Acute Myeloid Leukemia: From Clonal Hematopoiesis to Molecular Residual Disease', *International Journal of Molecular Sciences*. MDPI AG, 19(12), p. 3850. doi: 10.3390/ijms19123850.

Mastorodemos, V. *et al.* (2009) 'Human GLUD1 and GLUD2 glutamate dehydrogenase localize to mitochondria and endoplasmic reticulum', *Biochemistry and Cell Biology*, 87(3), pp. 505–516. doi: 10.1139/O09-008.

Matre, P., Velez, J., Jacamo, R., Qi, Y., Su, Xiaoping, Cai, T., Chan, Steven M, *et al.* (2016) 'Inhibiting glutaminase in acute myeloid leukemia: metabolic dependency of selected AML subtypes.', *Oncotarget*. Impact Journals, LLC, 7(48), pp. 79722–79735. doi: 10.18632/oncotarget.12944.

Medeiros, B. C. *et al.* (2017) 'Isocitrate dehydrogenase mutations in myeloid malignancies', *Leukemia*. Nature Publishing Group, pp. 272–281. doi: 10.1038/leu.2016.275.

Michael, D. R. *et al.* (2013) 'Differential regulation of macropinocytosis in macrophages by cytokines: Implications for foam cell formation and atherosclerosis', *Cytokine*. Academic Press, 64(1), pp. 357–361. doi: 10.1016/J.CYTO.2013.05.016.

Miraki-Moud, F. *et al.* (2015) 'Arginine deprivation using pegylated arginine deiminase has activity against primary acute myeloid leukemia cells in vivo.', *Blood*. American Society of Hematology, 125(26), pp. 4060–8. doi: 10.1182/blood-2014-10-608133.

Mussai, F. *et al.* (2015) 'Arginine dependence of acute myeloid leukemia blast proliferation: a novel therapeutic target.', *Blood*. American Society of Hematology, 125(15), pp. 2386–96. doi: 10.1182/blood-2014-09-600643.

National Cancer Institute Surveillance, Epidemiology, and End Results Program. Cancer stat facts: acute myeloid leukemia (AML). [cited 2020 Oct 24]. Available from: <https://seer.cancer.gov/statfacts/html/amyl.html> (2020). Available at: <https://seer.cancer.gov/statfacts/html/amyl.html> (Accessed: 24 October 2020).

Nelson, D. *et al.* (2009) *Lehninger Biochemie: Biosynthese von Aminosäuren, Nucleotiden und verwandten Molekülen*. Springer Verlag.

Nepstad, I. *et al.* (2020) 'The PI3K-AKT-MTOR signaling pathway in human acute myeloid

- leukemia (AML) cells', *International Journal of Molecular Sciences*. MDPI AG. doi: 10.3390/ijms21082907.
- Ni, F. *et al.* (2019) 'Critical role of ASCT2-mediated amino acid metabolism in promoting leukaemia development and progression', *Nature Metabolism*. Nature Publishing Group, 1(3), pp. 390–403. doi: 10.1038/s42255-019-0039-6.
- Nishimura, S. *et al.* (2008) 'Combinatorial targeting of the macropinocytotic pathway in leukemia and lymphoma cells.', *The Journal of biological chemistry*. American Society for Biochemistry and Molecular Biology, 283(17), pp. 11752–62. doi: 10.1074/jbc.M708849200.
- Palm, W. (2019) 'Metabolic functions of macropinocytosis', *Philosophical Transactions of the Royal Society B: Biological Sciences*. Royal Society Publishing, 374(1765), p. 20180285. doi: 10.1098/rstb.2018.0285.
- Palm, W. and Thompson, C. B. (2017) 'Nutrient acquisition strategies of mammalian cells', *Nature*. Nature Publishing Group, 546(7657), pp. 234–242. doi: 10.1038/nature22379.
- Papaemmanuil, E. *et al.* (2016) 'Genomic classification and prognosis in acute myeloid leukemia', *New England Journal of Medicine*. Massachusetts Medical Society, 374(23), pp. 2209–2221. doi: 10.1056/NEJMoa1516192.
- Parks, S. K., Cormerais, Y. and Pouysségur, J. (2017) 'Hypoxia and cellular metabolism in tumour pathophysiology', *The Journal of Physiology*. Wiley/Blackwell (10.1111), 595(8), pp. 2439–2450. doi: 10.1113/JP273309.
- Pavlova, N. N. and Thompson, C. B. (2016) 'The Emerging Hallmarks of Cancer Metabolism.', *Cell metabolism*. NIH Public Access, 23(1), pp. 27–47. doi: 10.1016/j.cmet.2015.12.006.
- Plaitakis, A., Kalef-Ezra, E., Kotzamani, D., Zaganas, I. and Spanaki, C. (2017) 'The glutamate dehydrogenase pathway and its roles in cell and tissue biology in health and disease', *Biology*. MDPI AG. doi: 10.3390/biology6010011.
- Plaitakis, A., Kalef-Ezra, E., Kotzamani, D., Zaganas, I., Spanaki, C., *et al.* (2017) 'The Glutamate Dehydrogenase Pathway and Its Roles in Cell and Tissue Biology in Health and Disease', *Biology*, 6, p. 11. doi: 10.3390/biology6010011.
- Pochini, L. *et al.* (2014) 'Membrane transporters for the special amino acid glutamine: structure/function relationships and relevance to human health.', *Frontiers in chemistry*. Frontiers Media SA, 2, p. 61. doi: 10.3389/fchem.2014.00061.
- Pollyea, D. A. *et al.* (2018) 'Venetoclax with azacitidine disrupts energy metabolism and targets leukemia stem cells in patients with acute myeloid leukemia', *Nature Medicine*. Nature Publishing Group, 24(12), pp. 1859–1866. doi: 10.1038/s41591-018-0233-1.
- Pollyea, D. A. *et al.* (2019) 'Venetoclax for AML: Changing the treatment paradigm', *Blood Advances*. American Society of Hematology, 3(24), pp. 4326–4335. doi:

10.1182/bloodadvances.2019000937.

Pulte, D. *et al.* (2016) 'Survival in patients with acute myeloblastic leukemia in Germany and the United States: Major differences in survival in young adults', *International Journal of Cancer*. Wiley-Liss Inc., 139(6), pp. 1289–1296. doi: 10.1002/ijc.30186.

Qvartskhava, N. *et al.* (2015) 'Hyperammonemia in gene-targeted mice lacking functional hepatic glutamine synthetase', *PNAS*, 112(17), pp. 5521–5526. doi: 10.1073/pnas.1423968112.

Ravandi, F., Walter, R. B. and Freeman, S. D. (2018) 'Evaluating measurable residual disease in acute myeloid leukemia', *Blood Advances*. American Society of Hematology, pp. 1356–1366. doi: 10.1182/bloodadvances.2018016378.

Recouvreux, M. V. and Commisso, C. (2017) 'Macropinocytosis: A metabolic adaptation to nutrient stress in cancer', *Frontiers in Endocrinology*. Frontiers Media S.A., p. 261. doi: 10.3389/fendo.2017.00261.

Recouvreux, M. V. and Commisso, C. (2017) 'Macropinocytosis: A Metabolic Adaptation to Nutrient Stress in Cancer', *Frontiers in Endocrinology*. Frontiers, 8, p. 261. doi: 10.3389/fendo.2017.00261.

Redelman-Sidi, G. *et al.* (2013) 'Oncogenic activation of Pak1-dependent pathway of macropinocytosis determines BCG entry into bladder cancer cells', *Cancer Research*. NIH Public Access, 73(3), pp. 1156–1167. doi: 10.1158/0008-5472.CAN-12-1882.

Reed, D. R. *et al.* (2019) 'Etrasidenib in acute myeloid leukemia: Clinical development and perspectives on treatment', *Cancer Management and Research*. Dove Medical Press Ltd, pp. 8073–8080. doi: 10.2147/CMAR.S162784.

Rezzonico, A., Gervasini, N. and Secchi, G. C. (1968) 'Observations on plasma ammonia in patients with leukemia', *Experientia*. Birkhäuser-Verlag, 24(1), pp. 28–28. doi: 10.1007/BF02136771.

Roboz, G. J. *et al.* (2020) 'Ivosidenib induces deep durable remissions in patients with newly diagnosed IDH1-mutant acute myeloid leukemia', *Blood*. American Society of Hematology, pp. 463–471. doi: 10.1182/blood.2019002140.

Roca-Portoles, A. *et al.* (2020) 'Venetoclax causes metabolic reprogramming independent of BCL-2 inhibition', *Cell Death and Disease*, 11(616), pp. 1–13. doi: 10.1038/s41419-020-02867-2.

Ronzio, R. A. and Ma1eister, A. (1967) 'Phosphorylation of methionine sulfoxamine by glutamine synthetase', *Biochemistry*, pp. 164–170.

Rosati, A. *et al.* (2013) 'Glutamine synthetase expression as a valuable marker of epilepsy and longer survival in newly diagnosed glioblastoma multiforme', *Neuro-Oncology*, 15(5), pp. 618–

625. doi: 10.1093/neuonc/nos338.

Rudman, D. *et al.* (1971) *Observations on the Plasma Amino Acids of Patients with Acute Leukemia, Cancer Research*. Available at: <http://cancerres.aacrjournals.org/content/canres/31/8/1159.full.pdf> (Accessed: 7 September 2018).

Schena, M. *et al.* (1992) 'Growth- and differentiation-associated expression of bcl-2 in B-chronic lymphocytic leukemia cells', *Blood*, 79(11), pp. 2981–2989. doi: 10.1182/blood.v79.11.2981.2981.

Seglen, P. O. (1978) 'Effects of amino acids, ammonia and leupeptin on protein synthesis and degradation in isolated rat hepatocytes', *Biochemical Journal*. Portland Press Ltd, 174(2), pp. 469–474. doi: 10.1042/bj1740469.

Sevindik, O. G. *et al.* (2015) 'Hypoalbuminemia is a surrogate biomarker of poor prognosis in myelodysplastic syndrome even when adjusting for comorbidities', *Leukemia & Lymphoma*, 56(9), pp. 1–4. doi: 10.3109/10428194.2015.1014362.

Shen, Y., Bai, J. and He, A. (2016) *Role of mTOR signaling pathway in acute myeloid leukemia, Int J Clin Exp Med*. Available at: www.ijcem.com/ (Accessed: 17 December 2018).

Shi, X. *et al.* (2014) '[¹³N]Ammonia Positron Emission Tomographic/Computed Tomographic Imaging Targeting Glutamine Synthetase Expression in Prostate Cancer', *Molecular Imaging*, pp. 1–10. doi: 10.2310/7290.2014.00048.

Shlush, L. I. *et al.* (2017) 'Tracing the origins of relapse in acute myeloid leukaemia to stem cells', *Nature*. Nature Publishing Group, 547(7661), pp. 104–108. doi: 10.1038/nature22993.

Short, N. J. *et al.* (2020) 'Advances in the treatment of acute myeloid leukemia: New drugs and new challenges', *Cancer Discovery*, 10(4), pp. 506–525. doi: 10.1158/2159-8290.CD-19-1011.

Simsek, T. *et al.* (2010) 'The distinct metabolic profile of hematopoietic stem cells reflects their location in a hypoxic niche', *Cell Stem Cell*. Cell Stem Cell, 7(3), pp. 380–390. doi: 10.1016/j.stem.2010.07.011.

Sohn, B. H. *et al.* (2018) 'Glutamine synthetase mediates sorafenib sensitivity in β -catenin-active hepatocellular carcinoma cells', *Experimental and Molecular Medicine*. Nature Publishing Group, 50(1). doi: 10.1038/emm.2017.174.

Sossa, C. L. *et al.* (2018) 'Prognosis and Survival of Acute Myeloid Leukemia: Experience of a Single Center in Colombia', *Blood*. American Society of Hematology, 132(Supplement 1), pp. 5184–5184. doi: 10.1182/blood-2018-99-119927.

Spencer, Joel A *et al.* (2014) 'Direct measurement of local oxygen concentration in the bone marrow of live animals', *Nature*, 508. doi: 10.1038/nature13034.

Spencer, Joel A. *et al.* (2014) 'Direct measurement of local oxygen concentration in the bone marrow of live animals', *Nature*. Nature Publishing Group, 508(7495), pp. 269–273. doi:

10.1038/nature13034.

Spinelli, J. B. *et al.* (2017) 'Metabolic recycling of ammonia via glutamate dehydrogenase supports breast cancer biomass', *Science*. American Association for the Advancement of Science, 358(6365), pp. 941–946. doi: 10.1126/science.aam9305.

Spodenkiewicz, M. *et al.* (2016) 'Minireview on Glutamine Synthetase Deficiency, an Ultra-Rare Inborn Error of Amino Acid Biosynthesis.', *Biology*. Multidisciplinary Digital Publishing Institute (MDPI), 5(4). doi: 10.3390/biology5040040.

Stehle, G. *et al.* (1997) *Plasma protein (albumin) catabolism by the tumor itself-implications for tumor metabolism and the genesis of cachexia*, *Critical Reviews in Oncology/Hematology*.

Szu-Wei Lee, Yijuan Zhang, Michael Jung, Nathalia Cruz, Basheer Alas, C. C. (2019) 'EGFR-Pak Signaling Selectively Regulates Glutamine Deprivation-Induced Macropinocytosis', *Developmental Cell*, 50, pp. 381-392.e5. doi: 10.1016/j.devcel.2019.05.043.

Tabe, Y. *et al.* (2017) 'Inhibition of mTOR kinase as a therapeutic target for acute myeloid leukemia', *Expert Opinion on Therapeutic Targets*, 21(7), pp. 705–714. doi: 10.1080/14728222.2017.1333600.

Tabe, Y., Konopleva, M. and Andreeff, M. (2020) 'Fatty Acid Metabolism, Bone Marrow Adipocytes, and AML', *Frontiers in Oncology*. Frontiers Media S.A., p. 155. doi: 10.3389/fonc.2020.00155.

Tabe, Y., Lorenzi, P. L. and Konopleva, M. (2019) 'Amino acid metabolism in hematologic malignancies and the era of targeted therapy', *Blood*. American Society of Hematology, 134(13), pp. 1014–1023. doi: 10.1182/BLOOD.2019001034.

Takubo, K. *et al.* (2010) 'Cell Stem Cell Regulation of the HIF-1a Level Is Essential for Hematopoietic Stem Cells', *Stem Cell*, 7, pp. 391–402. doi: 10.1016/j.stem.2010.06.020.

Tardito, S. *et al.* (2007) 'The inhibition of glutamine synthetase sensitizes human sarcoma cells to L-asparaginase', *Cancer Chemotherapy and Pharmacology*, 60(5), pp. 751–758. doi: 10.1007/s00280-007-0421-z.

Tardito, S. *et al.* (2015) 'Glutamine synthetase activity fuels nucleotide biosynthesis and supports growth of glutamine-restricted glioblastoma', *Nature Cell Biology*. doi: 10.1038/ncb3272.

Ünal, Ö., Ceylaner, S. and Akın, R. (2018) 'A Very Rare Etiology of Hypotonia and Seizures: Congenital Glutamine Synthetase Deficiency', *Neuropediatrics*. Georg Thieme Verlag KG, 50(01), pp. 051–053. doi: 10.1055/S-0038-1675637.

Vardiman, J. W., Harris, N. L. and Brunning, R. D. (2002) 'World Health Organization (WHO) classification of the myeloid neoplasmsThe', *Blood*, 100(7), pp. 2292–2302. doi: 10.1182/blood-2002-04-1199.

- Velasco-Hernandez, T. *et al.* (2014) 'HIF-1 α can act as a tumor suppressor gene in murine acute myeloid leukemia', *Blood*. American Society of Hematology, 124(24), pp. 3597–3607. doi: 10.1182/blood-2014-04-567065.
- Velasco-Hernandez, T. *et al.* (2019) 'Hif-1 α Deletion May Lead to Adverse Treatment Effect in a Mouse Model of MLL-AF9-Driven AML', *Stem Cell Reports*. Cell Press, 12(1), pp. 112–121. doi: 10.1016/j.stemcr.2018.11.023.
- Vidal, R. S. *et al.* (2018) 'Metabolic Reprogramming During Multidrug Resistance in Leukemias', *Frontiers in Oncology*. Frontiers, 8, p. 90. doi: 10.3389/fonc.2018.00090.
- Visnjic, D., Dembitz, V. and Lalic, H. (2018) 'The Role of AMPK/mTOR Modulators in the Therapy of Acute Myeloid Leukemia', *Current Medicinal Chemistry*, 26(12), pp. 2208–2229. doi: 10.2174/0929867325666180117105522.
- Vosberg, S. (2019) 'Clonal evolution of acute myeloid leukemia from diagnosis to relapse', (May), pp. 839–849. doi: 10.1002/gcc.22806.
- Wang, L. *et al.* (2018) 'Increased glutamine anabolism sensitizes non-small cell lung cancer to gefitinib treatment', *Cell Death Discovery*. Springer Nature, 4(1), pp. 1–16. doi: 10.1038/s41420-018-0086-x.
- Wang, N. *et al.* (2020) 'Prognostic value of hypoalbuminemia at diagnosis in de novo non-M3 acute myeloid leukemia', *Leukemia and Lymphoma*. Taylor & Francis, 61(3), pp. 641–649. doi: 10.1080/10428194.2019.1686499.
- Wang, Y. *et al.* (2011) 'Targeting HIF1 α eliminates cancer stem cells in hematological malignancies', *Cell Stem Cell*. Cell Stem Cell, 8(4), pp. 399–411. doi: 10.1016/j.stem.2011.02.006.
- Wang, Y. *et al.* (2013) 'Rapid Diagnosis and Prognosis of *de novo* Acute Myeloid Leukemia by Serum Metabonomic Analysis', *Journal of Proteome Research*, 12(10), pp. 4393–4401. doi: 10.1021/pr400403p.
- Wang, Y. *et al.* (2017) 'GLUL Promotes Cell Proliferation in Breast Cancer', *Journal of Cellular Biochemistry*. John Wiley & Sons, Ltd, 118(8), pp. 2018–2025. doi: 10.1002/jcb.25775.
- Watanabe, K. *et al.* (2011) 'The use of cationic nanogels to deliver proteins to myeloma cells and primary T lymphocytes that poorly express heparan sulfate', *Biomaterials*. Biomaterials, 32(25), pp. 5900–5905. doi: 10.1016/j.biomaterials.2011.04.058.
- Whitesides, G. M. (1985) 'Methods of Enzymatic Analysis. L-glutamine and L-glutamate; UV-method with glutaminase and glutamate dehydrogenase.', *Angewandte Chemie*. Wiley, 97(7), pp. 614–615. doi: 10.1002/ange.19850970739.
- Willems, L. *et al.* (2013) 'Inhibiting glutamine uptake represents an attractive new strategy for treating acute myeloid leukemia.', *Blood*. American Society of Hematology, 122(20), pp. 3521–

32. doi: 10.1182/blood-2013-03-493163.

Willems, L. *et al.* (2013) 'Inhibiting glutamine uptake represents an attractive new strategy for treating acute myeloid leukemia.', *Blood*. American Society of Hematology, 122(20), pp. 3521–32. doi: 10.1182/blood-2013-03-493163.

Wung, W., Ananthakrishnan, S. and Jonas, B. A. (2018) 'Proteinuria, Hypoalbuminemia, and Chronic Lymphocytic Leukemia: An Unusual Trio', *Journal of Investigative Medicine High Impact Case Reports*. SAGE Publications Ltd, 6. doi: 10.1177/2324709618764207.

Yang, H. *et al.* (2012) 'IDH1 and IDH2 mutations in tumorigenesis: mechanistic insights and clinical perspectives', *Clinical cancer research : an official journal of the American Association for Cancer Research*. NIH Public Access, 18(20), p. 5562. doi: 10.1158/1078-0432.CCR-12-1773.

Yang, L. *et al.* (2014) 'Metabolic shifts toward glutamine regulate tumor growth, invasion and bioenergetics in ovarian cancer', *Molecular Systems Biology*. Blackwell Publishing Ltd, 10(5). doi: 10.1002/msb.20134892.

Ye, H. *et al.* (2018) 'Subversion of Systemic Glucose Metabolism as a Mechanism to Support the Growth of Leukemia Cells', *Cancer Cell*. Cell Press, 34(4), pp. 659-673.e6. doi: 10.1016/j.ccell.2018.08.016.

Yoo, H. C. *et al.* (2020) 'Glutamine reliance in cell metabolism', *Experimental and Molecular Medicine*. Springer Nature, pp. 1496–1516. doi: 10.1038/s12276-020-00504-8.

Yuneva, M. O. *et al.* (2012) 'The metabolic profile of tumors depends on both the responsible genetic lesion and tissue type', *Cell Metabolism*. NIH Public Access, 15(2), pp. 157–170. doi: 10.1016/j.cmet.2011.12.015.

Zhang, Y. and Comisso, C. (2019) 'Macropinocytosis in Cancer: A Complex Signaling Network', *Trends in Cancer*. Elsevier Inc., 5(6), pp. 332–334. doi: 10.1016/j.trecan.2019.04.002.

Zhao, J., Zeng, X. and Hou, S. (2019) 'Glutamate-ammonia ligase promotes lung cancer cell growth through an enzyme independent upregulation of CaMK2G under a glutamine-sufficient condition', *bioRxiv Cancer Biology*. Cold Spring Harbor Laboratory, p. 818575. doi: 10.1101/818575.

Zheng, Y. *et al.* (2019) 'Inhibition of multiple myeloma-derived exosomes uptake suppresses the functional response in bone marrow stromal cell', *International Journal of Oncology*. Spandidos Publications, 54(3), pp. 1061–1070. doi: 10.3892/ijo.2019.4685.

Zhou, J. D. *et al.* (2019) 'BCL2 overexpression: Clinical implication and biological insights in acute myeloid leukemia', *Diagnostic Pathology*. BioMed Central Ltd., 14(1), p. 68. doi: 10.1186/s13000-019-0841-1.

7 Appendix

7.1 ¹⁵N- and non-labeled *Arthrospirulina maxima* cell extract preparation

¹⁵N- and non-labeled *Arthrospirulina maxima* cell extracts were obtained and prepared by Silantes (Germany) as described in the following:

1. 463 g centrifuged wet biomass resuspended in 1.2 L deionized water
2. Adding of 133 mL 5 M HCl to a final concentration of 0.5 M
3. Hydrolysis in autoclave at 121°C and 1 bar pressure above atmosphere for 3 hours
4. Reducing to a minimum with rotary evaporator
5. Resuspended in 200 mL deionized water and reduced in rotary evaporator in order to remove remaining HCl
6. Resuspended in 400 mL deionized water and centrifuged at 17,000 g for 10 minutes
Proceeded with supernatant
7. Added 5 g activated charcoal and stirred for 30 minutes
8. Filtering solution with 0.22 µm
9. Dark solution → adding 3 g charcoal and stirring for 30 minutes
10. Filtering solution with 0.22 µm
11. Dark solution → adding 3 g charcoal and stirring for 30 minutes
12. Filtering solution with 0.22 µm → clear solution
13. Neutralized with 67 mL 5 M NaOH → pH 7.0 (equals 0.335 mol → 19.5 g NaCl)
14. Frozen at - 60°C over night
15. Lyophilized in aluminium plates
→ 65 g powder in total (30% NaCl)

8 Declaration for collaborative work

Collaborative work and contributions from colleagues are explicitly referenced in the thesis. The material obtained in the context of collaborative work is listed below.

Figure 5. B. GS protein expression in primary AML blasts from 42 patients compared to HSPCs from 6 healthy donors. Prof. Dr. Jan Jacob Schuringa, University of Groningen, Netherlands

Figure 5. C. GS protein expression in primary AMLs blasts with different genetic backgrounds compared to an AML standard (consisting of NB4, MV411, KG1 cell lines) analyzed by SuperSILAC-based mass spectrometry. Prof. Dr. Thomas Oellerich, Goethe University Hospital Frankfurt, Germany

Figure 6. TCGA-based GS expression in AML with different genetic mutations and GS-based patient survival. Dr. Geoffroy Andreux, University of Freiburg, Germany

Figure 8. D. Overall survival of NOD SCID gamma mice transplanted with GS-knockdown THP1 compared to NTC controls. Dr. Rahul Kumar and Prof. Daniela Krause, Georg Speyer-House, Frankfurt, Germany

Figure 11. B./C. GC-MS analysis to determine the relative abundance of ¹⁵N-glutamine and ¹⁵N-glutamate in HEL and THP1 cells after treatment with 5 mM ¹⁵N-ammonium chloride. Prof. Dr. Marta Cascante, University of Barcelona, Spain

Figure 13. 2D 1H-15N HSQC NMR spectra of ¹⁵N-glutamate, ¹⁵N-glutamine reference samples and HEL cells fed with ¹⁵N-ammonium chloride. Islam Alshamleh and Prof. Dr. Harald Schwalbe group, Goethe University, Campus Riedberg, Frankfurt, Germany

Figure 19. Ammonium and glucose measurements in AML patients. Dr. Julius Enßle and Dr. Philipp Makowka, Goethe University Hospital Frankfurt, Germany

Figure 21. 2D ¹H-¹⁵N HSQC NMR spectra of HEL NTC cells and GPP cells fed with 2% ¹⁵N-labeled *Arthrospirulina maxima* hydrolysates. Islam Alshamleh and Prof. Dr. Harald Schwalbe group, Goethe University, Campus Riedberg, Frankfurt, Germany

9 Eidesstattliche Erklärung

Hiermit versichere ich, dass ich die vorliegende Dissertation selbständig und nur unter Zuhilfenahme der hier angegebenen Quellen und Hilfsmitteln verfasst habe. Die Dissertation wurde bisher keiner anderen Fakultät vorgelegt. Ich erkläre, dass ich bisher kein Promotionsverfahren erfolglos beendet habe und dass keine Aberkennung eines bereits erworbenen Doktorgrades vorliegt.

Frankfurt, den

Johanna Kreitz



Curriculum vitae JOHANNA KREITZ

johanna@kreitz.org +49 1601759593

24.01.1992
Troisdorf,
Germany Burgstraße 8
60316 Frankfurt,
Germany

EDUCATION

09/2016 - Present

[@HaemMetabolome1](#)

10/2014 - 06/2016

09/2012 - 06/2014

08/2002 - 07/2010

SCIENTIFIC ACHIEVEMENTS

TEACHING

VOLUNTARY WORK

PhD Double Degree



University Hospital Frankfurt, Germany



University of Barcelona, Spain

Project: HaemMetabolome - an EU funded research and innovation project
Focus: Finding metabolic vulnerabilities in acute myeloid leukemia (AML)
Research:
1. Metabolic screening in AML blasts using multi-omics approaches
2. Functional characterization of metabolic enzymes
3. Verification of potential therapeutic targets in cell lines, primary patient material and mouse models
Thesis title: Glutamine synthetase - a potential therapeutic target in AML
Supervision: Prof. Hubert Serve (Germany) and Prof. Marta Cascante (Spain)

MPhil



Robert Gordon University, Scotland

Focus: Characterizing enzymes for the bioremediation of cyanotoxins
Research:
1. Phylogenetic/functional characterization of bioremediating bacterial isolates
2. Heterologous expression of cyanotoxin degrading enzymes in *E. coli* strains
3. Functional characterization of cyanotoxin degrading enzymes
Thesis title: Evidence for functional drift of bacterial isolates in response to cyanobacterial microcystin-Lr and multiple peptide degradation in *Paucibacter toxinivorans*
Supervision: Prof. Linda Lawton and Prof. Christine Edwards

BSc Double Degree



Bonn-Rhein-Sieg University of Applied Sciences, Germany



Robert Gordon University, Scotland

Courses: Applied Biology; Bioscience with Biomedical Sciences
Focus: Human biology, Immunology, Biomedicine, Biochemistry, Clinical research, Genetics, Biotechnology, Microbiology, Quality assurance
Grades: 1.6 (Germany); 1st Class Honours Degree (Scotland)
Thesis title: Putting microbes to work - bioremedial strategies for removal of cyanotoxins from drinking water (Grade A)
Supervision: Prof. Linda Lawton and Prof. Christine Edwards

German Abitur

Albert-Einstein-Gymnasium, Germany (Grade: 1.7)

Publication

1. Kreitz, J. et al. (2019) 'Metabolic Plasticity of Acute Myeloid Leukemia', *Cells*. 8(8), p. 805. doi: 10.3390/cells8080805

Poster Prizes

1. DFG Sonderforschungsbereich 815 Summer School (Germany, 2018)
2. DTK Translational Cancer Research Summer School (Portugal, 2018)
3. DFG Sonderforschungsbereich 815 Summer School (Germany, 2019)

Tutor in Mathematics

at the Bonn-Rhein-Sieg University of Applied Sciences, Germany

Supervisor

of Master and medical students at the University Hospital Frankfurt, Germany

Kindergarten Teacher

in Ireland, as part of the European Voluntary Service (08/2010 - 07/2011)